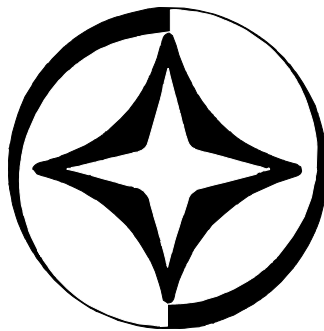


22nd SAINT PETERSBURG INTERNATIONAL CONFERENCE ON INTEGRATED NAVIGATION SYSTEMS

PANEL DISCUSSION

METHODS FOR NAVIGATION SENSOR PERFORMANCE DETERMINATION

PROCEEDINGS



27 May 2015

Saint Petersburg, Russia

CO-SPONSORED BY:

- SCIENTIFIC COUNCIL OF THE RUSSIAN ACADEMY OF SCIENCES ON THE PROBLEMS OF MOTION CONTROL AND NAVIGATION
- RUSSIAN FOUNDATION FOR BASIC RESEARCH
- INTERNATIONAL PUBLIC ASSOCIATION – ACADEMY OF NAVIGATION AND MOTION CONTROL (ANMC)
- NATIONAL RESEARCH UNIVERSITY ITMO, RUSSIA
- AMERICAN INSTITUTE OF AERONAUTICS AND ASTRONAUTICS (AIAA)
- INSTITUTE OF ELECTRICAL AND ELECTRONIC ENGINEERS – AEROSPACE AND ELECTRONIC SYSTEMS SOCIETY (IEEE – AESS), USA
- ASSOCIATION AERONAUTIQUE ET ASTRONAUTIQUE DE FRANCE (AAAF)
- INSTITUT FRANÇAIS DE NAVIGATION (IFN)
- DEUTSCHE GESELLSCHAFT FUER ORTUNG UND NAVIGATION (DGON)
GERMAN INSTITUTE OF NAVIGATION
- JOURNAL GYROSCOPY AND NAVIGATION, RUSSIA

The present book contains the papers of participants of the Panel Discussion held on the closing day of the 22nd Saint Petersburg International Conference on Integrated Navigation Systems (May 25-27, 2015, Concern CSRI Elektropribor, JSC).

CONTENTS

David W. Allan Historicity, Strengths, and Weaknesses of Allan Variances and Their General Applications	507
N.I. Krobka On the Topology of the Allan Variance Graphs and Typical Misconceptions in the Interpretations of the Gyro Noise Structure (Based on the Examples from Reports at the St. Petersburg International Conference on Integrated Navigation Systems)	525
O.A. Stepanov, I.B. Chelpanov, A.V. Motorin Accuracy of Sensor Bias Estimation and its Relationship with Allan Variance	551

HISTORICITY, STRENGTHS, AND WEAKNESSES OF ALLAN VARIANCES AND THEIR GENERAL APPLICATIONS

David W. Allan

President, Allan's TIME; Fountain Green, Utah 84632-0066

E-mail: david@allanstime.com

Web sites: www.allanstime.com www and ItsAboutTimeBook.com

Keywords: Allan variances, Time series analysis, Atomic clocks, Precision analysis, Non-stationary processes

Summary

Over the past 50 years, variances have been developed for characterizing the instabilities in precision clocks and oscillators. These instabilities are often modeled by non-stationary processes, and these variances have been shown to be well-behaved and to be unbiased, efficient descriptors of these processes. The time-domain and frequency-domain relationships are shown along with the strengths and weaknesses of these characterization metrics. These variances are also shown to be useful elsewhere, as in navigation.

Introduction

Nature gives us many non-stationary and chaotic processes. If we can properly characterize these processes, then we can use optimal procedures for estimation, smoothing, and prediction. During the 1960s through the 1980s, the Allan variance, the modified Allan variance, and the Time variance were developed to this end for the timing and the telecommunication communities. Since that time, useful refining techniques have been developed. This activity has been a learning endeavor, and the strengths and weaknesses of these variances will be enumerated herein. The applicability of these variances has been recognized in other areas of metrology as well, because the above processes are ubiquitous. Knowing the strengths and weaknesses is important not only in time and frequency but so that these variances may be properly utilized in other application areas, such as navigation.

Prior to the 1960s and before atomic clocks were commercially available, quartz-crystal oscillators were used for timekeeping. The greatest long-term-frequency instabilities in these oscillators were their frequency drifts. Also, it was commonly recognized that their long-term performance seemed to be modeled by what is commonly called flicker-noise frequency modulation (FM), which model is a non-stationary process, because this noise has a power-spectral-density proportional to $1/f$, where f is the Fourier frequency. In integrating this kind of noise to determine the classical variance, one observes that the integral is non-convergent.

In 1964, James A. Barnes developed a generalized auto-correlation function that was well behaved for flicker noise. I was fortunate to have him for my mentor at the National Bureau of Standards (NBS) in Boulder, Colorado. That same year, the IEEE and NASA held a special conference at NASA, Goddard, in Beltsville, Maryland, addressing the problem of how to characterize clocks with these non-stationary behaviors. Jim and I presented a paper at this conference, and it was well received. His work was the basis for his Ph.D. thesis, and it also gave me critical information that I needed for my master's thesis. We both finished our theses the following year. In addition to Jim's work, I relied heavily on the book that Jim had shown me by Sir James Michael Lighthill, *Fourier Analysis and Generalized Functions*. Along with Jim's work, this book was invaluable.

In my thesis I studied the effects on the classical variance as a function of how long the frequency was averaged (the averaging time, τ), how many samples were included in the variance, N , how much dead-time there was between frequency averages, $T-\tau$ (in those days it took time for a frequency counter to reset after a frequency had been measured over some interval τ ; so T was the time between the beginning of one measurement to the beginning of the next), and how it depended on the measurement system bandwidth, f_h . We developed a set of spectral-density, power-law noise models that covered the characterization of the different kinds of instabilities we were observing in clocks – resulting from the noise of the measurement systems, the clocks, and from environmental influences. Since then, we have observed that these noise models are much more general than we'd originally thought and have a broad application in metrology.

Both Jim's and my theses were published, along with several other papers from the 1964 IEEE/NASA conference, in a February 1966 special issue of the Proceedings of the IEEE on "Frequency Stability."

Modeling nature with power-law noise processes

The pioneering work of Mandelbrot and Voss introducing "fractals" shows the importance of these self-similar and non-stationary processes in modeling nature. Flicker noise is in that class. We found that five different kinds of noise were useful in modeling clocks. Many of these may be used as good models in other natural processes – including errors in navigation systems.

Modeling the noise processes in nature is revealing. The better we can model nature, the better we can use optimization to know more about the underlying processes masked by nature's noise.

We have been able to use the variances I will share in this paper in characterizing and modeling many different processes in nature. As I look back over the 50 years we have been doing this work, it has been rewarding to see the insights into nature that have been gained. I will show some exciting examples of these insights later in this paper.

For clocks, if the free-running frequency of a clock is $v(t)$ and we denote its nominal frequency as v_o , then we may write the normalized frequency deviation of a clock as $y(t) = (v(t) - v_o) / v_o$. The time-deviation of a clock may be written as $x(t)$, which is the integral of $y(t)$. Studying the time-domain and frequency-domain characteristics of $x(t)$ and $y(t)$ opens the opportunity to model the clock's behavior and then to perform optimum estimation, smoothing, and prediction of its "true" behavior in the midst of noise – even when the noise is non-stationary.

We symbolize the frequency-domain measures using spectral densities – denoted by $S_y(f)$ and $S_x(f)$. In the time domain we have found useful the Allan variance (AVAR), the modified Allan variance (MVAR), and the Time variance (TVAR). Other variances have been found useful as well. Often shown are the square-root of these variances:

• <u>SQUARE</u>	<u>SQUARE ROOT</u>
• $\sigma_y^2(\tau) = \text{AVAR}$	$\sigma_y(\tau) = \text{ADEV}$
• $\text{mod. } \sigma_y^2(\tau) = \text{MVAR}$	$\text{mod. } \sigma_y(\tau) = \text{MDEV}$
• $\sigma_x^2(\tau) = \text{TVAR}$	$\sigma_x(\tau) = \text{TDEV}$

Figure 1. Common nomenclature for the variances and their square-roots as used at the National Bureau of Standards (now National Institute of Standards and Technology) in the United States of America as well as in international scientific literature and as IEEE standards.

The power-law spectral densities may be represented as $S_y(f) \sim f^\alpha$ and $S_x(f) \sim f^\beta$, and because x is the integral of y , one may show that $\alpha = \beta + 2$. The models for the random variations for clocks, their measurement systems, and for their distribution systems that work well have values of alpha as follows: $\alpha = -2, -1, 0, +1, \text{ and } +2$. These models seem to reasonably fit the random frequency variations observed. These models seem to fit in many other areas of metrology as well. Flicker noise has been shown to be ubiquitous in nature. In the case of time and frequency, we have observed both flicker-noise FM ($\alpha = -1$) and flicker-noise PM ($\beta = -1$).

Figure 2 demonstrates how these models apply for different kinds of clocks. Typically, the noise model changes from short-term averaging times to long-term – almost always moving toward more negative values of α . Included in the following chart is the value $\alpha = -3$, as this is the long-term model for earth-rotation noise for Fourier frequencies below one cycle per year after subtracting all the systematic terms from the data.

**Given: $S_y(f) \sim f^\alpha$; $S_x(f) \sim f^\beta$;
and $\beta = \alpha - 2$**

Power-law spectra models

α	β	Earth	Qu	H-m	Cs	Rb	Optical
+2	0		•	•			
+1	-1		•				
0	-2		•	•	•	•	•
-1	-3	•	•	•	•	•	•
-2	-4		•	•	•	•	•
-3	-5	•					

Figure 2 Matrix showing the usefulness of power-law, spectral-density models for Earth = noise in the earth's rotation rate (after removing all systematics), in Qu = quartz-crystal oscillators, H-m = hydrogen masers, Cs = cesium-beam and cesium-fountain frequency standards, Rb = rubidium-gas-cell frequency standards, and in the new and most stable atomic clocks using frequencies in the optical region of the electromagnetic spectrum.

As one can see in the next figure, the visual appearance of these power-law spectra are very different, and the eye, in some sense, can be a good spectrum analyzer. One of the many reasons why in data analysis one should always visually look at the data is that the brain is an amazing and miraculous processor.

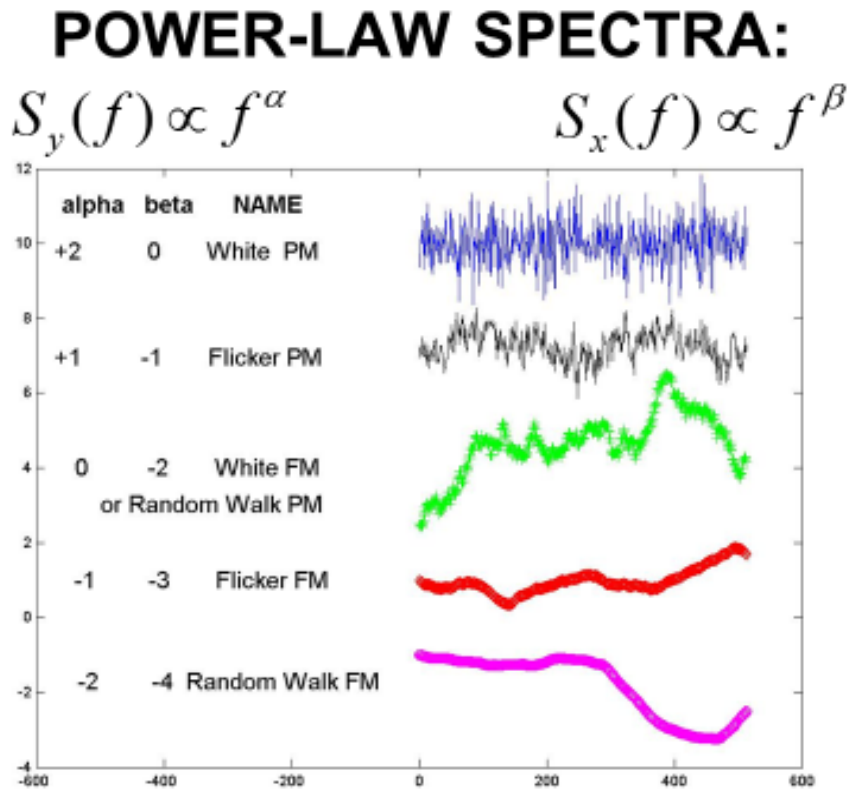


Figure 3. Illustration of visual difference for different power-law, spectral-density models.

Using Lighthill's book, we can transform these spectra to the time domain. In doing so we obtain figure 4.

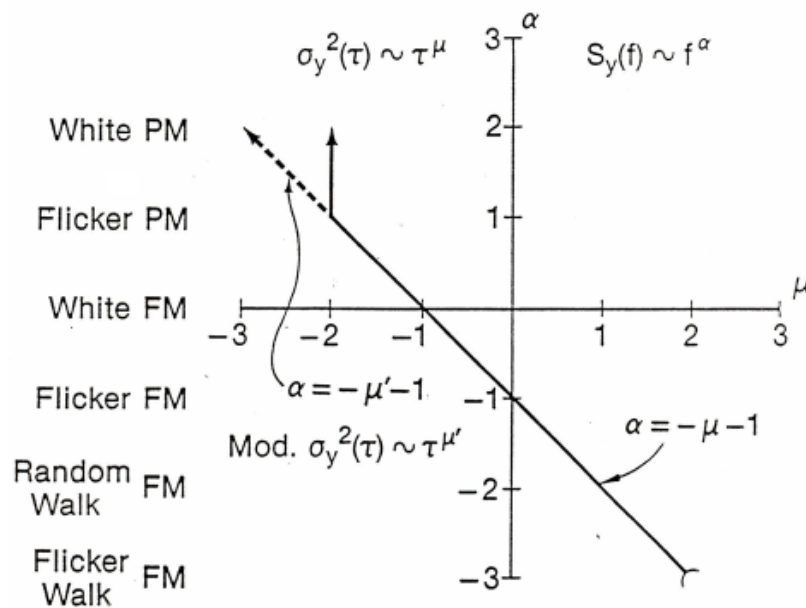


Figure 4. We have α as the ordinate and μ as the abscissa, where μ is the exponent on τ showing the time-domain dependence, and where $AVAR = \sigma_y^2(\tau)$ and $MVAR = \text{mod. } \sigma_y^2(\tau)$. We have an elegant Fourier transform relationship in the simple equation $\alpha = -\mu - 1$; we jokingly call it the super-fast Fourier transform, because the AVAR can be computed very quickly from an equally spaced set of data.

Since $\sigma_y^2(\tau) \sim \tau^\mu$, by plotting $\log \sigma_y(\tau)$ versus $\log \tau$, the slope will be $\mu/2$; hence, we can ascertain both the kind of noise as well as its level from such a plot. This sigma-tau plotting technique has been used literally thousands of times to great advantage – giving a quick “super-fast Fourier transform” of the data.

In Figure 4, we notice an ambiguity problem for AVAR at $\mu = -2$. The simple equation no longer applies, and we cannot tell the difference in the time domain between white-noise phase or time modulation (PM) and flicker-noise PM. This problem was a significant limitation in clock characterization for the time and frequency community for 16 years after AVAR was developed. Even though there was ambiguity in the τ dependence in this region, we knew that it could be resolved because there remained a measurement bandwidth sensitivity. Since it was inconvenient to modulate the measurement system bandwidth, this approach never became useful. But in 1981 we discovered a way to modulate the bandwidth in the software, and this was the breakthrough we needed. This gave birth to MVAR, and the concept is illustrated in the following figure.

One can think of software bandwidth modulation in the following way. There is always a finite measurement system bandwidth. We call it the hardware bandwidth, f_h . Let $\tau_h = 1/f_h$. Then every time we take a phase or time reading from the data, it inherently has a τ_h sample-time window. If we average n of these samples, we have increased the sample-time window using software by n , $\tau_s = n\tau_h$. Let $\tau_s = 1/f_s$, then if we increase the number of samples averaged as we increase τ , then one can show that we are decreasing the software bandwidth by $1/n$. We were able to show that by modulating the bandwidth in this way we removed the above ambiguity and maintained validity for our simple super-fast Fourier transform equation over all the power-law noise processes of interest; $\alpha = -\mu' - 1$. There is an unknown proportionality constant between the f_s shown below and the f_s in the above equations, but fortunately we don't need to know it to characterize the data.

Figure 5 is an illustration of this software bandwidth modulation for $n = 4$; in principle, n can take on any integer value from 1 to $N/3$.

In 1981 we learned how to modulate the bandwidth in the software;
fundamental breakthrough

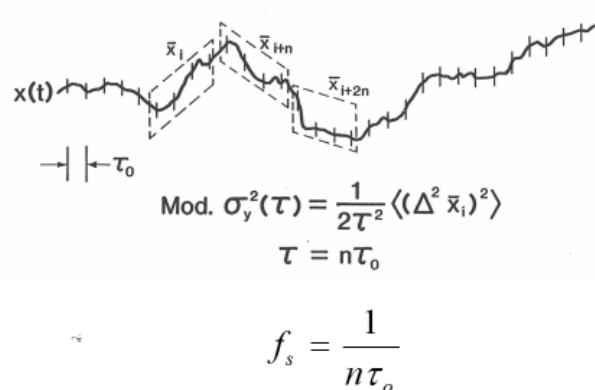


Figure 5. A pictorial of the software-bandwidth modulation technique used in the modified Allan variance to resolve the ambiguity problem at $\mu = -2$; Hence, this software modulation technique allows us to characterize all of the power-law spectral density models from $\alpha = -3$ to $\alpha = +2$. This covers the range of useful noise models for most clocks. Illustrated in this figure is the case for $n = 4$; n may take on values from 1 to $N/3$, where N is the total number of data points in the data set with a spacing of τ_0 .

Data length dependent variances are not useful

Going back to 1964, Dr. Barnes had shown that the second and third finite-difference operators on the time variations of a clock gave a convergent statistic in the presence of flicker noise FM. This was the basis of his PhD thesis in helping to use a quartz-crystal oscillator ensemble calibrated by the National Bureau of Standards primary cesium-beam-frequency standard to construct a time scale for generating time for NBS and hence for the USA civil sector; the USNO is the official time reference for the USA defense sector.

I had shown in my master's thesis the divergence of the classical variance or lack thereof for the above power-law noise processes as a function of the number of data points taken. The degree of divergence depends upon both the number of data points in the set as well as upon μ the kind of noise. In other words, the classical

variance was data-length dependent for all of the power-law noise models we were using to characterize clocks except for classical-white noise FM. Hence, the classical variance was deemed not to be useful in characterizing atomic clocks because other than white-noise FM models were needed. This divergence problem seems to exist in all areas of metrology as a result of nature’s natural processes and environmental influences on whatever we are measuring.

I used the two-sample variance as a normalizing factor because I knew from Lighthill and from Barnes’ work that it was convergent and well behaved for all of the interesting power-law spectral density processes that are useful in modeling clocks and measurement systems. The two-sample variance I used may be written as follows:

$$\sigma_y^2(\tau) = \frac{1}{2} \langle (\Delta y)^2 \rangle = \frac{1}{2\tau^2} \langle (\Delta^2 x)^2 \rangle,$$

where the brackets $\langle \rangle$ denote the expectation value, or ensemble average and the “2” in the denominator normalizes it to be equal to the classical variance in the case of classical white-noise FM. Don Halford, my Section chief at the time, named this the Allan variance, and the name persists. I don’t mind; jokingly, some ask if I am at variance with the world? When one takes the square root and it becomes the Allan deviation, I cringed a bit, but then as I thought about it, I said to myself, “I am not a deviant!” Deviation is the measure of performance – the change in a clock’s rate – the smaller the better. If I can help these be smaller and smaller, that is good and will help society, and I am all for that.

The ratio of the N-sample variance to the Allan variance as a function of N is shown in the figure 6. Realizing that the N-sample variance is the classical variance for N samples, one sees why it is not useful for characterizing these different kinds of noise, as it is not convergent in many cases and is biased as a function of N in all cases except for classical-white noise. One can turn this dependence to an advantage and use it to characterize the kind of noise using the B1 bias function: $B_1(N) = \sigma^2(N) / \sigma_y^2(\tau_0)$.

**This ratio is called the bias function, $B_1(N)$;
can be used to ascertain kind of noise:**

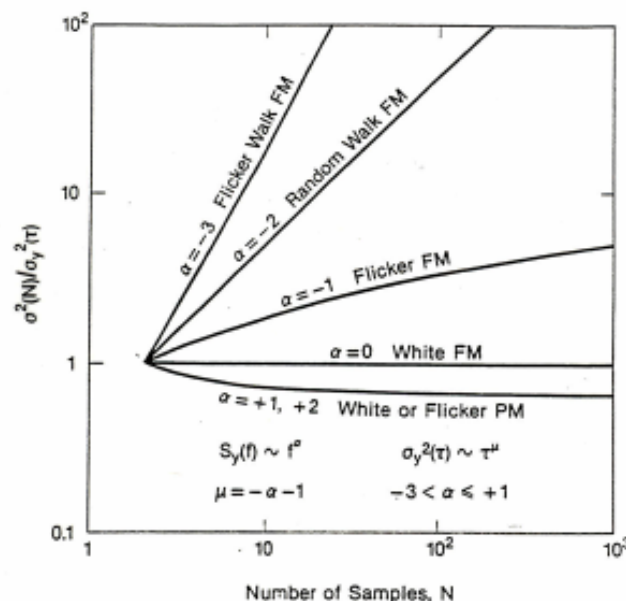


Figure 6. Illustration of the data-length dependence of the classical variance for the different kinds of power-law noise processes used in modeling precision oscillators and atomic clocks as a function of the data length.

Following the 1966 IEEE special issue on “Frequency Stability,” the IEEE asked Dr. Barnes to chair a panel of experts and to prepare a special paper on “Characterization of Frequency Stability.” That paper was published in 1971 in which they recommended the spectral density $S_y(f)$ and the two-sample variance as the recommended measures of frequency stability. They also called it the “Allan variance.” This paper is available on the NIST Time and Frequency Divisions web site: <http://tf.boulder.nist.gov/general/pdf/118.pdf> Dr. Leonard S. Cutler, who was one of these experts, was the first to write the equation for the time-domain variances in terms of the spectral density, and this is developed in this paper for, equation 23.

As a point of interest, many years ago I was asked to write a paper entitled, “Should the Classical Variance Be Used as a Basic Measure in Standards Metrology?” <http://tf.boulder.nist.gov/general/pdf/776.pdf> . I researched voltage standards and gage-blocks, and I found flicker-noise behavior in their long-term performance. A fundamental statement that came out of that research was that if the bias function $B_1(N)$ is not 1 (one) within some reasonable confidence limits, then the classical variance is not a good measure. That advice was not followed by the BIPM standard’s committee even though it has a solid scientific basis. Traditions seem too strong many times even when these traditions are not the best for progress when these flawed traditions continue to be followed.

Note also that the two-sample or Allan variance is without dead-time. In other words, the frequency measurements are sequentially adjacent. For example, the i^{th} frequency deviation taken over an averaging time, τ , may be derived from the time deviations as follows: $y_i = (x_i - x_{i-1})/\tau$. This equation gives us the true average frequency deviation over that interval; it may not be the optimum estimate of frequency. One notices that if the average is taken over the whole data set, then all the intermediate values cancel, and one is left with the true average frequency deviation over the data set: $y_{\text{avg}} = (x_N - x_0)/N\tau$. This is one of the benefits of no-dead-time data. Another is that for classical white-noise FM, as has been found to be the fundamental performance limitation in most atomic clocks, then $\sigma_y^2(\tau)$ is an optimum-variance estimator of the change of frequency over any averaging time, τ , and is equal to the classical variance for – the minimum data-spacing variance.

Dr. Barnes has also shown that $\sigma_y^2(\tau)$ is an unbiased estimator for the level of the power-law noise process of interest in modeling atomic clocks and that it is Chi-squared distributed. The value of τ in the software analysis can take on values for all $\tau = n \tau_0$ for any integer $n = 1$ to $N/2$. The confidence of the estimate is best at $\tau = \tau_0$ decreasing to $\tau = N/2$, where there is only one-degree of freedom for the confidence of the estimate and the Chi-squared-distribution function has a most probable value of zero for one degree of freedom. Even though it is unbiased, the probability of small values is significant. In a $\sigma_y^2(\tau)$ versus τ plot, one often observes too-low of values for $\sigma_y^2(\tau)$ as the value of τ approaches half the data length; then the degrees of freedom are too small for a good confidence on the estimate. David A. Howe and his group at NIST have addressed this problem and have come up with some elegant solutions by adding degrees of freedom to the long-term data; that work is still in progress and is extremely useful. <http://tf.boulder.nist.gov/tf-cgi/showpubs.pl>

In other areas of metrology, one needs to pay attention to this dead-time issue if the noise is not white (random and uncorrelated). As shown in my thesis, the dead-time has an impact on the resulting variance if the noise is not white. The dead-time problem was studied and subsequent papers written. The following link in Chapter 8 of Monograph 140 covers this issue for both the N dependence and dead-time with the bias functions B_1 and B_2 , respectively: <http://tf.boulder.nist.gov/general/pdf/771.pdf> Later, I will show this need not be a significant problem in general metrology applications; it seems to be a unique problem in time and frequency.

The time variance

In the later part of the 1980s the telecom industry in the United States came to me and asked if I would help them with a metric for characterizing telecommunication networks. I asked Dr. Marc Weiss, who was in my group at NIST at the time, to help me with this project. It was a fascinating work, as we analyzed a lot of their data to find the best metric. Out of this work we developed the time variance, TVAR. It is defined as follows: $\text{TVAR} = \tau^2 \text{MVAR}/3$. The “3” in the denominator normalizes it to be equal to the classical variance in the case of classical white-noise PM. Like as for AVAR for FM, one can show that for white-noise PM, TVAR is an optimum estimator of change in the phase or time residuals in a variance sense.

The work in the United States caught on and these three variances became international IEEE time-domain measurement standards in 1988. Interestingly, in their historic application we see that these three variances had three general regions of applicability:

1. AVAR for characterizing the performance of frequency standards and clocks.
2. MVAR for characterizing the performance of time and frequency distribution systems.
3. TVAR for characterizing the timing errors in telecommunication networks.

Following the development of each of these three variances, many other areas of applicability have arisen. Conveniently, TDEV (the square-root of TVAR) has no dead-time issues and has become a standard metric in the international telecommunications industry. All three have application capability in many other areas of

metrology. Navigation system errors and gyro errors are some examples. If you search Google for “Allan variance,” you will find about 50,000 results.

Equations and their transforms

The equations for computing AVAR, MVAR, and TVAR from the time-deviations and for N data points are respectively:

$$\sigma_y^2(\tau) = \frac{1}{2\tau^2(N-2n)} \sum_{i=1}^{N-2n} (x_{i+2n} - 2x_{i+n} + x_i)^2,$$

$$\text{mod.}\sigma_y^2(\tau) = \frac{1}{2\tau^2n^2(N-3n+1)} \sum_{j=1}^{N-3n+1} \left(\sum_{i=j}^{n+j-1} (x_{1+2m} - 2x_{i+n} + x_i) \right)^2,$$

$$\sigma_x^2(\tau) = \frac{1}{6n^2(N-3n+1)} \sum_{j=1}^{N-3n+1} \left(\sum_{i=j}^{n+j-1} (x_{1+2m} - 2x_{i+n} + x_i) \right)^2,$$

where the x_i are the time deviation data separated by a time interval, τ_0 , and $\tau = n\tau_0$.

For MVAR and TVAR, the computation involves a double sum. One may think that this could cause the computation time to increase as N^2 , but one can employ some computation tricks, such as simple drop-add averaging, to make it linear. Otherwise this could be a problem for large data sets. Such tricks have been successfully implemented, and the software references cited later include these computation techniques.

The following equations show how the three time-domain variances may be derived from frequency-domain information. One cannot do the reverse – derive the spectral densities from time-domain analysis. When possible, it is often very useful to analyze the data in both the frequency and time domains. Below we see the frequency-domain view of these variances.

Translation Between Frequency and Time Domains

$$\tau = n\tau_0$$

AVAR:

$$\sigma_y^2(\tau) = \int_0^\infty 2 \left[\frac{\sin^4(\pi f \tau)}{(\pi f \tau)^2} \right] S_y(f) df$$

MVAR:

$$\text{Mod } \sigma_y^2(\tau) = \int_0^\infty 2 \left[\frac{\sin^3(\pi f \tau)}{(n\pi f \tau) \sin(\pi f \tau_0)} \right]^2 S_y(f) df$$

TVAR:

$$\sigma_x^2(\tau) = \frac{8}{3n^2} \int_0^\infty \left[\frac{\sin^3(\pi f \tau)}{\sin(\pi f \tau_0)} \right]^2 S_x(f) df$$

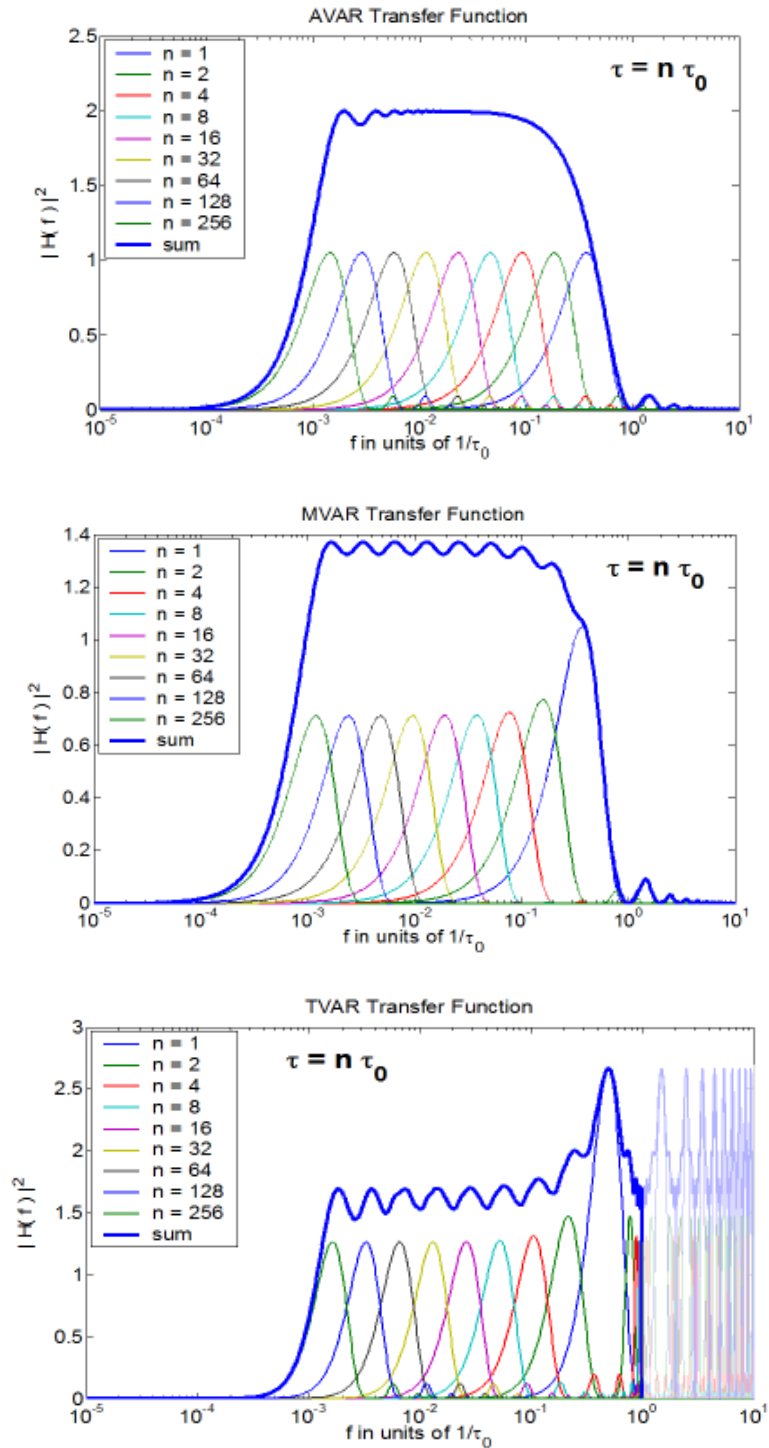


Figure 7 a, b, c, and d. Figure 7a shows the three time-domain equations as derived from spectral densities. Figures b, c, and d show the effective Fourier windows using the transfer functions of each of these three variances for $n = 1, 2, 4, 8, 16, 32, 64, 128, \text{ and } 256$.

Three years ago, I was asked to write a paper on “Conversion of Frequency Stability Measures from the Time domain to the Frequency domain, vice-versa and Power-law Spectral Densities.” This paper is available on our web site, and has a lot more detail about these conversion processes: http://www.allanstime.com/Publications/DWA/Conversion_from_Allan_variance_to_Spectral_Densities.pdf The conversion relationships are shown in the following table for the five noise types:

NOISE TYPE	$S_y(f)$	$S_x(f)$
White PM	$\frac{(2\pi)^2}{3f_h} [\tau^2 \sigma_y^2(\tau)] f^2$	$\frac{1}{\tau \sigma_x^2(\tau)} f^0$
Flicker PM	$\frac{(2\pi)^2}{A} [\tau^2 \sigma_y^2(\tau)] f^1$	$\frac{3}{3.37} [\tau^0 \sigma_x^2(\tau)] f^{-1}$
White FM	$2 [\tau^1 \sigma_y^2(\tau)] f^0$	$\frac{12}{(2\pi)^2} [\tau^{-1} \sigma_x^2(\tau)] f^{-2}$
Flicker FM	$\frac{1}{2\theta\tau^2} [\tau^0 \sigma_y^2(\tau)] f^{-1}$	$\frac{20}{(2\pi)^2 9\theta\tau^2} [\tau^{-2} \sigma_x^2(\tau)] f^{-3}$
Random Walk FM	$\frac{6}{(2\pi)^2} [\tau^{-1} \sigma_y^2(\tau)] f^{-2}$	$\frac{240}{(2\pi)^4 11} [\tau^{-3} \sigma_x^2(\tau)] f^{-4}$

$$A = 1.038 + 3 \ln(2\pi f_h \tau)$$

Estimation, smoothing, and prediction

■ Estimation and smoothing

Box and Jenkins in their book, *Time Series Analysis*, using the ARIMA process, do a great work on how to estimate and smooth for various kinds of random processes. I will not review their paramount work here.

There is a simple, powerful and useful statistical theorem that I will use for estimation, smoothing, and prediction. It is that the optimum estimate of the mean of a process with a white-noise spectrum is the simple mean. As examples, if we have white-noise PM, then the optimum estimate of the phase or the time is the simple mean of the independent phase or time residual readings added to the systmatics.

If we have white-noise FM, then the optimum estimate of the frequency is the simple mean of the independent frequency readings, which is equivalent to the last time reading minus the first time reading divided by the data length, if there is no dead-time between the frequency measurements. As we have shown before, the true average frequency is given by: $y_{avg} = (x_N - x_0)/N\tau$.

■ Prediction

Using the above theorem for optimum prediction, if we take the current time as “t,” and we wish to predict ahead an interval τ , then the optimum time prediction, for a clock having white-noise FM and an average offset frequency y_{avg} given by the above equation, is given by: $\hat{x}(t + \tau) = x_N + \tau y_{avg}$. A simple pictorial for the optimum time prediction using this theorem for the five different noise processes is shown in the figure 8; for white-noise FM, the y_{avg} is assumed to be zero.

The even-powered exponents are directly amenable to this theorem, but the flicker-noise (odd exponents) are more complicated. However, there is a simple prediction algorithm for flicker FM using what we call the second difference predictor. It is very close to optimum and is simple. If you desire to predict τ into the future then this prediction can be obtained by the following equation: $\hat{x}(t + \tau) = 2x(t) - x(t - \tau)$, where t is the current time. I have seen this equation used on the stock market, which is often flicker-like in its performance.

Knowing the stability, $\sigma_y(\tau)$, of a clock allows us to calculate its time predictability capability. As an approximate rule of thumb, the predictability is given by $\tau \sigma_y(\tau)$, Using this equation the figure 9 shows the time predictability of a variety of timing devices that have been used over human history.

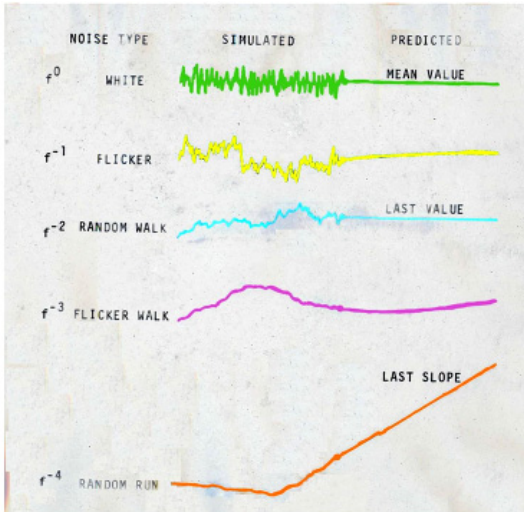


Figure 8. A pictorial illustrating optimum prediction for the five different power-law noise processes used in modeling the time deviations in precision clocks. These prediction algorithms have general application.

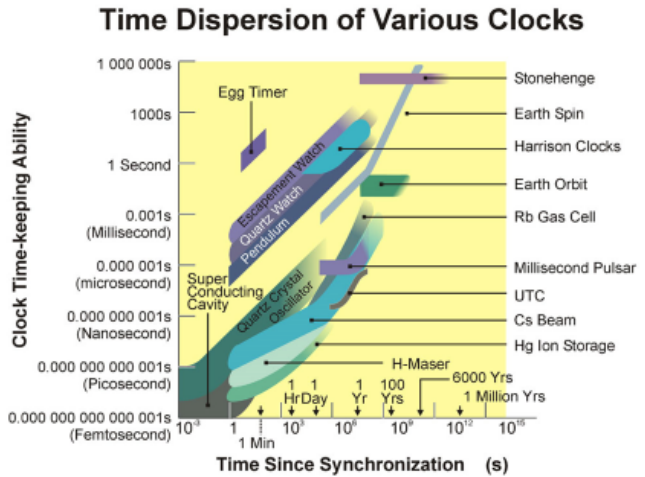


Figure 9. This chart was made back in 1997. If we were to include the ytterbium clock on this graph, it would be represented by a $\tau^{1/2}$ line crossing through 40 femtoseconds at seven hours; or it would be about 100 times better than the best clocks shown here.

A similar plot could be made for the navigation community showing the position dispersion rate for various navigation devices. This may be a useful tool to see which technologies could be brought together in combination to make a significant improvement in both the short-term and long-term performance.

Systematics

A good model for time deviations in a clock is: $x(t) = x_0 + y_0 t + \frac{1}{2} D t^2 + \epsilon(t)$, where x_0 and y_0 are, respectively, the synchronization error and syntonization error at $t = 0$, D is the frequency drift, and $\epsilon(t)$ represents the remaining random errors on top of the first three systematic error terms. It is good to subtract the systematics from the data so that the random effects can be viewed visually and then analyzed with better insights. Much can often be learned by this approach.

If frequency drift is present in a clock, and it usually is, then it affects AVAR, MVAR, and TVAR in the following way:

$$\sigma_y(\tau) = \text{mod.} \sigma_y(\tau) = \frac{D\tau}{\sqrt{2}} \quad \text{and} \quad \sigma_x(\tau) = \frac{D\tau^2}{\sqrt{6}} .$$

An example of the effect of frequency drift on an ADEV plot is shown in the next figure.

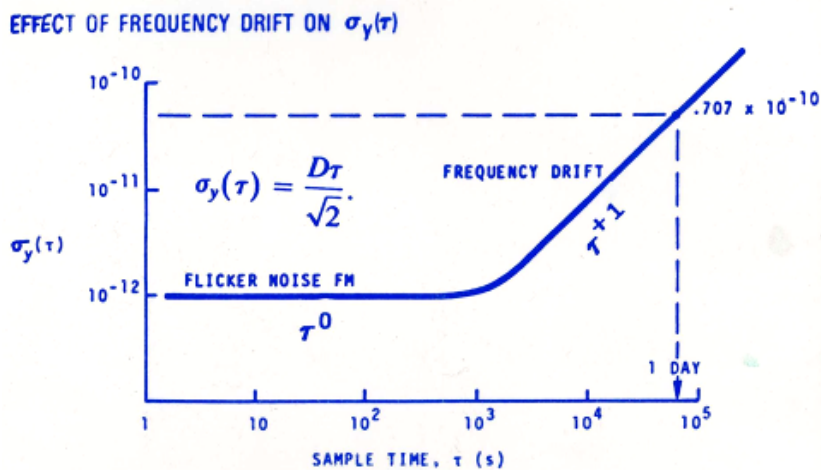


Figure 10. Illustration of the effects of frequency drift on an ADEV plot.

If there is frequency drift, the values of $\sigma_y(\tau)$, in that region where the drift is affecting the plot, will lie tightly on the τ^{-1} line. If there is random noise present then the values will not fit tightly to this line. If there is a frequency modulation, f_m , present in the data then it also has a systematic effect on the analysis in the following way for ADEV: $\sigma_y(\tau) = \frac{x_{pp}}{\tau} \sin^2(\pi f_m \tau)$, where x_{pp} is the peak-to-peak amplitude of the modulation. The following figure shows the effect on an ADEV plot.

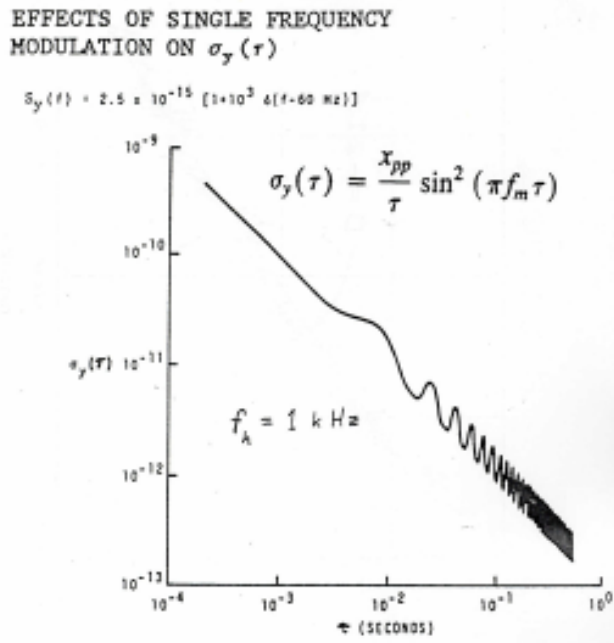


Figure 11. ADEV with frequency modulation, f_m , present on the data.

Both MVAR and TVAR are affected as well. A plot of the effect on TDEV is shown in the next figure.

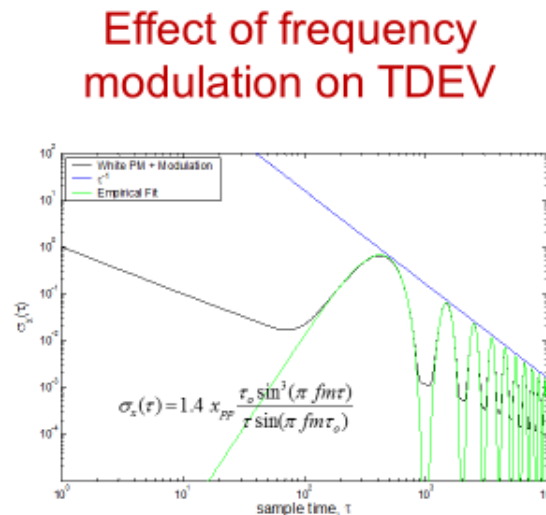


Figure 12. The effect of frequency modulation on a TDEV plot when that modulation is on top of the signal and noise. The white-noise PM causes the $\tau^{-1/2}$ behavior in the plot. Notice the modulation averages down as τ^{-1} . The equation fitting the effects of the modulation is empirical.

At $\tau = n/f_m$, the effect of the modulation is aliased away, where n is any positive integer. Recognizing this null effect allows these three variances to be used as low-frequency spectrum analysis techniques for bright Fourier-frequency lines in the data. It is my experience that low-frequency spectral lines can often be observed using this null approach in the time domain better than can be observed in the frequency domain. We will find this effect very useful in the EXAMPLES section of the paper, which is next.

Examples and some application opportunities of these variances

■ Clocks of the 1960s and 70s

In the following figure we have a sigma-tau plot of the frequency instabilities between a precision free-running, quartz-crystal oscillator and a commercial cesium-beam atomic clock. One sees for sample times, τ , shorter than one second a τ^{-1} behavior due to the measurement noise. This plot was made before MDEV was developed, so we are not sure of the noise type because of the ambiguity problem with ADEV for this slope. I have observed the same ambiguity problem in some of the navigation stability plots that I have seen. Whenever a τ^{-1} behavior occurs in an ADEV plot, one should then analyze the data using MDEV to hopefully resolve the ambiguity regarding the kind of noise modulation present in the data.

The rise in the value of $\sigma_y(\tau)$ as the sample or averaging time approaches 10 seconds is due to the attack time of the cesium-beam locking its quartz-crystal-slave-oscillator to the cesium resonance. Over the next decade we see a $\tau^{-1/2}$ behavior; or $\mu = -1$ which means $\alpha = 0$ from our simple "super-fast-Fourier" transform relationship, and this is classical white-noise being measured for this cesium-beam atomic clock. For the longest averaging times we see a τ^0 behavior, which then corresponds to $\alpha = -1$, and this is due to the flicker-noise FM of the precision, quartz-crystal oscillator. Even with the ADEV ambiguity problem, we were delighted in the 1960s and 70s to be able to characterize so easily the noise type and level of the clocks then being used for timekeeping for the USA.

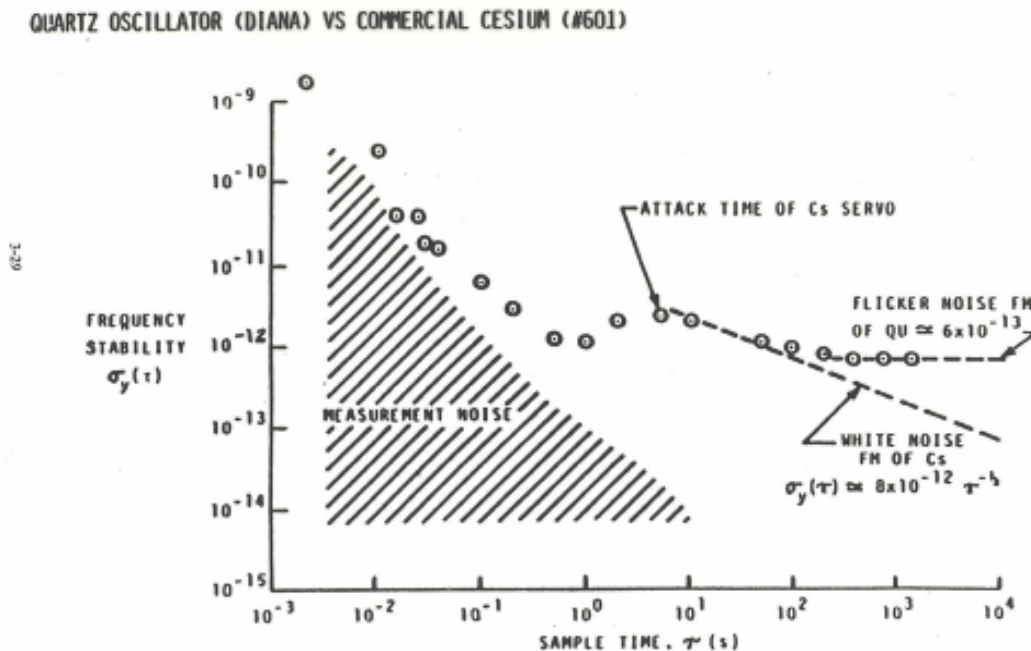


Figure 13. An ADEV plot for a precision, quartz-crystal oscillator versus a commercial cesium-beam atomic clock.

In 1965, we had a very interesting clock comparison at NBS in Boulder, Colorado. Bob Vessot brought his hydrogen maser from Boston, Massachusetts. Harry Peters brought his hydrogen maser from NASA Goddard, Beltsville, Maryland. Len Cutler brought his Hewlett Packard commercial-cesium-beam, atomic clock from Palo Alto, CA. We had the NBS primary frequency standard and data acquisition systems. This grand-clock-comparison effort resulted in an interesting 12 author paper. <http://tf.boulder.nist.gov/general/pdf/172.pdf>.

It was my responsibility at that time to provide the NBS reference time-scale for comparing all of these clocks. Up to this point, Jim's algorithm had been generating time for NBS and for the civil-sector of the USA. With Jim's ever-present help, I wrote a new time-scale algorithm, AT-1. With several refinements by Tom Parker and Judah Levine since that time, that algorithm is still generating time for the USA today. This time-scale algorithm was a major application of the "Allan variance" and generated a near real-time software clock with the following optimization features:

- Its software-clock output can be shown to be better than the best clock providing input;
- Even the worst clock enhances the output;
- If a clock misbehaves, it is rejected and not used – avoiding unnecessary perturbations;
- Each clock gets an optimum weighting factor for inclusion in the time computation;

- The weights are adaptive so that if a clock improves over time, its weight increases and vice versa;
- The optimum time of each clock as well as the optimum estimate of the frequency of each clock are estimated at each measurement cycle;
- Both the short-term as well as the long-term stability of the software ensemble output are optimized;
- And it is able to deal with white-noise FM, flicker-noise FM, and random-walk FM, which are the kinds of noise processes that well model the atomic clocks being used;

Originally, I used a PDP-8 computer and had eight clocks in the ensemble; AT-1 had 94 lines of code and provided error messages. I had to use some variables three times to not exceed the available logic limit. It is interesting to watch this algorithm's performance, because it is almost as if it is alive as it breathes with each clock's behavior. AT-1 has been generating the official time for the USA for nearly 50 years.

■ New optical clock stabilities using total ADEV

As we look at some of the exciting new optical clocks, the following ADEV plot is from data taken at NIST in Boulder, Colorado comparing two ytterbium optical lattice clocks in 2013. This plot utilizes the "Total ADEV" approach developed by David A. Howe and his group, which gives optimum confidence on the long-term stability estimates for ADEV. Long-term data are extremely valuable, so this "Total ADEV" technique adds greatly to the information one is able to learn from the data.

Here we see the best stability ever observed to that date of $\sigma_y(\tau = 25,000 \text{ seconds}) = 1.6 \times 10^{-18}$. This is like an error of 50 ps in a year. A picosecond is a million-millionth of a second (10^{-12} s); 50 ps is the time it takes light to travel 1.5 cm. This is 20 times better than the nanosecond accuracy that GPS needs and they have to upload their GPS corrections at least once a day. In this plot we see the nearly ideal atomic-clock ($\tau^{-1/2}$) white-noise FM behavior over about four decades of averaging time at a remarkable level of 3.2×10^{-16} at 1 second.

World record for stability NIST ytterbium optical lattice clock

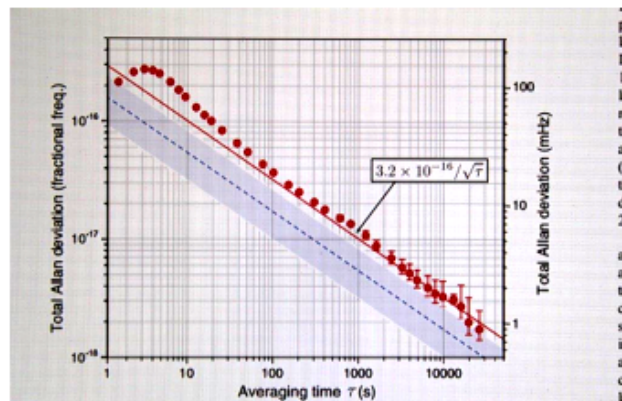


Figure 14. Comparison of two ytterbium optical-lattice atomic clocks operating at 518 295 836 591 600 Hz

Millisecond pulsar timing using MDEV

Going back to 1982, the first millisecond pulsar was discovered by Donald Backer, Shri Kulkarni, Carl Heiles, Michael Davis, and Miller Goss. Its name PSR B1937+21 is derived from the word "pulsar" and the declination and right ascension at which it is located, with the "B" indicating that the coordinates are for the 1950.0 epoch. This pulsar had the best astronomical timing performance of anything ever observed. I read their paper and was intrigued. I could see some ways we could help them, so I made contact with Dr. Michael Davis, who was the scientist in charge at the Arecibo Observatory where the data were being taken. Mike invited me down, and in 1984 I installed a GPS common-view receiver to tie their clock, which was making the pulsar measurements, to the world's best atomic clocks.

One can see in the next figure, the very complicated system for this millisecond pulsar measurement and the nominal behavior in each link of the measurement system chain.

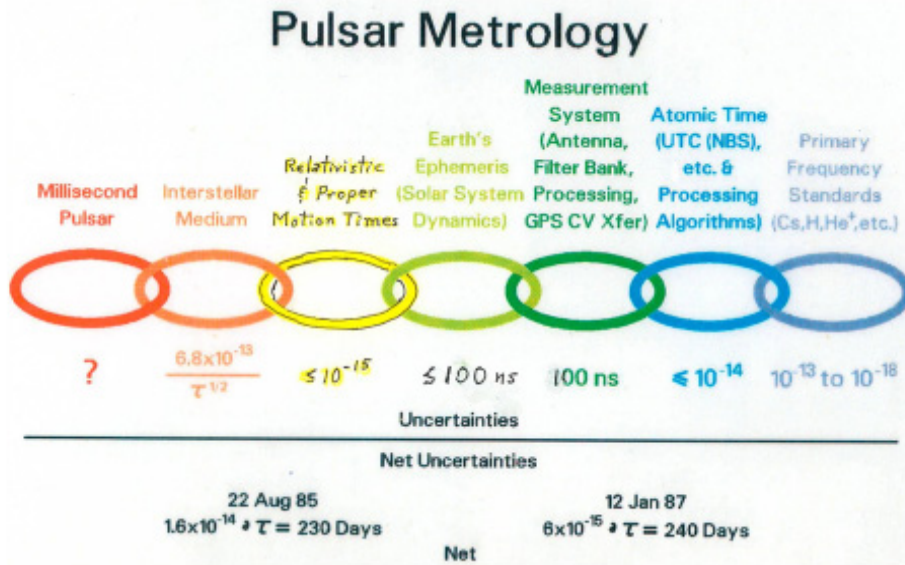


Figure 15. Measurement system for the millisecond pulsar. Note the improvement of nearly a factor of three in the stability measurements from 1985 to 1987 indicated at the bottom of the figure due to the help we were able to give them.

The next figure is an excellent example of the advantages of the modified Allan variance. As I studied the data, I was able to observe random-walk (f^2 spectrum) in the delay between two different observation frequencies for the pulsar. They had assumed that the electron content along the path was constant. This result showed that it was not, and when the $1/f^2$ ion content correction was applied the random-walk effect was suppressed leaving white-noise PM residuals as is shown in the next figure using MDEV to show this benefit.

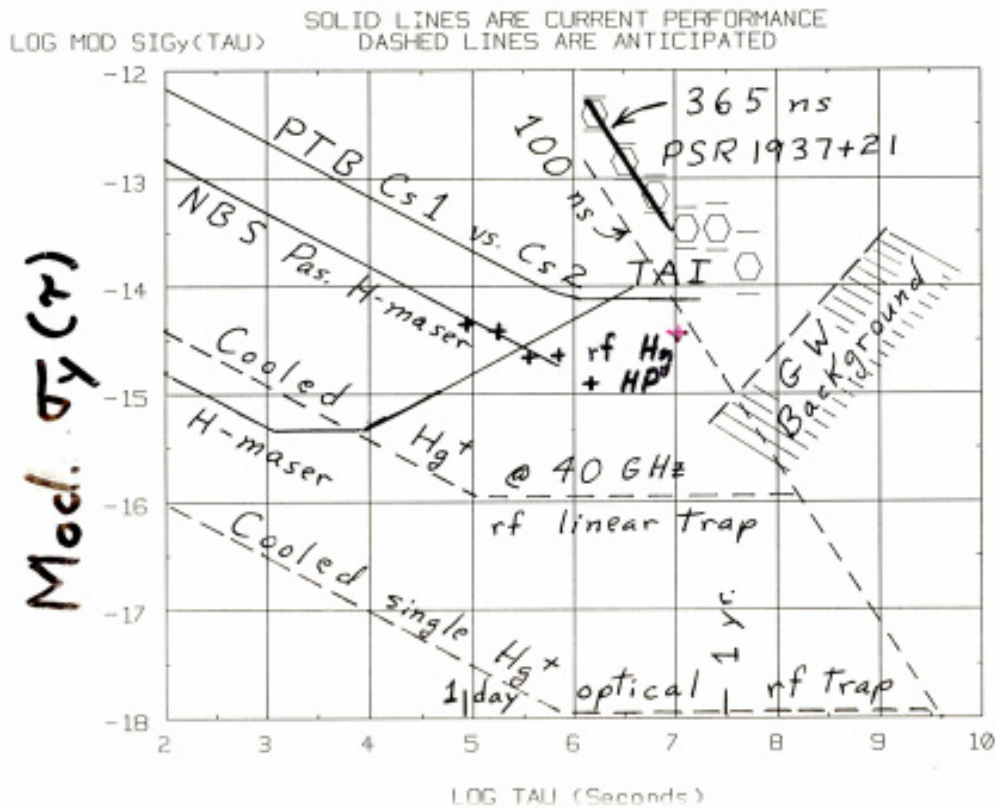


Figure 16. The PTB is the primary frequency standards laboratory for Germany. "Pas" stands for passive hydrogen maser. H-maser is for an active hydrogen maser. For shorter than 100-second averaging times, active hydrogen masers often exhibit white-noise PM, which is a $\tau^{-3/2}$ slope like the slope of the measurement noise of the pulsar. PSR 1937+21 is located about $1/7^{\text{th}}$ of the way across our galaxy, and the hope then was that we might see gravitational-wave perturbations in the path indicated by "GW Background."

Over the next several years, they did a 25-million dollar upgrade on the Arecibo telescope to bring about several major improvements and hoping to move the measurement noise down to the indicated 100 ns level.

In about 1990, I shared the following frequency stability plot at a UC Berkley, California, millisecond pulsar workshop. As these new fast spinning pulsars were thought to be competitive with atomic clocks, there is a very fundamental message in this plot. Even if they achieve the 100 ns white-noise PM measurement noise level with their upgrade, the data need to be averaged for about 200 years to reach a stability level of 10^{-18} , which is about where the best clocks are now. In other words, you would get one data point every 200 years at the 10^{-18} level – clearly not a competitive clock. I had no comments from my expert millisecond pulsar colleagues in the audience! One may further note that the ytterbium stability has, as of two years ago, surpassed by a factor of three that shown in the figure for the best anticipated performance of the cooled single Hg ion.

■ Opportunity for improving GPS accuracy

The GPS satellites (SVs) orbit the earth at about 4.2 earth radii. This distance creates a significant geometry problem for determining the vertical distance of the satellites from the center of the earth because the tracking stations' vectors are too close to parallel. GLONASS solves this problem by using retro-reflectors on the satellites and by doing round-trip-laser ranging from a ground station of known position to each of the satellites. This they can do to about 5-cm accuracy, which is about 12 times better than GPS.

Kepler's third-law has built into it the needed orthonality to solve this vertical-distance problem:

$T^2 = \frac{4\pi^2}{GM} r^3$, where T is the orbit period, G is the universal gravitational constant, M is the mass of the earth, and r is the radius from the center of the earth to the satellite. Since the orbit is tangential to the radius vector, if we can determine the point of closest approach to a tracking station of known coordinates, then we have the orthogonal information we need to determine the radius vector. The Doppler shift of an SV's clock will go to zero at its point of closest approach with respect to its tracking station. This zero-Doppler shift gives us a precise marker in its orbit period, T, with an uncertainty δT . From the above equation, we can derive the uncertainty in the radius vector: $\delta r = \frac{2}{3} r \frac{\delta T}{T}$. With current high-performance atomic clocks and using MDEV to assure that

the residuals are white-noise PM, so that all the systematics have been properly removed, then our calculations indicate that δr can be made to be less than a centimeter. The value of δT can be made very small because with white-noise PM being the limiting measurement noise, its value decreases as the data-length to the minus 3/2s power for the viewing-time of the satellite's pass.

There are some important contingencies associated with making this equation work properly. Professor Neil Ashby, who did the relativity equations for GPS, and I worked on modeling this approach in the 1990s and got some excellent results. Clocks have gotten significantly better since then, and the requirement for a zero-g environment as was done for Gravity Probe-B is now more readily available. There are some other contingencies, but the advantages are enormous; being an all-weather system is one. One of the biggest disadvantages is that this approach is a major change in system architecture, but these changes could be done in a meaningful step-wise process.

I felt that this-high accuracy technique was far enough along that I sent a letter to the GPS Headquarters folks for their consideration. I describe this some in Chapter 20 of my book, and the details may be found in Appendix K of the book's web site, www.ItsAboutTimeBook.com.

■ New unified field theory results validated using ADEV

Starting in 1999, we were working to understand a new concept in relationship to the UFT. This concept is explained in papers on our web site: www.AllansTIME.com/UFT_private and in Chapter 21 of my book. The book has exciting new information that has never been published before. The concept is that what we call diallel-field lines can carry all four of the force fields plus much more and connect everything to everything. The book by Lynne McTaggart, *The Field*, describes many experiments consistent with this new UFT.

We first did experiments to show the existence of these diallel-field-lines, and then that they had quantum states. Whereas the quantum states in atoms or molecules are generally thought of as being spherical or elliptical, they are nominally cylindrical in the diallel-field structure. In the fall of 2000 we observed for the first time quantum-transition emissions from these diallel-field-lines. This and some of the other experiments were performed in the laser physics lab at BYU. They kindly let me use it as an alumnus. All these experiments are described in Chapter 21 of my book. We have done seven experiments to date validating this new UFT diallel-field-line theory.

The following figure illustrates the diallel-field-line coupling of the planets to the sun and their effect on the sun-spot activity. I used 100 years of sunspot data and I analyzed it using ADEV as shown in the following figure. As predicted by this new UFT, we were delighted to find the periods of all the major planets present in the sun-spot data except for Uranus, where our 100 year data length was insufficient. I also used the masses, the magnetic fields, and the planet's orientations in space to see if I could nominally duplicate the sun-spot activity over the last 100 years. I had about an 80% correlation coefficient fit to the data. There is still a lot to be learned. We feel like infants exploring the biggest forest in the world.

Diallel-field line coupling of the planets to the sun shown in sunspot activity

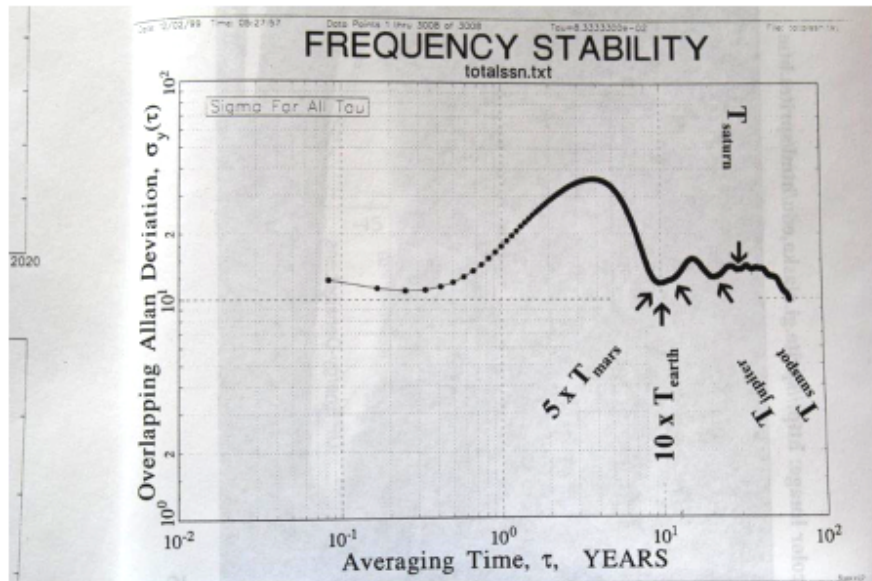


Figure 17. ADEV plot of 100 years of sun-spot data showing the periods of all the major planets except for Uranus, where our data length was too short to resolve its period.

Conclusions

It has been fifty years since I finished my master's thesis. With fifty years of experience in the time and frequency community, the use and improvements upon the Allan variance have matured significantly. I observe a similar maturing in its application in navigation scenarios and in other areas of metrology.

As I review the literature in this regard, there are three technical areas where I will make suggestions that I feel will be of most help in this maturing process.

First, for 16 years we lived with the ambiguity problem with the Allan variance when its square-root (ADEV) behaves as τ^{-1} – not being able to distinguish between white-noise phase modulation (PM) and flicker-noise PM. That ambiguity problem was resolved in 1981 with the development of the Modified Allan variance, which allowed us to modulate the bandwidth in the software. The quantization errors in integrated navigation systems have a white-noise spectrum; the use of MDEV would be very useful here. I have looked at several navigation papers by some of the best experts in the field using the Allan variance, and I have found very few using MDEV. In the case of quantization errors, MDEV allows to average the noise down as $\tau^{-3/2}$, which then allows the observation of other noise types and instability problems more quickly. MDEV is also the optimum averaging technique for such errors. In this same regard, if one desires to know the rate with white-noise residuals present, then a linear regression on the slope improves the knowledge of the slope as $N^{-3/2}$, where N is the number of data points in the regression analysis and is the optimum estimate of the slope for exactly the same reason that MDEV improves as $\tau^{-3/2}$. I am happy to see that it is beginning to be introduced by some navigation researchers.

Second, after the quantization errors are averaged down, ADEV works well and is an efficient metric for characterizing the intermediate and longer-term instabilities. But because the Allan variance is Chi-squared distributed, when the degrees of freedom get too small for the longest averaging times available from the data, then the ADEV values are often too small. This problem has in large measure been solved by David A. Howe

and his group at NIST, Boulder, Colorado, with “Total ADEV” and useful variations thereto (see the references). Their work, in a clever way, adds the needed degrees of freedom. Their work could be applied usefully to navigation error analysis as well. Long-term data are often very expensive to acquire, so Total ADEV and its cousins give a more efficient use of the data.

And Third, systematic errors are often hard to deal with. We have found it generally useful over the years to subtract the systematics from the data, as much as is reasonable, before analyzing the residuals for their noise characteristics. This practice is usually done after the fact, but can be done in real-time with proper filter functions and prediction algorithms that will estimate and remove the systematics. Since optimum estimation procedures depend upon the kind of noise, this problem can be solved recursively or from some prior knowledge of the noise characteristics of a given system. The principle of parsimony dictates that we use the simplest and most efficient metric in our noise analysis. ADEV satisfies that requirement in many areas of metrology, and I believe that is the main reason for its becoming as widely used as it is and ever growing in different areas of metrology. If the systematics are not subtracted from the data before the noise analysis, these systematics often adversely affect the long-term values in an ADEV plot. For this reason, the GPS program people went from Allan variance to the Hadamard variance, which is a third difference operator on the time residuals and is not sensitive to the systematic-frequency drift that plagues the performance of rubidium-atomic clocks used in the GPS satellites. The Hadamard variance is not parsimonious, and they would have better noise analysis confidence estimates by estimating and removing the frequency drift, and then use ADEV and Total ADEV (or similar) to analyze the noise characteristics of the residuals – from which they deduce their Kalman filter parameters for optimizing the GPS performance.

References

There are a very large number of publications about the three variances developed in this paper. I refer you to the NIST Time and Frequency Division publication web site for many of these. And I refer you to the 1988 IEEE Standard 1139-1988: *Standard Terminology for Fundamental Frequency and Time Metrology*, to the 1990 NIST Technical Note 1337, *Characterization of Clocks and Oscillators*, to the 1997 ITU HANDBOOK: “Selection and Use of Precise Frequency and Time Systems,” to the 1997 Hewlett Packard Application Note 1289, *The Science of Timekeeping*, to the 2000-2014 additional variance work at NIST giving additional degrees of freedom and providing efficiency & tighter confidences on the variance estimates – <http://tf.nist.gov/general/publications.htm>, to the “Handbook of Frequency Stability Analysis,” by W. J. Riley, NIST Special Publication, SP 1065 (2007), also available at www.wiley.com, and to Chapter 20 of my 2014 book www.ItsAboutTimeBook.com; Appendix J at this link is also the booklet *The Science of Timekeeping*. I also refer you to “publications” on my other web site: www.allanstime.com. The above publications by Bill Riley provide analysis software, which include the advantages of Total ADEV, etc. For this reason and others, his software is in common use in the time and frequency community.

As mentioned before, if you search using Google for “Allan variance,” there are about 50 thousand results. If you add navigation to that, there are about 3 thousand results. In reviewing some of the 3 thousand I found some very interesting papers. Though I have been around the navigation community and am a Fellow of the Institute of Navigation, I do not consider myself an expert in the literature of this community. I suggest here a few papers, which I found in my search, which I thought were outstanding: *Analysis and Modeling of Inertial Sensors Using Allan Variance* by El-Sheimy, N., Calgary University; Haiying Hou; Xiaoji Niu; *Allan Variance Analysis on Error Characters of MEMS Inertial Sensors for an FPGA-based GPS/INS System* by Xin Zhang, Yong Li, Peter Mumford, Chris Rizos; *School of Surveying and Spatial Information Systems University of New South Wales, Australia*; at the following link <http://www.vectornav.com/support/library/gyroscope> is a fascinating paper on using ADEV to measure gyroscope instabilities; *Allan Variance Analysis on Error Characters of Lowcost MEMS Accelerometer MMA8451Q* by Marin Marinov*, Zhivo Petrov* (*Aviation Faculty, NVU), V. Levski”, and Dolna Mitropolia, Bulgaria; *Modeling Inertial Sensors Errors Using Allan Variance*, http://www.ucalgary.ca/engo_webdocs/NES/04.20201.HaiyingHou.pdf (URL: <http://www.geomatics.ucalgary.ca/links/GradTheses.html>) by Haiying Hou September 2004; Department of Geomatics Engineering; *A Comparison between Different Error Modeling of MEMS Applied to GPS/INS Integrated Systems* by Alex G. Quinchia (Barcelona, Spain), Gianluca Falco (Torino, Italy), Emanuela Falletti (Torino, Italy), Fabio Dosis (Torino, Italy), and Carles Ferrer (Barcelona, Spain); *Notes on Stochastic Errors of Low Cost MEMS Inertial Units*, Yigiter Yuksel & Huseyin Burak Kaygisiz; *Two Methods for the Determination of Inertial Sensor Parameters*, Vladimir Vukmirica*, Ivana Trajkovski*, Nada Asanović*, *Military Technical Institute (VTI), Ratka Resanovića, Belgrade, Serbia; and *Modified Allan Variance Analysis on Random Errors of MINS* by Bin Fang and Xiaoqi Guo, TELKOMNIKA, Vol.11, No.3, March 2013, pp. 1227 ~ 1235 e-ISSN: 2087-278X. Even though these references are excellent resources in my opinion several of them suffer from the

ambiguity problem in ADEV when it behaves as τ^{-1} for the quantization noise problem. MDEV is a better metric in this case, as I have cited before.

Because $1/f$ noise and fractals are so ubiquitous in modeling nature, we expect non-stationary analysis techniques – like in the family of Allan variances – to be useful as efficient time-series analysis metrics. The usage seems to be growing, but there are many areas where these metrics seem to be unknown statistical tools. In my own research, I have shown these variances to be useful in analyzing the stability of gage blocks and volt standards. Richard F. Voss has demonstrated $1/f$ noise in a large variety of music. Musha and Higuchi have identified $1/f$ noise in traffic flow. The height of the River Nile at flood stage over the last some thousands of years for which there are data has a $1/f$ spectral density. Such noise is found in economics, psychology, and in neurons. Pink noise is another name for $1/f$ or flicker-noise. You will find a fascinating article in Wikipedia on “Pink Noise” – showing its ubiquitous nature – and a large number of references are given there.

As a fun health example, since neuron noise is $1/f$, if you were to stand on one foot and then map the motion of the top of your head, the time series would be a flicker-noise process. If now you get on a bicycle and ride it to follow a straight line, since you have to integrate when riding a bike to maintain balance, the front tire deviations from the straight line will be an f^3 spectral-density process. With a controlled set of parameters, this bicycle balancing activity could be used – using ADEV to analyze the deviations – in a very simple way to assess improvement or degradation in your balance. Since I am an avid mountain bike rider, I am observing this phenomenon a lot – especially on a narrow deer trail on a steep slope in the mountains near our home.

**ON THE TOPOLOGY OF THE ALLAN VARIANCE GRAPHS AND TYPICAL
MISCONCEPTIONS IN THE INTERPRETATIONS OF THE GYRO NOISE STRUCTURE
(BASED ON THE EXAMPLES FROM REPORTS AT THE ST. PETERSBURG INTERNATIONAL
CONFERENCE ON INTEGRATED NAVIGATION SYSTEMS)**

**PART I
ON THE DIFFERENCE OF LAWS OF GYRO NOISE ACCUMULATION
IN PLATFORM AND STRAPDOWN INERTIAL SYSTEMS**

**PART II
TECHNIQUE OF ALLAN $\sigma(\tau)$ – GRAPHS FOR IDENTIFICATION OF THE GYRO NOISE STRUCTURE**

N. I. Krobka¹

Federal State Unitary Enterprise “Center for ground-based space infrastructure operation”
(Branch “Research Institute of Applied Mechanics named after Academician V.I. Kuznetsov”),
Scientific and production company “Epsilon”, Ltd,
Moscow, Russia, e-mail: KrobkaNick@msn.com

*DEDICATED to the FATHERS of inertial navigation technology for rocket and space applications,
Charles Stark Draper and Victor Ivanovich Kuznetsov, and their development teams*

Abstract

Key words: gyro noise, noise structure, Allan variance, orientation, inertial navigation systems, accuracy

The report is dedicated to the methodological aspects of the interpretation of the Allan variance graphs and identification of the gyro noise structure. The main objectives of the work are the following: 1) methodological comment on common misconceptions and blunders in the interpretation of the Allan graphs concerning the identification of noise structure and estimation of noise parameters for different types of gyros, based on the examples from the papers published in the proceedings of the St. Petersburg International Conference on Integrated Navigation Systems of the previous years; 2) statement of the problem of extending the noise process basis and taking into account the gyro noise of different types unaccounted in the existing standards on gyros in order to correctly identify real gyro noise; 3) demonstration of types of noise (which has not been taken into account before) and partial contribution of this new noise into Allan deviation graphs. That was the main point of a short message proposed by the author a priori in his poster presentation.

Since the international program committee of the conference has made a decision to discuss this subject at the “round table”, allowing 5-fold time for this presentation, the author has complemented the report with one more section consisting of three parts: On the differences in orientation accuracy determined with SINS and platform INS with the same gyros, A new noncommutative kinematic effect, and What is “good” and what is “bad” in the part of noise in gyros for application in platform INS and SINS? They describe the difference between accurate kinematic error equations of platform INS and SINS; the necessity of the gyro noise structure identification; the form in which information on gyro noise should be represented; the difference in the required specification of the gyro noise structure for applications in platform INS and SINS; and the difference in noise identification problems in radio physics – in frequency standards (“time”) and in gyroscopy.

It is for the first time in the world that a new non-commutative kinematic effect is proposed: “The accuracy in determining orientation with platform INS and SINS, built on the same gyros, is different even (“even” is the keyword) when the errors and noise of these gyros are identically equal in platform INS and SINS”. One of the essential and most important manifestations of this effect is the following: “In zero frequency, gyro noise with zero power spectral density does not lead to significant increase in orientation error in time for platform INS (second-order “smallness” effect), but leads to rather significant increase in orientation error in time for SINS (first-order “smallness” effect)”. The difference in partial contribution of this noise to the accuracy of platform INS and SINS is some order of magnitude (10-, 100-, 1000-fold and more), depending on the specific gyro noise structure and form of the object rotation.

Three infinite (countable) set of new noises and the Allan variances corresponding to them are presented.

In order to better identify the gyro noise structure on the basis of the Allan variance method (and its generalizations), an Allan-Krobka functional–dispersion is proposed in addition to the Allan variance.

The real white noise level of Russian FOGs, less than $0.000001 \text{ deg}/(\text{hr})^{1/2}$ ($10^{-6} \text{ deg}/(\text{hr})^{1/2}$), is demonstrated by the example of an Optolink FOG.

¹ Cand. Sci. (Phys.-Math.), Corresponding Member, Academy of Engineering Sciences named after A.M. Prokhorov, Member, Academy of Navigation and Motion Control, Chief Scientist of Research Institute of Applied Mechanics named after Academician V.I. Kuznetsov; President, General Director, and Chief Designer of Scientific and Production Company “Epsilon”, Ltd.

Introduction

In the first part of the report for the first time the difference of errors accumulation in time for orientation determination (attitude position) of platform inertial navigation system (INS) and strapdown INS (SINS), based on the same gyros (on any physical principle) with arbitrary errors and noises is discussed in detail. There are two types of effects: first of them is wellknown, and the second is new and not a trivial. The first is that the orientation determination accuracy by platform INS (hereinafter, for brevity, sometimes – INS) and SINS, with the same gyros is different. This effect is obvious, because gyros on gyro-stabilized platform (GSP) “track” a narrower range of angular velocities, than gyros in SINS. Therefore, the components of gyro’s errors proportional to the angular velocity, caused by the errors in scale factor, (and nonlinear errors in the measured angular velocity for some types of non-linearity) for the same gyro in platform INS is less than in SINS. The second (more “subtle”), previously unpublished effect, is that the accuracy of platform INS and SINS, based on the same gyros, is different even (here “even” is the keyword) with identical gyros’ errors and noises in platform INS and SINS. For example, if gyros have only additive components (not depend on measured angular velocity) of errors (equals for platform INS and SINS), than the rate of orientation error accumulation for platform INS and SINS, i.e. accuracy, is different (except for some particular cases). The difference in orientation accuracy with platform INS and SINS may range in order of magnitude (in 10, 100, 1000 and in more time), depending on the noise structure and the type of object rotation. Moreover, platform INS or SINS may be more precise depending on the structure and the type of the object rotation. This effect explains the necessity of the correct identification of gyros noise structure. For gyroscopes for SINS accurate noise structure identification is more critical than for platform INS gyroscopes.

In the second part of the report on the example of reports at St. Petersburg International Conference on Integrated Navigation Systems in previous years, typical misconceptions of four different kinds in interpretation of gyro noise structure with Allan variance method are presented and commented:

- 1) Lack of understanding of Allan variance $\sigma(\tau)$ -graphs method’s “basis”. An example of incorrect white noise level estimation for micromechanical gyros (MMG) is shown (they incorrectly estimated on section of Allan variance graph with slope $\Delta = -1/2$). The error value is one-two orders of magnitude.
- 2) Misunderstanding of Allan deviation $\sigma(\tau)$ -graphs “summing” effect. Typical examples – determination of bias instability, using a tangent with slope $\Delta = 0$ in the minimum point of the $\sigma(\tau)$ -graph of Allan variance. So obtained upper bound differs from the actual value of bias instability in times.
- 3) Misunderstanding of “nuances” in Allan variance method. An example of incorrect white noise level estimation for fiber-optical gyros (FOG) is shown (due to effect of “screening” by Markov process with short correlation time. The error value is two-three orders of magnitude. It is shown that the level of Russian developed FOG’s white noises is less $0,000001 \text{ deg}/(\text{hr})^{1/2}$ ($10^{-6} \text{ deg}/(\text{hr})^{1/2}$).
- 4) Ignoring incompleteness of used “basis” of noises for gyros noise structure identification (in strict accordance with the algorithm of classic joke: “One should search lost thing under a lantern, because it is lighter under the lantern”) with Allan variance method.

The examples from practice, that are illustrating the presence of FOG noises, not recorded in the error model (standardized by IEEE Std 952-1997 and IEEE Std 952-1997 (R2008), are shown.

The problem of expansion of noise’ “basis” for correct noise structure identification is stated.

Three infinite (countable) set of new noises and the corresponding Allan variances are presented.

In order to better identify gyros noise structure on basis of Allan variance method (and its generalizations) the additional to Allan variance functional – Allan-Krobka dispersion is proposed.

The actual level of Russian design FOG’s white noise is demonstrated (on the example of RPC “Optolink” Ltd.) – less than $0,000001 \text{ deg}/(\text{hr})^{1/2}$ ($10^{-6} \text{ deg}/(\text{hr})^{1/2}$).

1. On the difference in accuracy of orientation determination by SINS and platform INS with the same gyros

In June 1960 on symposium “Frontiers of Science and Engineering Symposium” Dr. Charles Stark Draper – “father of inertial navigation”, also known as “father of inertial guidance”, as he is called in the USA [1-3], stated his personal forecast about the ways of INS development: “Author thinks, that high quality inertial systems based on fixing sensitive elements on object, are not among the perspective systems” [4].

Such opinion was based, obviously, on difference in principles of platform INS and SINS construction. Indeed: errors $\delta\omega(t)$ of any gyro contain components of three different type: additive $a(t)$ (independent of the measured angular velocity $\omega(t)$), linear $m(t)\omega(t)$ and nonlinear $n(t, \omega(t))$ in the measured angular velocity

$$\delta\omega(t) \equiv \delta\omega(\omega(t), t) = a(t) + m(t)\omega(t) + n(\omega(t), t). \quad (1.1)$$

Gyros in SINS are strictly attached to the object’s board and they “track” the whole range of object’s angular velocities $\omega(t) \in [-\Delta\omega\{\text{SINS}\}, +\Delta\omega\{\text{SINS}\}]$ (typical values $\Delta\omega\{\text{SINS}\} : 10 \text{ deg/s}, 100 \text{ deg/s}, 1000 \text{ deg/s}$ or more for

fast rotating object). The error in gyros has the form:

$$\delta\omega(t) \equiv \delta\omega(\omega(t), t) = a(t) + m(t)\omega(t) + n(\omega(t), t); \quad \omega(t) \in [-\Delta\omega\{\text{SINS}\}, +\Delta\omega\{\text{SINS}\}]. \quad (1.2)$$

In platform INS gyros, that are mounted on GSP, when the angular velocities of the object $\omega(t)$ is the same, “track” only narrow range of angular velocities $\omega'(t) \in [-\Delta\omega\{\text{GSP}\}, +\Delta\omega\{\text{GSP}\}]$, because GSP “works off” object rotation (for example, with the opposite sign: $-\omega(t)$ in the case of stabilized in inertial space GSP with the accuracy of gyros errors ($\delta\omega'(t)$) and imperfections of GSP subsystems $\delta\omega'(t)\{\text{GSP}\}$. Typical values $\Delta\omega\{\text{GSP}\}$: 0,1 deg/hr, 0,01 deg/hr, 0,001 deg/hr or less, depending on accuracy of gyros and implementation quality of GSP tracking systems.

Gyroscope error in GSP is following:

$$\delta\omega'(t) \equiv \delta\omega'(\omega'(t), t) = a(t) + m(t)\omega'(t) + n(\omega'(t), t); \quad \omega'(t) \in [-\Delta\omega\{\text{GSP}\}, +\Delta\omega\{\text{GSP}\}]. \quad (1.3)$$

The errors of the same gyros used in the platform INS (1.3) and in SINS (1.2) are different in strict accordance with (1.1) and with principles of platform INS and SINS construction. For example if GSP is stabilized in inertial space (this variant has been traditionally used in missile applications, for which Charles Draper with his team in USA and Viktor Ivanovich Kuznetsov with his team in USSR developed complex of command devices for control systems), then errors’ linear components $m(t)\omega(t)$ (due to inaccurate determination and noises of scale factor) of the same gyros, if used in platform INS and SINS, will differ by factor $\Delta\omega\{\text{GSP}\} / \Delta\omega\{\text{SINS}\}$. For example, when $\Delta\omega\{\text{SINS}\} \sim 10$ deg/s and $\Delta\omega\{\text{GSP}\} \sim 0,0001$ deg/hr ratio $\Delta\omega\{\text{GSP}\} / \Delta\omega\{\text{SINS}\}$ is $\sim 3 \cdot 10^{-9}$ – “as much as” – eight orders! Similarly (but with accuracy up to specific form of nonlinearity in function $n(\omega(t), t)$) and for nonlinear components of errors (1.1). In the extreme ideal case in platform INS

$$\Delta\omega\{\text{GSP}\} \rightarrow 0 \Rightarrow m(t)\omega'(t) \rightarrow 0, \quad (1.4)$$

but in reality one can reach values of linear and nonlinear gyro error components (1.3) in GSP much smaller, than the value of additive errors (1.3):

$$|m(t)\omega'(t)| \ll |a(t)|. \quad (1.5)$$

Charles Draper has no doubt that the platform INS has this advantage over SINS, and of course he was absolutely right. Any gyroscopes, mounted on GSP (which is stabilized in inertial space) are in more “comfort condition” because they don’t track the full range of objects’ angular velocities and “automatically” show the better accuracy performance in platform INS than in SINS. This is obvious. Charles Draper have fulfilled the technology of the platform INS to its perfection – the spherical floating platform – inertial measurement unit AIRS (Advanced Inertial Reference Sphere) [5, 6] was created. In AIRS a gimbal wasn’t used as it. It was gimbal free, but still platform INS.

And what would be in the case of gyros, which in the whole range of objects’ angular velocity *a priori* (“on table”, but not in GSP) have the following conditions

$$|m(t)\omega(t)| \ll |a(t)|; \quad \omega(t) \in [\omega_{\min}, \omega_{\max}] ? \quad (1.6)$$

There were no such gyroscopes in 1960. The problems had to be solved quickly, which was done. How? In the manner the problems are usually solved: “in three moves” [7]. The first move: the best at that time floating gyroscope was chosen by the criterion of a minimal drift – additive component $a(t)$. The second move: the error inherent in gimbal was eliminated (dialectically, it was no longer used: $\delta\omega'(t)\{\text{GSP}\} \rightarrow \min$). The third move: the goal was obtained owing to the workmen’s skillful hands:

$$\Delta\omega\{\text{GSP}\} \rightarrow \min \sim \max|a(t)|. \quad (1.7)$$

As a result, the accuracy of the angular orientation of inertial navigation units AIRS was $\sim 1 \cdot 10^{-5}$ deg/hr [5, 6], i.e. at the level of additive gyro drifts, as it should be.

And, forecast that the “high-quality” SINS “are not among the promising systems” was not proved. Why? Because gyroscopes satisfying (1.6) were soon developed. 6 months later, in December of the same 1960, neon-helium lasers were created [8], and 2 years later, laser gyro (LG) prototypes [9] were created, which became the basis for SINS development. SINS based on LG came to replace INS after 20 years of development since the early 1980s.

So. Here is the obvious known effect: «*The accuracy of orientation (attitude position) determined by SINS and platform INS built on the same gyros is different*».

But what happens in case of gyroscopes that satisfy *a priori* conditions (1.6) over the entire range of angular velocities? Simplify the task to the maximum. Let us consider a model gyro that has only additive error component (1.1): $\delta\omega(t) \equiv a(t)$. We shall use three gyros, which have only additive component of error: $\delta\omega_i(t) = a_i(t)$; $i = 1, 2, 3$. On the basis of these gyros, let us construct “ideal” INS and “ideal” SINS (by ideal we mean that these systems do not have any other sources of errors, except gyros additive noises and errors, which are the same for SINS and INS). Let us formulate the question as follows: “Will the accuracy of orientation determination (attitude position) of these two systems be the same or different?”

reproduce rotation of the object: $J(t) \equiv E(t)$. Transition $J \leftarrow E$ on diagram (2.4) describes GSP rotation relative to object's shell, which (while arbitrary object rotation $A(\bar{\omega}_E)$) provides the required rotation of GSP $A'(\bar{\omega}_J)$.

Next, let's look at the part of the diagram (2.4), which is interesting for discussing effect

$$\begin{array}{ccc} & A'(\bar{\omega}_J) & \\ & \rightarrow & \\ I & & J \end{array} \quad (2.5)$$

In the case of platform INS, the basis J physically "moves" relative to its program position, due to gyros errors and not ideal GSP (errors of GSP tracking system). Let's denote perturbed basis as J_* . The actual angular velocity of basis J_* in projections to its axes is denoted $\bar{\omega}_{J_*}$, and measured (by gyroscopes) angular velocity of its rotation (taking into account gyros errors) is denoted $\bar{\omega}_{*J_*}$. Gyroscope errors have the form: $\delta\bar{\omega}_{J_*} = \bar{\omega}_{*J_*} - \bar{\omega}_{J_*}$. Orientation of basis J_* relative to basis I is defined by matrix $A'_*(\bar{\omega}_{*J_*})$.

Kinematic diagram of perturbed GSP functioning has the form:

$$\begin{array}{ccc} & J & \\ & \nearrow & \\ & A'(\bar{\omega}_J) & \\ & \downarrow & \\ I & & \\ & \searrow & \\ & A'_*(\bar{\omega}_{*J_*}) & \\ & & J_* \end{array} \quad \begin{array}{l} \Delta A'(\Delta\bar{\omega}_{J_*}); \\ \Delta\bar{\omega}_{J_*} = \bar{\omega}_{*J_*} - \Delta A'(\Delta\bar{\omega}_{J_*})\bar{\omega}_J = \bar{\omega}_{*J_*} - \bar{\omega}_{J_*} = \bar{\omega}_{J_*} + \delta\bar{\omega}_{J_*} - \bar{\omega}_{J_*} = \delta\bar{\omega}_{J_*}; \\ \Delta\bar{\omega}_J = \Delta B'(\Delta\bar{\omega}_{J_*})\Delta\bar{\omega}_{J_*} = \Delta B'(\Delta\bar{\omega}_{J_*})\delta\bar{\omega}_{J_*}. \\ B'(\bar{\omega}_J) = A'(\bar{\omega}_J)^{-1}; \quad \Delta B'(\Delta\bar{\omega}_{J_*}) = \Delta A'(\Delta\bar{\omega}_{J_*})^{-1}. \end{array} \quad (2.6)$$

In case of SINS the orientation error is described by any of two equivalent diagrams, where angular velocity vector of basis I_* rotation relative to basis I is defined by components in basis I_* , or in basis I (2.3):

$$\begin{array}{ccc} \Delta A(\Delta\bar{\omega}_{I_*}) & & \Delta A(\Delta\bar{\omega}_I) \\ I & \rightarrow & I_* \quad \Leftrightarrow \quad I & \rightarrow & I_* \\ \Delta\bar{\omega}_{I_*} = -B_*(\bar{\omega}_{*E})\delta\bar{\omega}_E & & \Delta\bar{\omega}_I = -B(\bar{\omega}_E)\delta\bar{\omega}_E \end{array} \quad (2.7)$$

In case of INS the orientation error can be described by any of two equivalent diagrams, on which the angular velocity vector of basis J_* rotation relative to basis J is given by components either in basis J_* , or in basis J (2.6):

$$\begin{array}{ccc} \Delta A'(\Delta\bar{\omega}_{J_*}) & & \Delta A'(\Delta\bar{\omega}_J) \\ J & \rightarrow & J_* \quad \Leftrightarrow \quad J & \rightarrow & J_* \\ \Delta\bar{\omega}_{J_*} = \delta\bar{\omega}_{J_*} & & \Delta\bar{\omega}_J = \Delta B'(\Delta\bar{\omega}_{J_*})\delta\bar{\omega}_{J_*} \end{array} \quad (2.8)$$

In case of GSP stabilization for platform INS in inertial space ($J \equiv I$):

$$\begin{array}{ccc} \Delta A'(\Delta\bar{\omega}_{J_*}) & & \Delta A'(\Delta\bar{\omega}'_I) \\ I & \rightarrow & J_* \quad \Leftrightarrow \quad I & \rightarrow & J_* \\ \Delta\bar{\omega}_{J_*} = \delta\bar{\omega}_{J_*} & & \Delta\bar{\omega}'_I = \Delta B'(\Delta\bar{\omega}_{J_*})\delta\bar{\omega}_{J_*} \end{array} \quad (2.9).$$

Another notation is used after replacement $J \rightarrow I$ in (2.9):

$$\Delta\bar{\omega}_I = \Delta B'(\Delta\bar{\omega}_{J_*})\delta\bar{\omega}_{J_*} \rightarrow \Delta\bar{\omega}'_I = \Delta B'(\Delta\bar{\omega}_{J_*})\delta\bar{\omega}_{J_*}.$$

Let's limit ourselves by commenting diagrams (2.7) and (2.9), i.e. SINS and INS, which has stabilized in inertial space GSP. In case of INS "physical" basis J_* (fixed to GSP) rotates ("moves") relative to inertial basis I with angular velocity vector $\Delta\bar{\omega}'(t)\{\text{GSP}\}$. In case of SINS "mathematical" basis I_* ("physical" GSP basis analog) rotates ("moves") relative inertial basis I with absolute angular velocity vector $\Delta\bar{\omega}(t)\{\text{SINS}\}$.

$$\Delta\bar{\omega}(t)\{\text{SINS}\} \equiv \Delta\bar{\omega}(t) \Leftrightarrow \begin{cases} \Delta\bar{\omega}_{I_*} = -B_*(\bar{\omega}_{*E})\delta\bar{\omega}_E \\ \Delta\bar{\omega}_I = -B(\bar{\omega}_E)\delta\bar{\omega}_E \end{cases}; \quad \Delta\bar{\omega}(t)\{\text{GSP}\} \equiv \Delta\bar{\omega}'(t) \Leftrightarrow \begin{cases} \Delta\bar{\omega}_{J_*} = \delta\bar{\omega}_{J_*} \\ \Delta\bar{\omega}'_I = \Delta B'(\Delta\bar{\omega}_{J_*})\delta\bar{\omega}_{J_*} \end{cases}. \quad (2.10)$$

Let gyros errors in cases of SINS and INS (in bases, in which the absolute angular velocity is measured, i.e. in basis E in case of SINS and in basis J_* in case of INS) be identical:

$$\delta\bar{\omega}_{J_*}(t) \equiv \delta\bar{\omega}(t) \equiv \delta\bar{\omega}_E(t); \quad \delta\bar{\omega}(t) = (\delta\omega_1(t), \delta\omega_2(t), \delta\omega_3(t))^T. \quad (2.11)$$

Rotation of basis I_* (SINS) and rotation of basis J_* (INS) have different angular velocity

$$\Delta\bar{\omega}(t)\{\text{SINS}\} \neq \Delta\bar{\omega}'(t)\{\text{GSP}\}, \quad (2.12)$$

what is obvious from (2.10), comparing $\Delta\bar{\omega}(t)\{\text{SINS}\}$ and $\Delta\bar{\omega}'(t)\{\text{GSP}\}$ and taking into account (2.11) in the same

basis I :

$$\Delta\bar{\omega}_I = -B(\bar{\omega}_E)\delta\bar{\omega}; \Delta\bar{\omega}'_I = \Delta B'(\Delta\bar{\omega}_{J_*})\delta\bar{\omega}. \quad (2.13)$$

The gyroscopes errors and noises vector $\delta\bar{\omega}$ (mathematical vector – column matrix) in case of SINS is modulated by object rotation: $\Delta\bar{\omega}_I = -B(\bar{\omega}_E)\delta\bar{\omega}$, and in case of INS by rotation (“move”) of GSP: $\Delta\bar{\omega}'_I = \Delta B'(\Delta\bar{\omega}_{J_*})\delta\bar{\omega}$ (2.13). Therefore, rotating with different angular velocity vectors (despite the fact, that vectors modules are identical),

$$|\Delta\bar{\omega}(t)\{\text{SINS}\}| = |\Delta\bar{\omega}'(t)\{\text{GSP}\}| = (\delta\bar{\omega}^T(t)\delta\bar{\omega}(t))^{1/2}, \quad (2.14)$$

basis $J_*(t)$ relative to basis I (INS) and basis $I_*(t)$ relative to basis I (SINS) are turned (for the same time) on different angles of resulting Euler rotation – on angle $\Delta s(t)$ (in case of SINS) and on angle $\Delta s'(t)$ (in case of INS), i.e. SINS and INS accuracies in general case (with rare exceptions) of arbitrary object rotation and arbitrary gyroscopes errors $\delta\bar{\omega}$ are different:

$$\Delta s(t)\{\text{SINS}\} \equiv \Delta s(t) \neq \Delta s'(t) \equiv \Delta s'(t)\{\text{GSP}\}. \quad (2.15)$$

The Euler turn angle $\Delta s(t)$ and Euler turn angle $\Delta s'(t)$ are the natural criteria of orientation accuracy by SINS and INS. Let's comment effect (2.15) and some of its manifestations.

Let's parameterize matrices ΔA and $\Delta B = \Delta A^{-1} = \Delta A^T$ of SINS orientation errors and matrices $\Delta A'$ and $\Delta B' = \Delta A'^{-1} = \Delta A'^T$ of INS orientation errors by Euler turn vectors $\Delta\bar{S}$ and $\Delta\bar{S}'$

$$\begin{aligned} \Delta A^{\pm 1} = \Delta B^{\mp 1} &= I_0 \mp (\sin \Delta s / \Delta s) \Omega(\Delta\bar{S}) + [(1 - \cos \Delta s) / \Delta s^2] \Omega^2(\Delta\bar{S}); \quad \Delta s = +(\Delta\bar{S}^T \Delta\bar{S})^{1/2}; \quad \Delta\bar{S} \equiv \Delta\bar{S}(t); \\ \Delta A'^{\pm 1} = \Delta B'^{\mp 1} &= I_0 \mp (\sin \Delta s' / \Delta s') \Omega(\Delta\bar{S}') + [(1 - \cos \Delta s') / \Delta s'^2] \Omega^2(\Delta\bar{S}'); \quad \Delta s' = +(\Delta\bar{S}'^T \Delta\bar{S}')^{1/2}; \quad \Delta\bar{S}' \equiv \Delta\bar{S}'(t). \end{aligned} \quad (2.16)$$

Vectors $\Delta\bar{S}$ and $\Delta\bar{S}'$ and angles Δs and $\Delta s'(t)$ can be expressed by matrices ΔA and $\Delta A'$:

$$\begin{aligned} -(\sin \Delta s / \Delta s) \Omega(\Delta\bar{S}) &= (\Delta A - \Delta A^T) / 2; \quad \cos \Delta s = (\text{Sp} \Delta A - 1) / 2 = (\text{Sp} \Delta A^T - 1) / 2; \\ -(\sin \Delta s' / \Delta s') \Omega(\Delta\bar{S}') &= (\Delta A' - \Delta A'^T) / 2; \quad \cos \Delta s' = (\text{Sp} \Delta A' - 1) / 2 = (\text{Sp} \Delta A'^T - 1) / 2. \end{aligned} \quad (2.17)$$

The two forms of KE for the four matrices (2.16) can be obtained on the basis of general form KE (2.2), which are corresponding to rotation of some basis relative to stable basis, taking into account the two forms of angular velocity representation (2.10) for these rotations. Of the eight KE the next pairs are the most convenient

$$\Delta \dot{A}' = -\Omega(\delta\bar{\omega})\Delta A' \Leftrightarrow \Delta \dot{B}' = \Delta B'\Omega(\delta\bar{\omega}); \quad \Delta A'|_{t=0} = \Delta B'|_{t=0} = I_0; \quad (2.18)$$

$$\Delta \dot{A} = \Delta A\Omega(B\delta\bar{\omega}) \Leftrightarrow \Delta \dot{B} = -\Omega(B\delta\bar{\omega})\Delta B; \quad \Delta A|_{t=0} = \Delta B|_{t=0} = I_0. \quad (2.19)$$

The equations (2.18) and (2.19) are the accurate errors KE (without any assumption of “smallness” of perturbation) respectively for INS and SINS, in general case of arbitrary gyroscopes errors and noises $\delta\bar{\omega} = \delta\bar{\omega}(t) = \delta\bar{\omega}(\bar{\omega}_E(t), t)$ and arbitrary object's rotation $B = B(t) = B(\bar{\omega}_E(t))$.

The errors KE for INS (2.18) and SINS (2.19) are different. The KE solutions (2.18) depends only from gyroscopes errors, and KE solutions (2.19) depends both from gyroscopes errors and the form of rotation. The INS accuracy on GSP is a functional of one parameter, and SINS accuracy is a functional of two parameters:

$$\Delta s'(t) = \Delta s'(\delta\bar{\omega}(t)); \quad \Delta s(t) = \Delta s(\delta\bar{\omega}(t), B(t)). \quad (2.20)$$

To compare KE solutions (2.18) and (2.19) it's convenient to consider the KE pairs, for which KE either “right” or “left” (i.e. in KE coefficients matrix is located either from the right or from the left of required matrix). Let's choose pair of “left” KE forms from (2.18) and (2.19):

$$\Delta \dot{A}' = -\Omega(\delta\bar{\omega})\Delta A'; \quad \Delta A'|_{t=0} = I_0; \quad \Delta \dot{B} = -\Omega(B\delta\bar{\omega})\Delta B; \quad \Delta B|_{t=0} = I_0 \quad (2.21)$$

and represent their solutions by absolute and uniformly convergent series of successive approximation:

$$\Delta A' = \sum_{n=0}^{\infty} \Delta A'_n; \quad \Delta A'_0 = I_0; \quad \Delta A'_{n+1} = -\int_0^t \Omega(\delta\bar{\omega}(\tau))\Delta A'_n(\tau)d\tau; \quad \Delta B = \sum_{n=0}^{\infty} \Delta B_n; \quad \Delta B_0 = I_0; \quad \Delta B_{n+1} = -\int_0^t \Omega(B(\tau)\delta\bar{\omega}(\tau))\Delta B_n(\tau)d\tau. \quad (2.22)$$

Similarly for vectors and angles of Euler turn, taking into account (2.22) and (2.17)

$$\begin{aligned} -\frac{\sin \Delta s}{\Delta s} \Omega(\Delta\bar{S}) &= \frac{1}{2} \sum_{n=0}^{\infty} (\Delta A_n - \Delta A_n^T); \quad \cos \Delta s = 1 + \frac{1}{2} \sum_{n=2}^{\infty} \text{Sp} \Delta A_n = 1 + \frac{1}{2} \sum_{n=2}^{\infty} \text{Sp} \Delta A_n^T; \\ -\frac{\sin \Delta s'}{\Delta s'} \Omega(\Delta\bar{S}') &= \frac{1}{2} \sum_{n=0}^{\infty} (\Delta A'_n - \Delta A_n'^T); \quad \cos \Delta s' = 1 + \frac{1}{2} \sum_{n=2}^{\infty} \text{Sp} \Delta A'_n = 1 + \frac{1}{2} \sum_{n=2}^{\infty} \text{Sp} \Delta A_n'^T. \end{aligned} \quad (2.23)$$

Taking into account (2.21)-(2.23), it's easy to understand and prove the result (2.15). Indeed, despite the fact, that the modules of angular velocities are equal (2.14) or in equivalent form

$$+\{[\delta\bar{\omega}(t)]^T [\delta\bar{\omega}(t)]\}^{1/2} \equiv +\{[B(t)\delta\bar{\omega}(t)]^T [B(t)\delta\bar{\omega}(t)]\}^{1/2}, \quad (2.24)$$

the modules of vectors' $\delta\bar{\omega}(\tau)$ and $B(\tau)\delta\bar{\omega}(\tau)$ integral in general case (if $B(\tau) \neq I_0$) aren't the same

$$+\left\{\int_0^t \delta\bar{\omega}(\tau)d\tau\right\}^T \left\{\int_0^t \delta\bar{\omega}(\tau)d\tau\right\}^{1/2} \neq +\left\{\int_0^t B(\tau)\delta\bar{\omega}(\tau)d\tau\right\}^T \left\{\int_0^t B(\tau)\delta\bar{\omega}(\tau)d\tau\right\}^{1/2}. \quad (2.25)$$

The effect (2.15) appears in any N -th ($N \geq 1$) order of successive approximation method

$$\begin{aligned} \Delta A' &\approx \Delta A'^{\{N\}} = \sum_{n=0}^N \Delta A'_n; \quad \Delta B \approx \Delta B^{\{N\}} = \sum_{n=0}^N \Delta B_n \Rightarrow \\ -\frac{\sin \Delta s^{\{N\}}}{\Delta s^{\{N\}}} \Omega(\Delta \bar{S}^{\{N\}}) &= \frac{1}{2} \sum_{n=0}^N (\Delta A_n - \Delta A_n^T); \quad \cos \Delta s^{\{N\}} = 1 + \frac{1}{2} \sum_{n=2}^N \text{Sp} \Delta A_n = 1 + \frac{1}{2} \sum_{n=2}^N \text{Sp} \Delta A_n^T; \\ -\frac{\sin \Delta s'^{\{N\}}}{\Delta s'^{\{N\}}} \Omega(\Delta \bar{S}'^{\{N\}}) &= \frac{1}{2} \sum_{n=0}^N (\Delta A'_n - \Delta A_n'^T); \quad \cos \Delta s'^{\{N\}} = 1 + \frac{1}{2} \sum_{n=2}^N \text{Sp} \Delta A'_n = 1 + \frac{1}{2} \sum_{n=2}^N \text{Sp} \Delta A_n'^T \Rightarrow \end{aligned} \quad (2.26)$$

$$\Delta \bar{S}^{\{N\}} = \sum_{n=1}^N \varepsilon^n \Delta \bar{S}_n; \quad \Delta \bar{S}'^{\{N\}} = \sum_{n=1}^N \varepsilon^n \Delta \bar{S}'_n; \quad \Delta s^{\{N\}} = (\Delta \bar{S}^{\{N\}T} \Delta \bar{S}^{\{N\}})^{1/2}; \quad \Delta s'^{\{N\}} = (\Delta \bar{S}'^{\{N\}T} \Delta \bar{S}'^{\{N\}})^{1/2} \quad (2.27)$$

and can be confirmed by this method with any precision. Parameter $\varepsilon = 1$ added to (2.27) for the convenience of series $\Delta \bar{S}^{\{N\}}$ and $\Delta \bar{S}'^{\{N\}}$ construction by method of successive approximation on the basis (2.26).

The author knows only three strict exceptions in general rule (2.15): 1) In the rare (but possible) for gyroscopes applications case of complete lack of object rotation $B(t) \equiv I_0$ for arbitrary gyroscopes errors and noises $\delta\bar{\omega}$. This is obvious, since KE of errors for SINS and INS (2.21) are equal in the absence of object rotation. 2) In the rare (but possible) case, when the vector of gyroscopes errors is an eigenvector, which is corresponding to eigenvalue +1 of object rotation matrix: $\delta\bar{\omega}(t) = B(t)\delta\bar{\omega}(t)$. 3) In the unreach by now case of presence of only white Gaussian noises (while arbitrary object rotation) in gyroscopes error $\delta\bar{\omega}$.

In order to estimate the effect (2.15) size when performed in practice conditions of "small" gyroscopes errors and orientation errors (it is independent conditions) of INS and SINS

$$\left\{\int_0^t \delta\bar{\omega}(\tau)d\tau\right\}^T \left\{\int_0^t \delta\bar{\omega}(\tau)d\tau\right\}^{1/2} \ll 1; \quad \Delta s'(t) \ll 1; \quad \left\{\int_0^t B(\tau)\delta\bar{\omega}(\tau)d\tau\right\}^T \left\{\int_0^t B(\tau)\delta\bar{\omega}(\tau)d\tau\right\}^{1/2} \ll 1; \quad \Delta s(t) \ll 1 \quad (2.28)$$

it is possible (except in the case of non-commutative kinematic effects (NKE) of N -th order, $N > 2$ [11-13]) to limit ourselves by second order of successive approximation method (2.29) [14-22]

$$\Delta \bar{S}(t) \equiv \varepsilon \int_0^t \Delta \bar{\omega}(t_1) dt_1 + \frac{1}{2} \varepsilon^2 \int_0^t dt_2 \int_0^{t_2} [\Delta \bar{\omega}(t_2) \times \Delta \bar{\omega}(t_1)] dt_1; \quad \Delta \bar{\omega}(t) = -B(t)\delta\bar{\omega}(t); \quad (2.29)$$

$$\Delta \bar{S}'(t) \equiv \varepsilon \int_0^t \delta\bar{\omega}(t_1) dt_1 + \frac{1}{2} \varepsilon^2 \int_0^t dt_2 \int_0^{t_2} [\delta\bar{\omega}(t_2) \times \delta\bar{\omega}(t_1)] dt_1. \quad (2.30)$$

In a first approximation the KE of errors solutions (this approximation coincides with the accurate solution of widely used KE of errors "in variations") have the form

$$\Delta \bar{S}(t) \equiv \varepsilon \int_0^t \delta\bar{\theta}(t) dt \equiv -\varepsilon \int_0^t B(t_1)\delta\bar{\omega}(t_1) dt_1; \quad \Delta \bar{S}'(t) \equiv \varepsilon \int_0^t \delta\bar{\theta}'(t) dt \equiv \varepsilon \int_0^t \delta\bar{\omega}(t_1) dt_1. \quad (2.31)$$

To calculate the variance of the SINS and INS orientation angle error (considering noises in $\delta\bar{\omega}(t)$)

$$\sigma_{\Delta s}^2(t) = \langle \Delta s^2(t) \rangle - \langle \Delta s(t) \rangle^2; \quad \Delta s(t) = +[\Delta \bar{S}^T(t) \Delta \bar{S}(t)]^{1/2}; \quad \sigma_{\Delta s'}^2(t) = \langle \Delta s'^2(t) \rangle - \langle \Delta s'(t) \rangle^2; \quad \Delta s'(t) = +[\Delta \bar{S}'^T(t) \Delta \bar{S}'(t)]^{1/2} \quad (2.32)$$

when using N -th approximations (2.27), including first approximation (2.31), it is necessary to know the distribution function of the random vector process $\delta\bar{\omega}(t)$. To calculate the mean square angles (2.31) it's sufficient to use only statistical moments of $2N$ order, but to calculate the average angles (including a non-linear operation – square root extraction) it's not enough to have only moments, one needs a distribution function, which isn't easy to determine experimentally. There are components with different statistics in the mixture of noises. For example, photo-counts statistics is Poisson [23] and it would be a mixture of Poisson and Gaussian noises in FOG. But LG doesn't have such problem, due to the different type of information output: photocurrent is measured in FOG, and the number of interference fringes, which are "running through" two areas of the photodetector is counted in LG.

But it's possible to overcome this difficulty by using (instead of the dispersion) another similar in meaning functional [11], (called by colleagues in the Scientific and Research Institute of Applied Physics in the early 1980s: "the Krobka dispersion"), which is traditionally called by author "SINS orientation error dispersion" (or INS orientation error dispersion)

$$\sigma_{\Delta s+}^2(t) \equiv \langle \Delta \bar{S}^T(t) \Delta \bar{S}(t) \rangle - \langle \Delta \bar{S}^T(t) \rangle \langle \Delta \bar{S}(t) \rangle; \quad \sigma_{\Delta s'+}^2(t) \equiv \langle \Delta \bar{S}'^T(t) \Delta \bar{S}'(t) \rangle - \langle \Delta \bar{S}'^T(t) \rangle \langle \Delta \bar{S}'(t) \rangle. \quad (2.33)$$

To calculate the “dispersion” (2.33) noise distribution function $\delta\bar{\omega}(t)$, obviously, isn’t required.

The orientation “error dispersions” of SINS and INS (2.33) are exceed the dispersions of angles $\Delta s(t)$ or $\Delta s'(t)$ by value, but don’t exceed value of second moments (a margin of precision does not hinder anybody)

$$\langle \Delta s^2(t) \rangle \geq \sigma_{\Delta s+}^2(t) \geq \sigma_{\Delta s}^2(t); \quad \langle \Delta s'^2(t) \rangle \geq \sigma_{\Delta s'+}^2(t) \geq \sigma_{\Delta s'}^2(t), \quad (2.34)$$

what is obvious, because it doesn’t follow, that mean values of Euler rotation vectors are equal to zero from equality to zero of gyroscopes errors vector mean value:

$$\langle \delta\bar{\omega}(t) \rangle = \bar{0} \leftrightarrow \langle \Delta \bar{S}(t) \rangle \neq \bar{0}; \quad \langle \Delta \bar{S}'(t) \rangle \neq \bar{0}. \quad (2.35)$$

In the case of Gaussian noise statistics (taking into account known effect “correlation decay” of any even order moments on product of second order moments) to estimate the accuracy of SINS and INS orientation in any order of successive approximation method it’s sufficient to know only noises correlation matrix (nonstationary in general case)

$$K(t_1, t_2) = \langle \delta\bar{\omega}(t_1) \delta\bar{\omega}^T(t_2) \rangle - \langle \delta\bar{\omega}(t_1) \rangle \langle \delta\bar{\omega}^T(t_2) \rangle = \|k_{ij}(t_1, t_2)\|; \quad i, j = 1, 2, 3. \quad (2.36)$$

For example, for quantum noises of gyroscopes, modeled by stationary Gaussian white noise ($\delta(t_1 - t_2)$ – is Dirac delta function, δ_{ij} – is Kronecker symbol, $[D_i^{1/2}] = \text{deg}/(\text{hr})^{1/2}$):

$$\delta\bar{\omega}(t) = \bar{\xi}(t); \quad \langle \bar{\xi}(t) \rangle = \bar{0}; \quad \langle \xi_i(t_1) \xi_j(t_2) \rangle = D_i \delta_{ij} \delta(t_1 - t_2); \quad i, j = 1, 2, 3, \quad (2.37)$$

by averaging and summing series (2.22), we obtain accurate average value of SINS error KE solution (for compactness of result representation let’s take $D_1 = D_2 = D_3 \equiv D$) [11, 22]

$$\langle \Delta A(t) \rangle = \langle \Delta B(t) \rangle = \langle \Delta A'(t) \rangle = \langle \Delta B'(t) \rangle = e^{-Dt} \mathbf{I}_0. \quad (2.38)$$

The dispersions of SINS and INS orientation errors (2.33) for arbitrary object rotation don’t depend on the specific type of rotation $B(t)$ and coincide in magnitude, and in case $Dt \ll 1$ have the form

$$\sigma_{\Delta s+}^2(t) = \sigma_{\Delta s'+}^2(t) = 3Dt + O((3Dt)^2). \quad (2.39)$$

SINS or INS may be more accurate depending on the structure of gyroscopes errors and noises (let’s limit ourselves by additive components (1.1): “slowly” time-varying zero drifts of gyroscopes $\delta\bar{\omega}_m(t)$ and “quickly” time-varying noises $\bar{\zeta}_n(t)$)

$$\delta\bar{\omega}(t) = \sum_m \delta\bar{\omega}_m(t) + \sum_n \bar{\zeta}_n(t) \quad (2.40)$$

and on the form of object rotation ($\bar{S} = \bar{S}(t)$ – object’s Euler turn vector in inertial space)

$$B(\bar{S}) = \mathbf{I}_0 + (\sin s/s)\Omega(\bar{S}) + [(1 - \cos s)/s^2]\Omega^2(\bar{S}); \quad s = +(\bar{S}^T \bar{S})^{1/2}; \quad \bar{S} = \bar{S}(t). \quad (2.41)$$

The partial contributions of different gyroscopes errors and noises (2.40) to resulting SINS and INS orientation error may vary not only in times, but in orders.

First example. Because gyroscopes errors in case of SINS are modulated by object rotation, then “carousel” mode is automatically realized in SINS. To illustrate, let’s consider the simple case of constant gyroscopes biases and object rotation with constant angular velocity

$$\delta\bar{\omega}_m(t) \rightarrow \delta\bar{\omega}_0; \quad \delta\dot{\bar{\omega}}_0 = \bar{0}; \quad \bar{\omega}_E(t) = \bar{\omega}_I(t) = \bar{\omega}; \quad \dot{\bar{\omega}} = \bar{0}; \quad (\delta\bar{\omega}_0^T \delta\bar{\omega}_0)^{1/2} = \delta\omega_0; \quad (\bar{\omega}^T \bar{\omega})^{1/2} = \omega. \quad (2.42)$$

The accurate expressions are obvious in the case of INS: $\Delta \bar{S}'(t) = \delta\bar{\omega}_0 t \Rightarrow \Delta s'(t) = (\delta\bar{\omega}_0^T \delta\bar{\omega}_0)^{1/2} t$. In the case of SINS in a first approximation one obtains: $\Delta \bar{S}(t) = [\bar{\omega}(\bar{\omega}^T \delta\bar{\omega}_0)/\omega^2] t$ (only accumulated in time contribution is withheld). Assuming equal directional probabilities of angular velocity vector, the ratio of SINS error and INS error is following: $|\Delta s(t)|/|\Delta s'(t)| = 2/\pi$. Constant biases and “slowly” time-varying gyros drifts $\delta\bar{\omega}_m(t)$ (2.40) in the presence of the object rotation ($B(t) \neq \mathbf{I}_0$) make a smaller contribution to the orientation error in case of SINS $\Delta s(t)$ than in case of platform INS $\Delta s'(t)$.

Second example. For “quickly” time-varying gyros noises $\bar{\zeta}_n(t)$ (2.40) the situation is opposite. There is a wide class of stationary noises with zero power spectral density in angular velocity $S_\omega(v)$ at zero frequency

$$S_\omega(0) \equiv S_\omega(v=0) \equiv S_\omega(v)|_{v=0} = 0, \quad (2.43)$$

which are in the first approximation ($\sim \varepsilon$) don’t lead to INS orientation error growth in time. This is obvious, because the dispersion of the random process integral, which has a noise power spectral density of the form (2.43), doesn’t grow in time, when the times exceed correlation time of such process. However, such noises in the same first approximation ($\sim \varepsilon$) lead to growth in time of SINS orientation error when object rotates arbitrary ($B(t) \neq \mathbf{I}_0$)

$$S_{\omega}(0) \equiv S_{\omega}(v=0) \equiv S_{\omega}(v)|_{v=0} = 0 \Rightarrow \begin{cases} \sigma_{\Delta s'+}^2(t) \leq \text{const}; \\ \sigma_{\Delta s'+}^2(t) \sim t. \end{cases} \quad (2.44)$$

Derivatives of n-th order of white noise $\xi(t)$ are the convenient model for estimation of stationary noises of the form (2.43) impact to platform INS and SINS orientation error

$$\xi^{(n)}(t) \equiv \frac{d^n}{dt^n} \xi(t) \Rightarrow k^{[n]}(\tau) \equiv \langle \xi^{(n)}(t) \xi^{(n)}(t+\tau) \rangle = (-1)^n \frac{d^{2n}}{d\tau^{2n}} D\delta(\tau); \quad S_{\omega}^{[n]}(v) = v^{2n} \cdot \text{const}. \quad (2.45)$$

Autocorrelation functions $k^{[n]}(\tau)$ and noise power spectral densities $S_{\omega}^{[n]}(v)$ of n-th order derivatives $\zeta^{(n)}(t)$ (if they exist) for stationary process $\zeta(t)$ with autocorrelation function $k(\tau) = \langle \zeta(t) \zeta(t+\tau) \rangle$ and noise power spectral density $S_{\omega}(v)$ are connected with functions $k(\tau)$ and $S_{\omega}(v)$ by relations [25]

$$\zeta^{(n)}(t) \equiv \frac{d^n}{dt^n} \zeta(t) \Rightarrow k^{[n]}(\tau) \equiv \langle \zeta^{(n)}(t) \zeta^{(n)}(t+\tau) \rangle = (-1)^n \frac{d^{2n}}{d\tau^{2n}} k(\tau); \quad S_{\omega}^{[n]}(v) = v^{2n} S_{\omega}(v); \quad (2.46)$$

$$k(\tau) = \int_{-\infty}^{\infty} S_{\omega}(v) e^{iv\tau} dv \Leftrightarrow S_{\omega}(v) = \frac{1}{2\pi} \int_{-\infty}^{\infty} k(\tau) e^{-iv\tau} d\tau; \quad k^{[n]}(\tau) = \int_{-\infty}^{\infty} S_{\omega}^{[n]}(v) e^{iv\tau} dv \Leftrightarrow S_{\omega}^{[n]}(v) = \frac{1}{2\pi} \int_{-\infty}^{\infty} k^{[n]}(\tau) e^{-iv\tau} d\tau.$$

Here $\langle \dots \rangle$ – is ensemble averaging, $\langle \zeta(t) \rangle = 0 \Rightarrow \langle \zeta^{(n)}(t) \rangle = 0$.

In the absence of rotation the gyroscopes noises of the type (2.45) and (2.46) lead to growth in time of INS and SINS orientation errors, which are equal. Depending on the steepness of spectra (2.45), (2.46) near the zero frequency $\sim v^{2N}$, orientation errors, which grow in time, are counted starting only with (N+1)-th approximation ($\sim \varepsilon^{N+1}$) of error KE solutions. This is obvious, because non-stationary random process can be obtained from n times differentiated stationary random process, only after integrating it (N+1) times. When N grows the N-th effect decreasing in magnitude $\sim \mu^N$, where $\mu \ll 1$.

In the presence of rotation, the noises (2.45), (2.46) lead to SINS orientation errors growth in first approximation ($\sim \varepsilon$) of error KE solutions [11, 17].

In the general case of arbitrary stationary gyroscopes noises, but in particular case of object rotation with constant angular velocity, the partial contribution of such noises to SINS orientation error growths in time as diffusion. The diffusion coefficient depends on module of object angular velocity ω in accordance with the dependence of noise power spectral density versus frequency (when uncorrelated noises in three channels of a three-axis gyroscope with equal intensity) [26]:

$$\sigma_{\Delta s'+}^2(t) \equiv D(\omega)t; \quad D(\omega) = [S_{\omega}(0) + 2S_{\omega}(\omega)]; \quad S_{\omega}(0) \equiv S_{\omega}(v)|_{v=0}; \quad S_{\omega}(\omega) \equiv S_{\omega}(v)|_{v=\omega}. \quad (2.47)$$

The SINS orientation error dispersion depends only on the magnitude of angular velocity vector, in the general case of the arbitrary object rotation, but in particular case of noises in the form of first order derivative of the white noise [11, 15]

$$\langle \delta\bar{\omega}_E(t_1) \delta\bar{\omega}_E^T(t_2) \rangle = Q\tau_0^2 \frac{d^2}{dt_1 dt_2} \delta(t_1 - t_2) I_0 \Rightarrow \sigma_{\Delta s'}^2(t) \equiv 2Q\tau_0^2 \int_0^t |\bar{\omega}(\tau)|^2 d\tau. \quad (2.48)$$

The sources for noises of type (2.43) in the various gyroscopes are different. In the LG it's uncompensated components of “frequency biasing” of the types (2.45), (2.46) [11, 27].

3. What is “good” and what is “bad” in the terms of gyroscopes noises, designed for applications in platform INS and SINS

This section is written for young developers, who were involved in SINS gyroscopes development with no experience in development of platform INS and gyroscopes for such systems.

Let's comment manifestation (2.44) of NKE (2.15), which turned out to be surprisingly actual on transition phase – from platform INS to SINS.

The NKE (2.15), which was seen from the first steps of accurate SINS on LG theory construction [11] (on the phase of derivation of accurate SINS errors equations at the turn of 1979-1980 [28]), was only a “by-product” for author and have never been published “for unnecessary”.

Since the beginning of 1950s, for INS errors analysis [29], and later for SINS, by everyone and everywhere

(in the USA, and in the USSR) approximate errors equations (equations in variations [30, 31]) were used, including errors KE [32-34], independent of used formalisms. This trend continues to date in the USA [35], and in Russia [36]. Therefore, the author's primary concern was to "restore order" within the established SINS theory, – LG were developing for SINS.

The situation was a paradoxical: in mechanical gyroscopy "nonholonomic error" have long been known (A. Yu. Ishlinsky's theorem "On solid angle" [37, 38]), and approximation equations in variations (which ignore these effects of the second order $\sim \varepsilon^2$ in principle) were used as the errors KE in the inertial navigation theory, instead of accurate errors KE [29-31, 39-41].

In the study of features for LG applications in SINS, the nonholonomic errors "antithesis" was discovered, which is identical in mathematical terms, but opposite on the physical meaning effect of the second order ($\sim \varepsilon^2$). – Non compensated periodic frequency LG biasing

$$\delta\bar{\omega}(t) = (\alpha_1 \sin(\nu t + \varphi_1) \quad \alpha_2 \sin(\nu t + \varphi_2) \quad \alpha_3 \sin(\nu t + \varphi_3))^T = \bar{c}_1 \sin \nu t + \bar{c}_2 \cos \nu t \quad (3.1)$$

corresponds to fictitious not finitely rotation (when phases φ_i aren't equal). – SINS orientation error (in the absence of object rotation) growth with speed $\Delta s(t)/t = \varepsilon^2 \alpha^2 \nu \cdot \text{const}$, where $\alpha \sim \alpha_1 \sim \alpha_2 \sim \alpha_3$, for equiprobable distribution of phases φ_i in range $(-\pi, +\pi)$, $\text{const} \sim (3/2)^{1/2}/8$. For typical parameters values $\alpha = (2-10)$ arc. min, $\nu/2\pi = (100-500)$ Hz, effect's magnitude is $\alpha^2 \nu \cdot \text{const} \sim (7-700)$ deg/hr. Accurate KE solution in quadratures for rotation with angular velocity (3.1) in particular cases $\bar{c}_1^T \bar{c}_1 = \bar{c}_2^T \bar{c}_2$; $\bar{c}_1^T \bar{c}_2 = 0$ is known [11]. Paradoxically but true: such a "big" in magnitude effect (although it's second-order effect $\sim \varepsilon^2$) didn't allow (and don't allow) to be noticed with throughout used approximate errors KE in variations.

In the research process of the various LG errors and noises influence on SINS orientation accuracy with accurate errors KE, general patterns of accumulation of various LG errors and noises components to resulting SINS orientation error were clarified [11, 14]:

$$1) \Delta \bar{S}(t) = \sum_{n=1}^{\infty} \varepsilon^n \Delta \bar{S}_n(t) \rightarrow \Delta \bar{S}(t) \cong \varepsilon^1 \Delta \bar{S}_1(t) = \Delta \bar{\theta}(t); \Delta \bar{\theta}(t) \equiv \int_0^t B(\tau) \delta \bar{\omega}(\tau) d\tau; \quad (3.2)$$

$$2) \Delta \bar{S}(t) = \sum_{n=1}^{\infty} \varepsilon^n \Delta \bar{S}_n(t) \rightarrow \Delta \bar{S}(t) \cong \varepsilon^1 \Delta \bar{S}_1(t) = \delta \bar{\theta}(t); \delta \bar{\theta}(t) \equiv \int_0^t \delta \bar{\omega}(\tau) d\tau; \quad (3.3)$$

$$3) \Delta \bar{S}(t) = \sum_{n=1}^{\infty} \varepsilon^n \Delta \bar{S}_n(t) \rightarrow \Delta \bar{S}(t) \cong \varepsilon^1 \Delta \bar{S}_1(t) + \varepsilon^n \Delta \bar{S}_n(t). \quad (3.4)$$

In the expressions (3.2), (3.3) and (3.4) only the main term of series (2.27) of errors KE solutions was retained, i.e. the rest of the series (2.27) can be neglected due to smallness in comparison with retained ones. The first type 1) includes many components of gyroscopes errors and noises. For these and only for these errors and noises it's possible to limit ourselves by solution of approximate errors KE in variations. The second type 2) includes (for arbitrary object rotation) white noises in angular velocity and nonlinear LG errors, caused by the lock-in effect in LG [27]. The third type 3) includes periodic errors (3.1) and noises of types (2.43), (2.45). The ratio of values for terms of first and N-th orders depends on the type of the object rotation.

All results of the research of gyros errors and noises influence on SINS orientation accuracy by changing: $B(t) \rightarrow I_0$ turn into research of gyroscopes errors and noises influence on platform INS orientation accuracy.

Paradoxically but true: only recently, the author noted that the new generation of SINS and different types SINS' gyroscopes (including gyroscopes upgrades developed in 1950-1980 for application in platform INS) developers, don't know the effect (2.15) and can make mistakes due to ignorance of the following effect – one of the most striking manifestation of NKE (2.15). – See Fig. 3.1.

The result (Fig. 3.1) would have pleased Dr. Charles Stark Draper as an additional argument in platform INS benefit to argument described in Part 1. Charles Stark Draper had such a chance, papers [26, 27] were published in the English version [43, 44] and were seen by NASA [45].

And the essence of the matter is following. In 1950-1980s Charles Stark Draper team in USA and V.I. Kuznetsov team in USSR were developing command devices complexes, competing in their accuracy, for control systems of creating and continually upgrading rocket technology, [51]. GSP "drift" was a natural criteria of quality (accuracy) of GSP. Therefore, during the improvement of gyros all the errors sources, which lead to GSP "drift" were eliminated. And on the elimination of other errors of the gyroscopes that do not lead to GSP

, did not pay much attention. In part, because there was no time for this. – It was a hard race for the accuracy of the GSP. ¹

“Gyros noises with equal to zero power spectral density on zero frequency $S_{\omega}(\nu=0)=0$ don't lead to significant increase of orientation determination error in time for platform INS (second order “smallness” effect), but lead to pretty significant increase of orientation determination error in time for SINS (first order “smallness” effect). The difference of partial contribution of these noises to accuracy of platform INS and SINS is in order of magnitude (in 10, 100, 1000 and more time) depending on the specific structure of gyro noises structure and on form of the object rotation”.

(SRI AP Engineer, 1979-1980, N.I. Krobka)



Fig. 3.1. “Byproduct” of accurate SINS on LG theory construction on the basis of accurate errors equations [11]

Fig. 3.2. Learning is never too late to anyone. “Live a century and learn a century” (the folk wisdom) [42]

In the same time, in mechanical gyroscopy has a tradition: determine the quality of gyroscopes by “integral” parameter (taking into account hundreds of different imperfection sources, but that doesn’t matter): “gyroscope drift”: X_m arc. min/min или X_s arc. sec/sec. And that, indeed, was enough for GSP gyroscopes (up to second-order effects). But for SIOS or SINS gyroscopes everything is different. It’s not enough to know only “inegral” parameter of “gyroscope drift”. It’s necessary to know gyroscopes errors and noises structure, because different components, firstly, differently accumulate in SIOS error, secondly, significantly depend on the type of object rotation, – see (2.20), (3.2)-(3.4).

Fig. 3.3 and Fig. 3.4. represent Allan deviation $\sigma(\tau)$ -graphs for two model gyroscopes (No. 1 and No. 2) with *a priori* known (given) parameters of the three noises. Difference only in bias instability magnitude: 10^{-4} deg/hr (Fig. 3.3) and 10^{-5} deg/hr (Fig. 3.4).

Question: which gyro is better? If gyros are used for the platform INS, then, obviously, second gyro (Fig. 3.4) is better. White noise “in angle” contributes in GSP “drift” only in the second order, it can be neglected (with relative accuracy $\sim 1,8 \times 10^{-6}$) compared with two other noises. GSP “drift” would be almost in order of magnitude less, independent from the form of the object rotation. And in the case of SIOS and SINS applications of gyros the answer is not simple – all depends on the specific form of the object rotation $B(t)$. For the simplicity of explanation, let’s assume that as a result of various efforts (“gyroscope, it’s simple” [52]), a

¹ Did Charles Stark Draper or his team of developers in the USA know about existence of the effect (2.15) and its display (Fig. 3.1), the author doesn’t know. But it is authentically known that “such effect was not ever noticed” from lips of “fathers of inertial navigation and inertial targeting” (“leaders of domestic gyroscopy” [46]) as they were called in the USSR and are called in Russia, the Academician V. I. Kuznetsov (during the two-hour conversation on October 1, 1986 which took place at the initiative of the Chief designer of NPO “Rotor” V. I. Kuznetsov according to the “Midgetman” program and modernization of the AIRS block designed by Charles Starck Draper and mastered by Northrop company which has been already used in MX IBM, Litton and Honeywell developed navigation blocks based on LG, and the accuracy of LG blocks surpassed AIRS accuracy in advertizing forecasts by 10 times [47, 28])) and the Academician A.Yu. Ishlinsky (in a series of the meetings which took place at the initiative of A.Yu. Ishlinsky since November, 1993 till May, 1994 [48, 49]).

In 1991, after security classification removal from subject of LG, some first general-theoretical results of the author on strict LG-based SINS theory created in 1979-1981, were prepared in the form of reports on the first international symposiums on inertial technology in St. Petersburg [14, 15]. For “public release” of these results (the strict dynamic and kinematic equations of SINS errors and researched on their basis regularities of accumulation of LG errors and noise in SISO and SINS) the author had to discuss texts of [14, 15] with experts of gyroscopic and inertial technology of team of V. I. Kuznetsov (I.N. Sapozhnikov, V.I. Reshetnikov, I.D. Blyumin, M.L. Effa, S.A. Kharlamov). Scientific novelty and practical value of the results was confirmed by all experts, approval on the publication of reports [14, 15] was received. But more than others M.L. Effa [50] became interested in works [14, 15]. He worked with V. I. Kuznetsov since student years, over time he has become the leading developer of all mechanical gyroscopes designed by SRI AM of NPO “Rotor”. At that time M.L. Effa helped to start LG production for LG-based SINS – SINS-90 which has been developing in SRI AM and therefore sought to study LG features [47]. Mainly, texts [14, 15] were written, specially to bring M.L. Effy up to date on LG and LG-based SINS features quickly. In parallel M.L. Effa modernized a spherical floating platform designed by SRI AM [51], similar to modernization of the AIRS block by Charles Starck Draper. Therefore first-order effect (2.48) incredibly interested M.L. Effu. He wanted to understand: 1) What is the difference in the accumulation of the derivative of white noise “in the angular velocity” (white noise “in the angle”) in SINS and platform INS; 2) What causes such difference as such “strong” effect was never observed in GSP. Author needed to explain this matters, starting with strict error KE SINS and platform INS differences (2.18), (2.19). M.L. Effa understood everything and thought: what if it is possible to construct SINS on float-operated gyroscopes, which were designed for use in GSP? As a developer, knowing his gyroscopes errors sizes, M.L. Effa made numerical estimates and put to the end the discussion of the effect (Fig. 3.1) with his short and capacious, widely known in circles of gyroscopes developers in USSR and in Russia, exclamation: “Nothing to yourself!” (Do not confuse with expression: “Wow!”).

new generation of gyroscopist-developers has created gyros (in any physical principles) without bias instability – Fig. 3.5, – gyros noise is just a mix of two white noises: “in angular velocity” and “in angle”. For the simplicity of model let’s assume, that the noises are Gaussian, independent and have equal intensity in three gyros:

$$\delta\bar{\omega}(t) = \bar{\xi}_1(t) + \bar{\xi}_2(t); \quad \langle \bar{\xi}_i(t) \rangle = \bar{0}; \quad \langle \dot{\bar{\xi}}_i(t) \rangle = \bar{0} \Rightarrow \langle \delta\bar{\omega}(t_1) \delta\bar{\omega}^T(t_2) \rangle = [D\delta(t_1 - t_2) + Q\tau_0^2 \frac{d^2}{dt_1 dt_2} \delta(t_1 - t_2)]I_0. \quad (3.5)$$

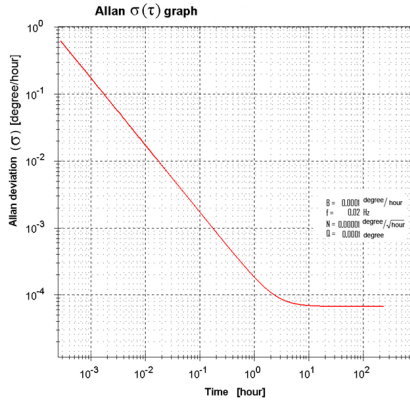


Fig. 3.3. Allan deviation $\sigma(\tau)$ -graph for model gyroscopes No. 1

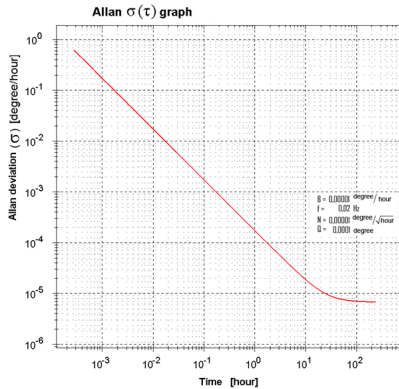


Fig. 3.4. Allan deviation $\sigma(\tau)$ -graph for model gyroscopes No. 2

extraction, in years work”.

The author had tried to reach a different result, as formulated by V.V. Maykovsky: “Joyful boy went and decided: “I’ll do good and I’ll not do bad”. – See example in Fig. 3.6.

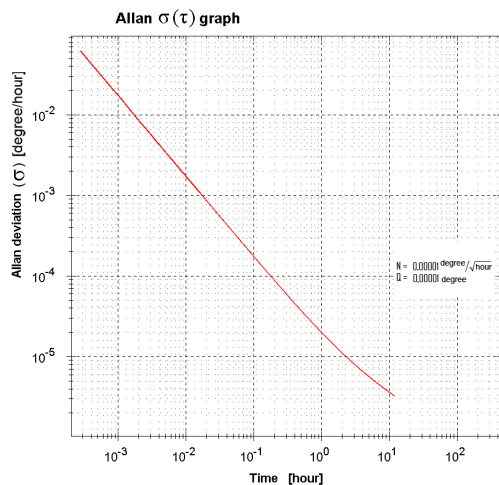


Fig. 3.5. Allan deviation $\sigma(\tau)$ -graph for model gyroscopes No. 3

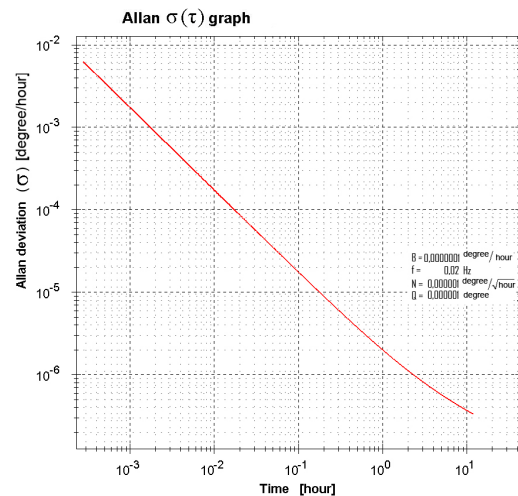


Fig. 3.6. Allan deviation $\sigma(\tau)$ -graph for model gyroscopes No. 4

“What a good gyroscope!” (Fig. 3.5), – a new generation of gyroscopist-developers exclaims.

Yes, not bad (it’s possible, in principle, to do better [22]) gyros (Fig. 3.5), but for platform INS application. Indeed, the GSP “drift” on such gyros would be diffusion (orientation error for 1 hour would be $\sqrt{3} \cdot 10^{-5}$ deg, for 100 hours – $\sqrt{3} \cdot 10^{-4}$ deg, independent on object rotation). Charles Stark Draper would like such gyroscope (accuracy exactly corresponds to AIRS unit accuracy after 1 hour, and much better after 100 hours):

$$\sigma_{\Delta S'+}^2(t) \cong 3Dt. \quad (3.6)$$

And everything would be principally different in the case of SIOS and SINS applications of the such gyros:

$$\sigma_{\Delta S'+}^2(t) \cong 3Dt + 2Q\tau_0^2 \int_0^t |\bar{\omega}(\tau)|^2 d\tau. \quad (3.7)$$

The ratio of SINS (3.7) and INS (3.6) orientation errors dispersion for arbitrary object rotation ($B(t) \neq I_0$) greater than unit and has the form:

$$\frac{\sigma_{\Delta S'+}^2(t)}{\sigma_{\Delta S'+}^2(t)} = 1 + \frac{2Q\tau_0^2}{3Dt} \int_0^t |\bar{\omega}(\tau)|^2 d\tau. \quad (3.8)$$

The numerical values of the ratio $\sigma_{\Delta S'+}(t)/\sigma_{\Delta S'+}(t)$ (3.8) are easy to evaluate by any gyroscopist-developer for own gyros if one is really a developer [53]. For LG [47, 54, 55] such estimates were obtained. Estimates for some other gyroscopes were obtained too. The author would not be surprised if some of the developers of gyros for SIOS and SINS, a quarter of a century later, will repeat M.L. Effa exclamation: “Nothing to yourself” Perhaps, some of the developers will realize, that about one order of magnitude reduction of gyros bias instability (Fig. 3.3 and Fig. 3.4), without reduction of the other noises, poet V.V. Mayakovsky had noticed: “In gram

4. The task of identifying the structure of noise gyros. The strategy “Gasoline is your, ideas are our”

With methods of researches of noises, including Allan variance [56], the author is familiar since student years (1973-1979) in the Moscow Institute of Physics and Technology (MIPT) [57, 58] where he had studying simultaneously on three specialties: the first – “physical and quantum electronics”; the second – “IBM control systems” [59, 60]; the third – “statistical radiophysics”. The practise course (1975-1979) took place according to the “Fiztech’ System” at chair of physical electronics of MIPT [61] (1975-1979) in Scientific Research Institute of Applied Physics (SRI AP) in which since the beginning of the 1960th LG [62] were developed. And the diploma thesis was connected with noises, not LG noises but the optical quantum amplifiers (OQA) noises [63].

In the 1960-1970th in the USSR for researches of noises of LG, which were created in the USA (1962) and in the USSR (1963) with a half-year interval [64] radio engineering and radio physical methods, and also methods of statistical physics and mathematical statistics were used. Research problems of LG noises were the following. Based on the results of LG tests: 1) to separate technical fluctuations, which can be eliminated or reduced by means of design-technological decisions during LG working off, from “natural” fluctuations – principally ineradicable quantum noise caused by spontaneous radiation; 2) to estimate precisely the intensity of the quantum noise which is determining achievable accuracy of LG; 3) to find out: whether quantum noise of LG is white noise or the power spectral density of quantum noise at zero frequency is equal to zero (there were two such models). The accuracy of a laser gyrocompass at the set measurement time (ΔT) depended on it as follows:

$$\sim \Delta T^{-1/2} \text{ or } \sim \Delta T^{-1}.^2$$

Allan variance [56] has the following form:

$$\sigma_{\omega}^2(\tau) \equiv \frac{1}{2} \left\langle (\omega_{k+m} - \omega_k)^2 \right\rangle = \frac{1}{2\tau^2} \left\langle (\theta_{k+2m} - 2\theta_{k+m} + \theta_k)^2 \right\rangle \equiv \frac{1}{2\tau^2(N-2m)} \sum_{k=1}^{N-2m} (\theta_{k+2m} - 2\theta_{k+m} + \theta_k)^2; \quad (4.1)$$

$$\omega_k(\tau) \equiv \frac{\theta(t_k + \tau) - \theta(t_k)}{\tau}; \quad \theta(t_k) \equiv \theta_k; \quad \theta(t) \equiv \int_0^t \omega(z) dz; \quad t_k \equiv k\tau_0; \quad \tau = m\tau_0.$$

From the second half of the 1960th the Allan variance method was used in the USA not only for researches of noises of the frequency standards (“time”). All the firms which developed LG technology and SINS based on LG (Honeywell, Litton, Singer, Sperry, Raytheon, etc.) used the Allan variance method in the 1960-1980th. In the USSR, the Allan variance method in those years in a gyroscopy, including quantum gyroscopy, widely wasn't used. But the last 10-20 years, at working off of MEMS-gyros and FOG, the Allan variance method is used in Russia wider every year. The author uses Allan graphs since 2007. After the break, which was connected with “perestroika”, the Scientific Research Institute of Applied Mechanics named after Academician V.I. Kuznetsov (SRI AM) has restored the works on FOG (in 1985-1995, in SRI AM FOGs were investigated in parallel with development of LG). The standard [66] already regulated the error model of FOG with

² At working off of LG the measurements lasting 10000-100000 hours without switching off of devices were taken. The author, at that time – the student, had to work part-time laboratory assistant on tests of LG in non-working days. Laboratory assistant's responsibility consisted in replacing rolls of tape in recorders (there were no computers in that time) without violation of a continuity of measurements. It was impossible to simply look at recorders and not to think of anything else. One of methods of research of noise of LG at that time was $\sigma(\Delta T)$ – graph – a standard deviation (SD) as function of time of averaging (or time of integration of angular speed, since LG is an integrating gyroscope). Two options of formation of statistical ensemble from primary data of one realization are obvious to construction $\sigma(\Delta T)$ – graphs assuming ergodicity [65] of a random process. First option: the cycle of measurements with quantity of steps $N = T/\tau$ (τ – a step of gathering information, T – duration of measurement) is primary ensemble on which SD $\sigma(\tau)$ is calculated. Further the data of two next steps are summarized (the first from the second, third with the fourth, etc.) and SD $\sigma(2\tau)$ is calculated. And so on for receiving SD $\sigma(n\tau)$, i.e. $\sigma(\Delta T)$ -graph ($\Delta T = n\tau$) of the first type. With an increase of n , the size of the ensemble, obviously, reduced $\sim N/n$. With decreasing the size of ensemble, obviously, the reliability of an assessment $\sigma(n\tau)$ also decreases. For increase reliability of $\sigma(n\tau)$ it is possible to increase the ensemble size. Why not, if the hypothesis of ergodicity has already been accepted? Second option: For calculation $\sigma(2\tau)$ it is used not only $[N/2]$ elements of primary ensemble (a symbol [...] – is function of the whole part), but also additional $[(N-1)/2]$ elements (if N – is odd number) or $[(N-2)/2]$ element (if N – is even number), which are obtained by summation of primary data: second with the third, third with the fourth, etc. Similarly for calculation $\sigma(n\tau)$, by shifting on n steps “to the right” the summation of data of n neighboring steps. In other words: for preparation of statistical ensemble for the purpose of calculation of SD $\sigma(n\tau)$ all possible options of the sums of primary data of n steps continuously following one after another are used. Dispersion for the $\sigma(\Delta T)$ – graph of the second type looks like the following:

$$\sigma_{\omega(\Delta T)}^2 \equiv \left\langle (\omega_{k+m})^2 \right\rangle - \left\langle (\omega_{k+m}) \right\rangle^2; \quad \omega_k(\Delta T) \equiv \frac{\theta(t_k + \Delta T) - \theta(t_k)}{\Delta T}; \quad \theta(t_k) \equiv \theta_k; \quad \theta(t) \equiv \int_0^t \omega(z) dz; \quad t_k \equiv k\tau; \quad \Delta T = m\tau, \quad (*)$$

where ω – is an angular velocity, θ – is an angle of so called apparent turn, τ – is a step of gathering information.

The functional (*) is close to Allan variance [56] (there are three differences) in spite of the fact that it arose from other reasonings.

determination of parameters of noise. Finally, it was realized that the author sought at conferences since the early 1980s from the developers of SINS and gyros intended for SINS on the example of LH [68], realizing that the different noises are making a different contribution to the orientation error of SINS. In standards [66, 67] the “dynamic” model of errors [68] of gyroscopes for SINS [16, 17] is already required.

At the end of 2006, working on the request of the Chief designer to analyze the current situation with the FOG development in Russia, the author spoke with the FOG designers in Moscow, asking three questions: 1. How many FOGs are there on resource tests? 2. What is the FOG accuracy; what is the averaging time? 3. How much does the FOG cost and why? The additional question what the noise structure of their FOGs was caused a puzzling question: “What do you mean? Can the noise have a structure? Noise is white!” That was the answer the author heard from many Russian FOG designers at the boundary of 2006–2007 (except for the designers from Fizoptika [69], who, like the author, passed the school of quantum gyroscopy at the SRI AP in the 1960–1980s, where LG (1963) [64], and FOG (1975) [70] were created for the first time in the USSR. “The answer is not correct!” the author used to answer. “Have a look!” the author offered. No sooner said than done.

In Fig. 4.1 the autocorrelation functions of noises (of three different Russian FOG, not important, whose development) constructed by results of the tests in SRI AM in 2007-2008 [71, 21], are presented. In standards [66, 67] there was not such noises of FOGs (Fig. 4.1).³

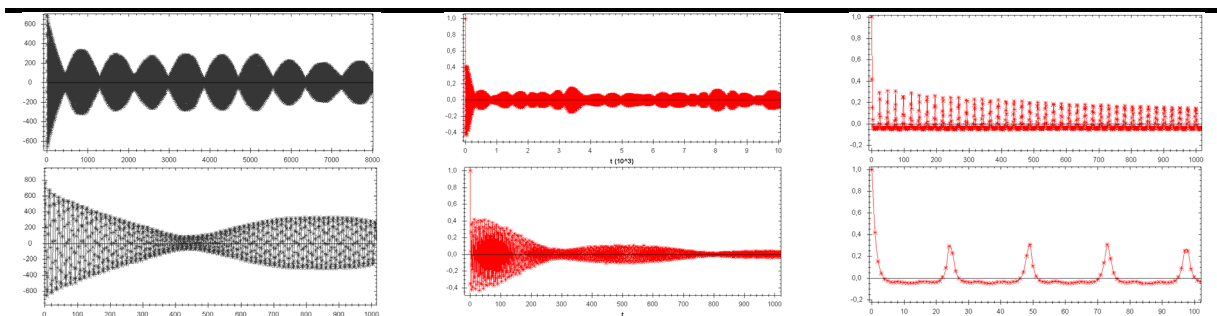


Fig. 4.1. The autocorrelation function and the correlation coefficients of noise for three FOG samples of Russian design (the scale does not matter) built on the results of tests

The statement of the problem for the development of software and programm-mathematical complex (PMC) for identify the structure of noises was more laconic in comparison with the statement of the problem in [48]: “Guys! We work further. Let’s develop PMC with the following features: PMC has to: 1) To be able to do all (“all” is a keyword here) that was known earlier for identification of noise structure in physics and technology; 2) To allow you to expand opportunities for the implementation of any new ideas. All the rest is to your taste. For any questions contact at any time and ask about details”.

5. The topology of graphs of Allan deviation. Partial contributions of different noises to $\sigma(\tau)$ – graphics

Basic designations and definitions are following: $S_{\omega}(f)$ – noise power spectral density of noise; $K_{\omega}(\tau)$ – autocorrelation function; $\sigma(\tau)$ – Allan deviation.

The link between Allan variance and power spectral density (in angular velocity) is following

³ During deployment works on FOG in SRI AM in 2007-2008, communicating with young specialists, author with surprise understood that the new generation of developers of gyroscopes doesn’t understand elementary things: how to define gyroscope’s noises structure by the results of test and why is it necessary?; how to define the source of the noise by its type in gyroscope’s elements and subsystems for the purpose of noise elimination or reduction to improve gyroscope’s accuracy? how various gyroscope noises accumulate over time in SISO and SINS errors?; which noise components are more crucial in concrete applications regarding influence on orientation, navigation and control systems accuracy, for which the concrete gyroscope is designed?; what is the difference between white noises “in angle”, “in angular velocity” and “in angular acceleration” regarding influence of these gyroscope noises on the accuracy of systems for which these gyroscopes are designed?; how numbers $X_1, X_2, X_3, X_4, X_5, X_6$ are interconnected regarding accuracy: X_1 arc. sec/sec., X_2 arc. min/min., X_3 deg/hr, X_4 deg/day, X_5 deg/month, X_6 deg/year; whether it is possible to define numbers $X_1, X_2, X_3, X_4, X_5, X_6$ if the seventh number X_7 – SKO of an angular velocity determination error during measurement of 100 seconds is known? After seeing (Fig. 4.1) and hearing the answers it became clear – everything should be started almost “from scratch”, – today it is simply not taught in any of those institutions whose graduates come to SRI AM.

In an initiative order three informal groups were created. The first group (Y) consisted of everyone who was interested in dealing with noises; the second group (Z) consisted of postgraduates; the third group (X) consisted of students whom the author coached for research work as a mentor. Work with all groups was realized on the base of strategy “Gasoline – your, ideas – our” [72]. Today each developer in SRI AM knows: 1) noises of gyroscopes are not white but are represented as a mix of different noises; 2) how to understand which types of noises there are in the mix using Allan deviation ; 3) how to assess the upper estimates of bias instability and angle random walk.

Group X knows and can much more.

$$\sigma^2(\tau) = 4 \int_0^\infty S_\omega(f) \frac{\sin^4(\pi f \tau)}{(\pi f \tau)^2} df. \quad (5.1)$$

N – is the angle random walk (ARW) coefficient [67]:

$$S_\omega(f) = N^2 \rightarrow \sigma^2(\tau) = \frac{N^2}{\tau}. \quad (5.2)$$

B – is the bias instability (B) coefficient [67]:

$$S_\omega(f) = \begin{cases} \frac{B^2}{2\pi} \frac{1}{f} & f \leq f_0 \\ 0 & f > f_0 \end{cases} \rightarrow \sigma^2(\tau) = \frac{2B^2}{\pi} \left[\ln 2 - \frac{\sin^3 x}{2x^2} (\sin x + 4x \cos x) + Ci(2x) - Ci(4x) \right]; \quad Ci(x) \equiv -\int_x^\infty \frac{\cos t}{t} dt, \quad (5.3)$$

where f_0 – is the cutoff frequency, Ci – is the cosine-integral function, $x = \pi f \tau$. K – is the rate random walk (RRW) coefficient [67]:

$$S_\omega(f) = \left(\frac{K^2}{2\pi} \right) \frac{1}{f^2} \rightarrow \sigma^2(\tau) = \frac{K^2 \tau}{3}. \quad R - \text{the rate ramp (RR) coefficient [67]:} \quad (5.4)$$

$$S_\omega(f) = \frac{R^2}{(2\pi f)^3} \rightarrow \sigma^2(\tau) = \frac{R^2 \tau^2}{2}. \quad (5.5)$$

Q – the quantization noise (Q) coefficient [67]:

$$S_\omega(f)(f) = \begin{cases} \frac{4Q^2}{\tau_0} \sin^2(\pi f \tau_0) & f < \frac{1}{2\tau_0} \\ \approx (2\pi f)^2 \tau_0 Q^2 & \end{cases} \rightarrow \sigma^2(\tau) = \frac{3Q^2}{\tau^2}. \quad (5.6)$$

Exponentially correlated (Markov) noise (M) [67]:

$$S_\omega(f) = \frac{(q_c T_c)^2}{1 + (2\pi f T_c)^2} \rightarrow \sigma^2(\tau) = \frac{(q_c T_c)^2}{\tau} \left[1 - \frac{T_c}{2\tau} \left(3 - 4e^{-\frac{\tau}{T_c}} + e^{-\frac{2\tau}{T_c}} \right) \right], \quad (5.7)$$

q_c – is the amplitude of Markov noise; T_c – is the correlation time of Markov noise.

Harmonic perturbation (“sinusoidal noise”) [67]:

$$S_\omega(f) = \frac{1}{2} \Omega_0^2 [\delta(f - f_0) + \delta(f + f_0)] \rightarrow \sigma^2(\tau) = \Omega_0^2 \left(\frac{\sin^2(\pi f_0 \tau)}{\pi f_0 \tau} \right)^2. \quad (5.8)$$

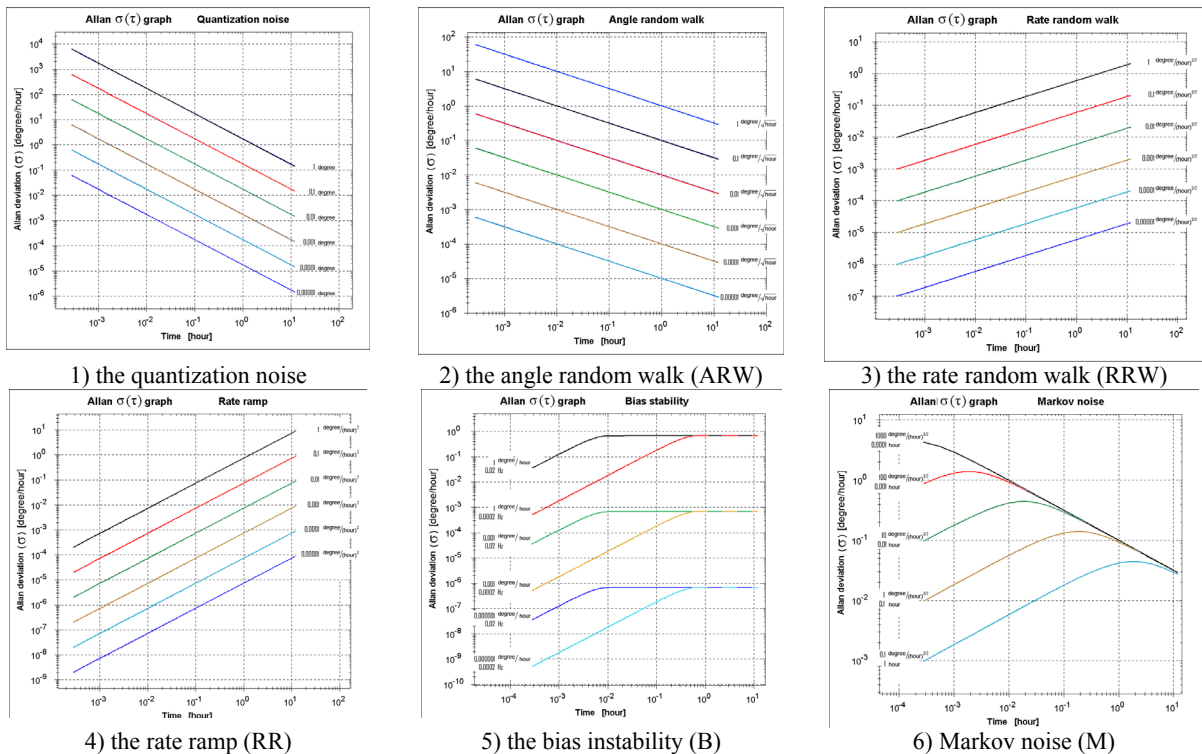


Fig. 5.1. The topology of $\sigma(\tau)$ – graphs of Allan deviation of the “basic” noises provided by the standard [67]

In Fig. 5.1 the graphs of Allan deviation of the noise provided by the standard [67] are presented. These graphs were simulated by PMC (the developer of the software of this subsystem of PMC – A.I. Bidenko).

The topology (*analysis situs* [73]) of $\sigma(\tau)$ – graphs of Allan deviation of the noises is presented in Fig. 5.1. It is rather simple and clearly. Four noises: 1) the quantization noise, 2) the angle random walk (ARW), 3) the rate random walk (RRW) and 4) the rate ramp (RR) are one-parametrical. Change of the corresponding parameters leads to parallel shift of graphs of Allan deviation “up” or “down” (Fig. 5.1). Two noises: 5) the bias instability (B) and 6) exponentially correlated (Markov) noise (M) are two-parametrical. Change of parameters of these noises leads to two-parametrical “deformation” of graphs of Allan deviation (Fig. 5.1). For n-parametrical noise the topology of graphs of Allan deviation depends on n of parameters, in particular, on 3 parameters for three-parametrical noises.

The resulting $\sigma_{\Sigma}(\tau)$ – graph of Allan deviation of the mix of statistically independent noises depends on the partial contributions $\sigma_i(\tau)$ of Allan deviations of separate noises nonlinearly:

$$\sum_i \zeta_i(t) \Rightarrow \sigma_{\Sigma}(\tau) = \left(\sum_i \sigma_i^2(\tau) \right)^{1/2}. \quad (5.9)$$

In Fig. 5.2 the $\sigma(\tau)$ – graphs of Allan deviation of harmonic perturbation (“sinusoidal noise”) provided by the standard [67], simulated by means of PMC, are presented.

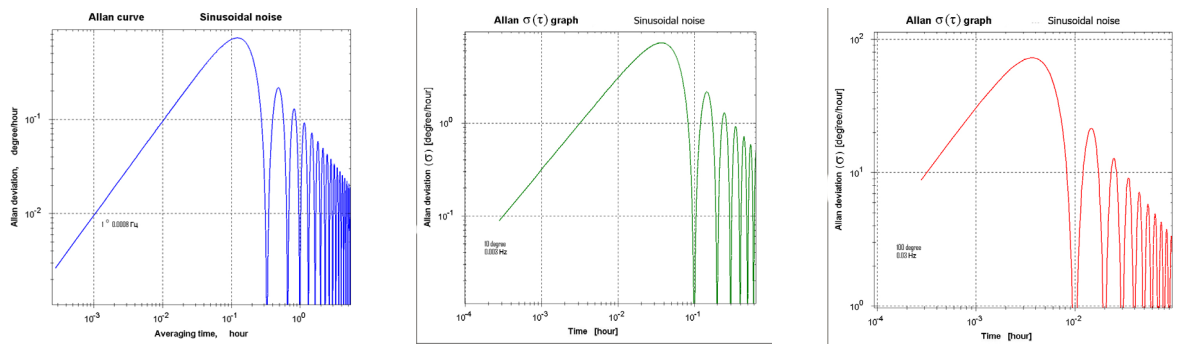


Fig. 5.2. The topology of $\sigma(\tau)$ – graphs of Allan deviation “sinusoidal noises” provided by the standard [67]

Here it is pertinent to explain the following. Despite the used dispersion symbol σ^2 , Allan variance $\sigma^2(\tau)$ [56] isn't the dispersion. Allan variance is a statistical moment of the second order, – the “average square” of some value, averaged on ensemble depending on parameter τ (4.1). Therefore in Allan variance and in $\sigma(\tau)$ – graph of Allan deviation not only random processes (noises), but also any determined (not random) processes (except constants) make contributions.

Why the author for an assessment of influence of noise of gyroscopes on the accuracy of orientation of SINS uses the functional $\sigma_{\Delta s+}^2(t)$ (2.33) instead of dispersion $\sigma_{\Delta s}^2(t)$ (2.32) is explained in item 2. It is a consequence of rotation in three-dimensional space. Why D. Allan in a one-dimensional case where such problems aren't present, uses not dispersion, but only a mean square (the second moment) of a scalar random variable without “minus the square of average value”? – Questions to D. Allan. But one aspect is obvious. The Allan variance method was developed for researches of fluctuations of frequency and a phase of standards of the frequency (“time”). The “drift” of a phase for this or that interval of time irrespective of, this drift is caused by stationary or non-stationary random processes or the determined processes changing in time is important for standards of “time”.

In gyroscopy there is a close situation, but a bit different. Not only such errors and noises in the angular velocity (analog of frequency) which lead to an error of an angle of the seeming turn (analog of “drift” of phase), but also such noises in the angular velocity which, though don't lead to growth in time of an error of the angle of the seeming turn, but lead to growth in time of an error of an angle of the valid turn are important. It is a consequence of not commutativity of rotations around a point (but not around an axis). In platform INS there are such effects of the second order, in SINS there are such effects of the first order.

For identification the structure of noises of gyroscopes more detailed tools, than for identification of structure of noises of frequency and a phase in standards of “time”, namely, for identification the structure of noises of gyroscopes type (2.43), (2.45) are necessary. For the accounting of fluctuations of onboard “time scales” on accuracy of SINS (and INS) information of noise structure not only of “time” (phase) and first derivative of “time”(frequency), but also the second derivative of “time” (the first derivative of frequency of standards of time) are needed [74].

In Fig. 5.3 the graphs of Allan deviation, modified Allan deviation and Hadamard deviation created by the Alavar 5.2 program are submitted. The file with primary information of laboratory tests of four-axis FOG is

used. But instead of the data in columns with information of four FOG channels, the numbers in column No. 1 with sequence of counting: 1, 2, 3, etc, is used. In other words, the graphs in Fig. 5.3 correspond to the function t (time). The graph of Allan deviation is a ray of a straight line with an inclination +1, the graph of Hadamard deviation is a ray of a straight line with an inclination 0 (identical to 1), as well as has to be. To functions t^2 and t^3 correspond the graphs of Allan deviation also in the form of ray of a straight line with an inclination +1, but with shift of the beginning of a ray.

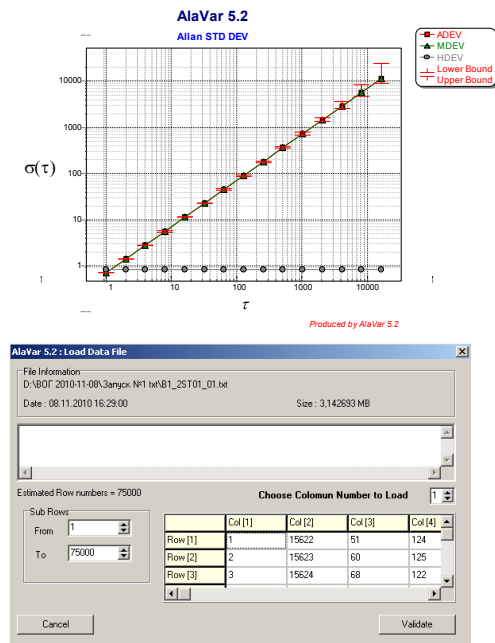


Fig. 5.3. The graphs of Allan deviation, modified Allan deviation and Hadamard deviation created by the Alavar 5.2 program on the base of the first 75000 natural numbers: 1,2,3, ..., 75000

methods [75], the author has not heard. The author didn't use such names, because the essence is not in the title. But, if David Allan doesn't object, and Nikolay Krobka won't object if these generalizations will be called as such in the future and outside of SRI AM. But with one condition: if use of dispersions along with variances will bring benefit for identification of noises.

Physical intuition suggests that the use of two functionals type (5.10) simultaneously, can, in some cases, enhance the ability to identify the structure of the noises ⁴.

6. Typical misconceptions and blunders in the interpretation of noise structure and the estimates of parameters of noises of gyroscopes based on $\sigma(\tau)$ – graphs of Allan deviation

The first example ("two in one").

Of the many well-known publications, which did not correctly assess the structure and parameters of noises of gyroscopes based on $\sigma(\tau)$ -graphs of Allan deviation, let's choose as a bright example, the report of 2007-year [79]. The choice of this report namely is made, first of all, because it contains half of the "bouquet" of common

⁴ Two examples from author's practise to double the volume of initial information:

1) If the angular velocity vector in general case of arbitrary object rotation is set only in the rotating basis or only in immovable basis, then KE (2.2) nobody managed to integrate in quadratures more than 250 years – from the moment of creation of kinematics of rotations by Leonard Euler. And if to use at the same time two representations, pair KE are integrated in quadratures [76], and without of integration [77]. Simultaneous information can be received by using gyros of SINS and platform INS, stabilized in inertial space [78].

2) The new algorithm of inertial navigation [19, 22] which is following: in regular algorithm of calculation the trajectory of object, based on accelerometers and gyroscopes data, gravitational acceleration isn't used completely, but the accurate error equations are used. The unaccounted contribution of gravitational acceleration in "regular" algorithm is precisely considered in the solution of the accurate error equations. Thus both the "regular" algorithm and accurate error equations are linear and are integrated in quadratures. As a result the valid trajectory of object is expressed in quadratures without the need to integrate nonlinear differential equations [19, 22].

misconceptions and blunders in the interpretation of $\sigma(\tau)$ -graphs of Allan deviation formulated in the Introduction. Secondly, it is one of the few reports at the Saint Petersburg International Conference on Integrated Navigation Systems, written by Russian authors, first in English and then translated into Russian. Therefore, anyone who can not read in Russian will be able to evaluate the logic of estimating the parameters of the noise of the gyroscope reading literate English text [79] (except for an unfortunate typo in the title of the report: “Coliolis” instead of the “Coriolis”). Thirdly, since one of the authors who wrote the text [79], has three higher technical education: the Moscow State Technical University named after N.E. Bauman, with honors, 1998; University of Illinois, Urbana-Champaign, USA, a Master of Science, 2001; University of Calgary, Canada, PhD, 2005 [80], it is possible, with a minimum amount of irony, because it is not the worst universities in Russia, USA and Canada, to conclude: “Allan variance method to identify the structure of the noise of gyros competently do not teach neither in Russia, nor in the USA, nor in Canada”.

So. Following the “iron logic” of the classic anecdote [81] (up to isomorphism [82, 83]): “If the box is square, it means something in it is round. If it is the round, then it is orange. If the orange, then it is orange!”, the action takes place in three acts [79]. Act One: Enjoying the $\sigma(\tau)$ -graph of Allan deviation (Fig. 6.1). Act Two: Compare the graph (Fig. 6.1) with the graph in Fig. 6.2. Act Three: Determine (what could be easier?) the value of N (the angle random walk (ARW) coefficient) and the value of B (the bias instability (B) coefficient) by comparing graphs on Fig. 6.1 and Fig. 6.2. Specific considerations [79] presented to quote in Fig. 6.3

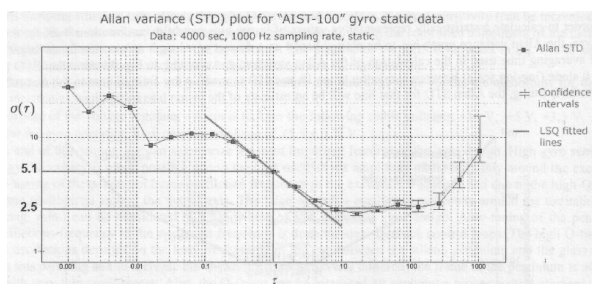


Fig. 6.1. Allan $\sigma(\tau)$ -graph, built according to the testing MMG "AIST-100" [79]

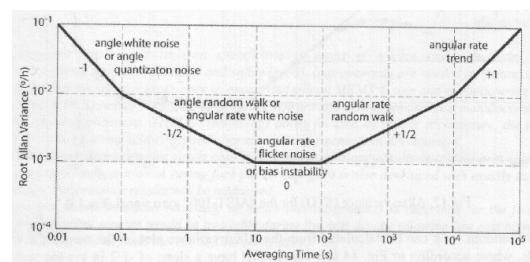


Fig. 6.2. Schematic representation of the resulting Allan deviation [79, 84], which introduced many astray

Random drift corresponds to the slope $-1/2$ (see Fig. 6.2). We find on the graph (Fig. 6.1) the slope $-1/2$. Is it logically? See again Fig. 6.1 and Fig. 6.2. It is logically! We seek in the segment with a slope of $-1/2$ point from which the perpendicular to the horizontal axis passes through the point 1 sec. (In this, to the authors of the report [79] were just lucky. There is such point on Fig. 6.1). Next, see Fig. 6.3.

An estimate of random walk can be calculated from the Allan variance plot on the range of averaging times from 0.1 to 10 seconds, where according to Fig. 14 this curve must have a slope of $-1/2$ in log-log scale. After fitting an LSQ line on this range with slope $-1/2$, a random walk estimate (ARW) can be computed as following:

$$ARW = \sigma_a(\tau) \sqrt{\tau}, \quad (6)$$

where, σ_a – Allan STD (deg/hour) at averaging time τ (hour) for any point on this line between 0.1 and 10 seconds.

As can be seen from Fig.17, the ARW value for the “AIST-100” gyro can be found as:

$$ARW = 5.1 \sqrt{\frac{1}{3600}} = 0.085 \text{ deg}/\sqrt{\text{hour}}. \quad (7)$$

In-run bias instability for the gyro between averaging times 10 and 100 seconds is equal to 2.5 deg/hour, which can be considered as a very good value for a low-cost and miniature gyro that can be produced in large volume.

Fig. 6.3. The quote from the report [79] in the analysis of the parameters of the noise on the basis of Allan graph (Fig. 6.1)

What are the misconceptions and mistakes? This is obvious to a triviality. Firstly, from the graph in Fig. 6.1 can not be determined not only the magnitude of the angle random walk, but even its presence in the mixture of noises. The maximum that can be done is to accept the hypothesis (it is believable, basing on the experience) that the white noise in angular velocity exists and estimate an upper its magnitude. See Fig. 5.1. Line segment with slope $-1/2$ in Fig. 6.1 can be associated with the contribution of a Markov process in Allan $\sigma(\tau)$ -graph, but not angle random walk, which partial contribution to the ray (not segment) with a slope of $-1/2$ passes through the leftmost point of Allan graph. – See again Fig. 5.1. For the upper estimate the value of N it is necessary through the leftmost point of Allan $\sigma(\tau)$ -graph to carry out the ray with tilt $-1/2$ (See Fig. 6.1). If such ray crosses the Allan $\sigma(\tau)$ -graph, the ray needs to be displaced below (by parallel translation) to contact with Allan $\sigma(\tau)$ -graph in one point. On the base of the ray, constructed thus, it is possible to determine (by known algorithm [66]) the assessment of N (the upper assessment). Even visually (“approximately”) from Fig. 6.1 it is visible that the upper assessment of N is less than $0.085 \text{ deg}/\text{hr}^{1/2}$ [79] (Fig. 6.3) approximately in (10–20) times. Besides, owing to effect of “summation” (4.8) N is less than upper assessment, at least, in some times. Visually from Fig. 6.1 (taking into account the experience), N is estimated in the range (0.006–0.001) $\text{deg}/\text{hr}^{1/2}$. The bias instability coefficient B on the basis of the graph (Fig. 6.1) taking into account the graph (Fig. 6.2) is determined in [79] by

a tangent arrangement to the minimum value of Allan $\sigma(\tau)$ -graph (Fig. 6.1). First, if to follow the “logic” of Fig. 6.2, it would be necessary to consider coefficient $1/0,664$ [66] (see Fig. 6.4). But in the presence of mix of noises, the tangent to the minimum value of Allan $\sigma(\tau)$ -graph, as a rule, gives the overestimated assessment. In Fig. 6.5 and Fig. 6.6 the examples of two mixes of noises are given. These examples demonstrate that the real bias instability coefficient B is less than its assessment based on a tangent to local a minimum of Allan $\sigma(\tau)$ -graph respectively in 4 times and in 20 times.

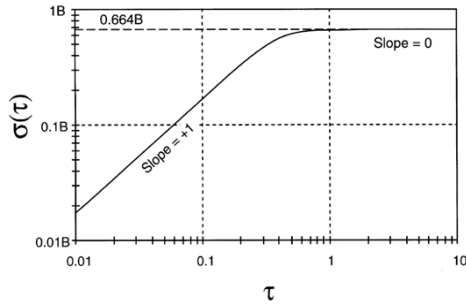


Fig. 6.4. Contribution of bias instability in Allan $\sigma(\tau)$ -graph

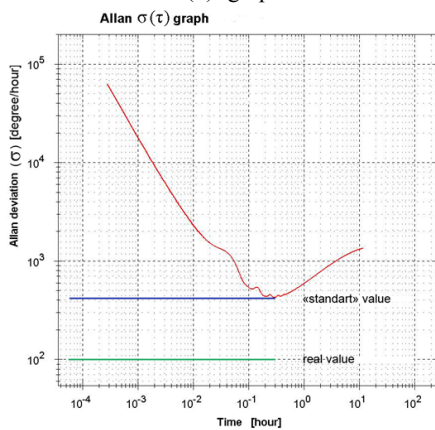


Fig. 6.5. 4-fold difference B value, compared with the estimate

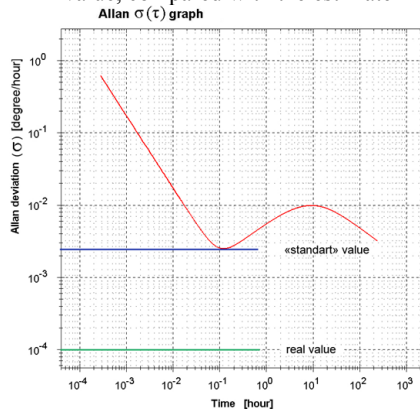


Fig. 6.6. The difference is 20 times B values, compared with the estimate

Authors of the report [79] sincerely misinterpreted regarding interpretation of Allan $\sigma(\tau)$ -graph (Fig. 6.1) since they were mistaken in estimates of precision characteristics of their gyroscope “not in their favor”. From Fig. 6.1 it is obviously that precision characteristics of MMG “AIST-100” [79] is significantly better: coefficient N is not $0.085 \text{ deg/hr}^{1/2}$, but no more than $(0.006-0.001) \text{ deg/hr}^{1/2}$; coefficient B is not 2.5 deg/hr , but no more than 1 deg/hr . These improved estimates can be improved still, analyzing primary data.

This help the author makes for O.A. Mezentsev – the co-author of the report [79] in gratitude for that that namely he in 2007 told the author about the existence of program Alavar 5.2 in the Internet.

The second example – the report of 2012-year [85]. That FOGs of the leading developers have long-term stability $\sim 0.0001 \text{ deg/hr}$ doesn't raise doubts. Estimates follow from Allan $\sigma(\tau)$ -graph submitted in Fig. 6.7 for iXblue FOG (Astrix 200): the bias instability $\sim 4 \times 10^{-5} \text{ deg/hr}$, the angle random walk $\sim 2 \times 10^{-4} \text{ deg/hr}^{1/2}$. Only for LG is “offensive” since in the report [85] as comparison of FOG and LG the level of accuracy of modern LG is specified $(0.01-0.003) \text{ deg/hr}$. Apparently, the author of the report [85] didn't notice that LG accuracy level: the bias instability – less than 0.0001 deg/hr ; the angle random walk – less than $0.00001 \text{ deg/hr}^{1/2}$, instability of scalefactor – less than 0.01 ppm was reached in LG on different schemes DILAG in the USA slightly earlier year of the publication the book [86], and in the People's Republic of China – a bit later. But an essence is not in it. In the text of the report [85] there is not Allan $\sigma(\tau)$ -graph. But in presentation of the report [85] Allan $\sigma(\tau)$ -graphs were presented (Fig. 6.7 and Fig. 6.8). We shall use these graphs for explanation one more typical misconception in interpretation of structure and an assessment of parameters of noises. We shall explain the “screen”-effect when the white noise in angular velocity is screened by contribution of Markov process with small time of correlation. From Fig. 6.8 it is visible that in the left part of Allan $\sigma(\tau)$ -graph there is “logjam” or typical for FOG “hump” (or several “humps” as it is in Fig. 6.8). What is it? Obviously, it is partial contributions of Markov processes with small times of correlation.

We shall explain in details by means of Fig. 6.9 and Fig. 6.10. In Fig. 6.9 Allan $\sigma(\tau)$ -graph of noises of FOG of JSC

NPK Optolink OIUS 1000 is presented. In Fig. 6.9 the dimension $[\tau]$ is the number of cycles of FOG output; frequency of output is 100 Hz , the dimension $[\sigma(\tau)]$ is deg/hr . The upper assessment of angle random walk is $4 \times 10^{-4} \text{ deg/hr}^{1/2}$. What is the real angle random walk coefficient? Whether it is possible to reduce the upper assessment? Yes, it is possible. – See Fig. 6.10. But for this purpose it is necessary to know parameters of Markov process – amplitude and time of correlation. It is possible to arrive more simply, by changing the time of correlation of Markov process with the aim to move the “hump” on Allan $\sigma(\tau)$ -graph to the right. No sooner said than done. For the first time such type target experiment was made by NPK Optolink Ltd.

In Fig. 6.11 and Fig. 6.12 the result of target experiment – Allan $\sigma(\tau)$ -graphs based on results of tests of the same FOG OIUS 1000 (No. 12020) with a frequency of output 2000 Hz is presented. The only change which was made for the “purity of experiment”, – only parameters of Markov process were changed with other things being equal. Primary data were processed by the same Alavar 5.2 program.

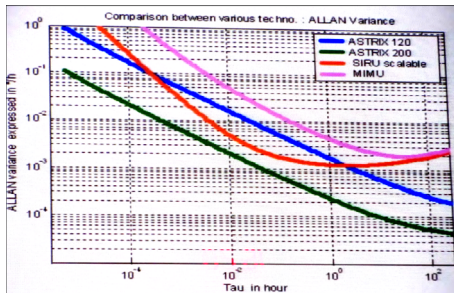


Fig. 6.7. Photo of the presentation of the report [85]

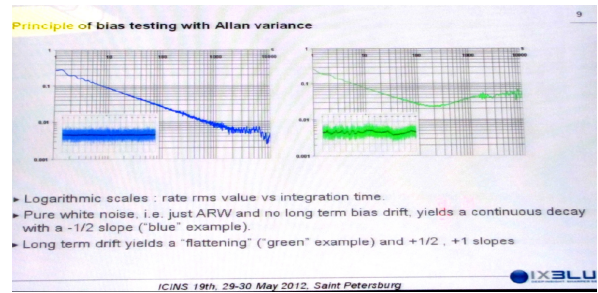


Fig. 6.8. Photo of the presentation of the report [85]

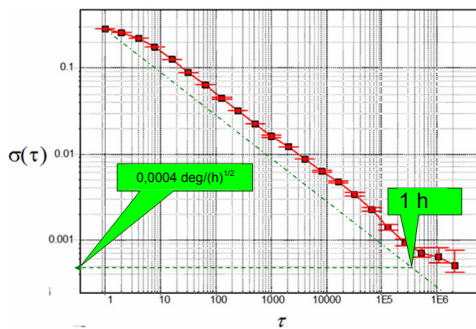


Fig. 6.9. Allan $\sigma(\tau)$ -graph of noises of FOG OIUS 1000

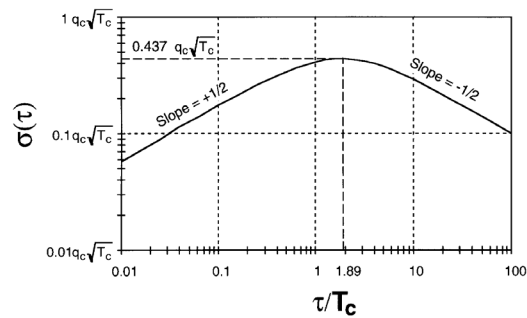


Fig. 6.10. The partial contribution of Markov noise in Allan $\sigma(\tau)$ -graph [67]

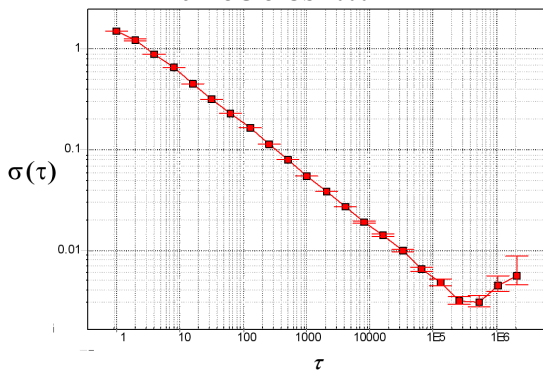


Fig. 6.11. Allan $\sigma(\tau)$ -graph of noises of FOG OIUS 1000 (option No. 1 of parameters of a Markov process)

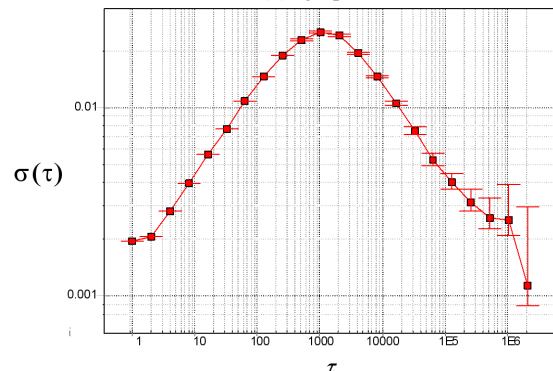


Fig. 6.12. Allan $\sigma(\tau)$ -graph of noises of FOG OIUS 1000 (option No. 2 of parameters of a Markov process)

From the graphs in Fig. 6.11 and Fig. 6.12 it is obvious: upper estimate of the white noise of FOG reduced by three orders of magnitude. Indeed, from $\sigma(\tau)$ -graph in Fig. 6. 11 the upper estimate is as follows:

$$\frac{1}{(3600 \cdot 2000)^{1/2}} = \frac{1}{600(20)^{1/2}} = \frac{(5)^{1/2}}{6} \cdot 10^{-3} \text{ [deg/hr}^{1/2}\text{]}.$$

From $\sigma(\tau)$ -graphs in Fig. 6.12 the upper estimate is as follows:

$$\frac{0,002}{(3600 \cdot 2000)^{1/2}} = \frac{0,002}{600(20)^{1/2}} = \frac{2 \cdot (5)^{1/2}}{6} \cdot 10^{-6} = \frac{(5)^{1/2}}{3} \cdot 10^{-6} < 10^{-6} \text{ [deg/hr}^{1/2}\text{]}.$$

So. Level of white noise of FOG of the Russian development is less than $10^{-6} \text{ deg/hr}^{1/2}$ and not inferior to the best samples of FOG of the leading developers [87, 88]. More exact estimates (still reducing the abovementioned estimate) of real level of white noise of FOG will be published soon by the developer – RPC OPTOLINK Ltd. Visually (according to graphs in Fig. 6.10 and Fig. 6.12): $\sim (10^{-7} - 10^{-8}) \text{ deg/hr}^{1/2}$.

This help the author makes for H.C. Lefevre in connection with his report [85] and for all FOG developers.

The author equally well applies to LG, FOG and new quantum gyros [89]. Why is that? ⁵

The third (and the last) example – in many reports real noises of various sensitive elements the authors try to spread out on the base of five known noises which make a partial contribution in Allan $\sigma(\tau)$ -graph with slopes: $-1, -1/2, 0, +1/2, +1$ (Fig. 6.2). What it is possible to tell? It is obvious that other noises existing in mix (except these five) are converted into uncertainty of estimates of parameters of five “basic” noises. What to do, – under the lamp, really, is lighter.

But it is possible to work differently, – systematically study noises to find new types and bring them in “basic” noises for error models of the corresponding sensitive elements.

7. Allan variances and Allan $\sigma(\tau)$ -graphics for new, previously not considered, types of noise

Allan variance (4.1) can be calculated for any temporary row, but on the basis of (5.1) analytical expression is possible to calculate only for such types of the noises which are given by the power spectral density of noise for which the integral (5.1) converges.

In table 7.1, Allan variances for three infinite (calculating) sets for new (unaccounted in the IEEE standards on gyroscopes) noises with spectral density of power noise which are equal to zero at a zero frequency are presented. The existence of a symbol of imaginary unit i ($i^2 = -1$) in two of three formulas for real functions shouldn't mislead. See the prompt from Leonard Euler: $e^{i\pi} = -1$.

Table 7.1

$S_{\omega}(f)$	$\sigma^2(\tau)$
$\alpha f^n e^{-\beta f}$	$\frac{\alpha \Gamma(n-1)}{4\pi^2 \tau^2} [6\beta^{1-n} - 4(\beta - 2i\pi\tau)^{1-n} - 4(\beta + 2i\pi\tau)^{1-n} + (\beta - 4i\pi\tau)^{1-n} + (\beta + 4i\pi\tau)^{1-n}];$ $\Gamma(z) = \int_0^{\infty} t^{z-1} e^{-t} dt \text{ — Euler gamma function; } n > 1$
$\alpha f^n e^{-\beta f^2}$	$\frac{\alpha}{4\pi^2 \tau^2} \beta^{1/2-n/2} \Gamma\left(\frac{1}{2}(n-1)\right) \left[3 + F_1\left(\frac{1}{2}(n-1), \frac{1}{2}, -\frac{4\pi^2 \tau^2}{\beta}\right) - 4F_1\left(\frac{1}{2}(n-1), \frac{1}{2}, -\frac{\pi^2 \tau^2}{\beta}\right) \right];$ $\Gamma(z) = \int_0^{\infty} t^{z-1} e^{-t} dt; \quad F_1(a, b, c) = \sum_{k=0}^{\infty} \frac{(a)_k}{(b)_k} \frac{z^k}{k!} \text{ — hypergeometric function of the first kind;}$ $(a)_n \equiv \frac{\Gamma(x+n)}{\Gamma(x)} = x(x+1) \dots (x+n-1) \text{ — Pochhammer symbol; } n > 1$
$\alpha f^n e^{-\beta f} \cos(cf)$	$\frac{4\alpha}{\pi^2 \tau^2} \frac{\Gamma(1+n)}{32} \{ 6(b-ic)^{-1-n} + 6(b+ic)^{-1-n} + [b-i(c-4\pi\tau)]^{-1-n} + [b+i(c-4\pi\tau)]^{-1-n}$ $-4[b-i(c-2\pi\tau)]^{-1-n} - 4[b+i(c-2\pi\tau)]^{-1-n} - 4[b-i(c+2\pi\tau)]^{-1-n} - 4[b+i(c+2\pi\tau)]^{-1-n}$ $+ [b-i(c+4\pi\tau)]^{-1-n} + [b+i(c+4\pi\tau)]^{-1-n} \}$

⁵ First, in October, 1975 at the excursion in SRI AP, preceding distribution of third-year students (MIPT group 355 FFKE) to “base” laboratories, the author saw for the first time with his own eyes various models of LG, some of which were mastered in mass-produced and accepted to operate on various objects (earlier than in the USA) and various model samples of FOG which were developed for some years. The author gave advice then (of course, already the third-year Fystekh student, already something understanding in physics) to the FOG developers of SRI AP: "Use the solitonic mode in FOG. Dispersion of solitons in fiber is minimum. Receive the best stability of zero". No, the author doesn't mistake with dates. The author perfectly knows that there was half a year before first publications concerning FOG [90]. And the first published result [90] was trivial: the interferential picture from the laser radiation missed through 10 meter piece of the light guide. Therefore at youth conferences to which (after the report [89]) invite, the author isn't tired to speak: "Dear colleagues! If you have received a result, – publish it! Don't shelve! I am a witness myself of USSR lost a world priority in creation of FOG. And don't follow my example; I can publish results 10 years, and 20 years, and 30 years [91] and even 40 years later [48]". And today – 35 years later.

Secondly, in August, 1979 to the author, already young engineer, it was necessary to work at one table in laboratory No. 69 of SRI AP with Nikolay Glavatskikh – a young engineer too, the graduate of physical faculty of MSU. On the one half of a table the author tried to integrate error KE of SINS (2.19) in quadratures [7] that one formula would be able to consider a contribution of any noise (any gyroscope) to an error of orientation of SINS and not to consider commensurable deposits of different noise in the first and any n-number order (2.22). On the second half of the table Nikolay Glavatskikh assembled the FOG model according to some new optic-physical scheme. He had no equipment. The author advised him: "Nikolay! Have you not been taught at physical faculty how to solve problems [7]? Stop torturing yourself, make all from one piece of fiber". The all-fiber technology of FOG really took place. Such technology also was invented by Physics and Technology faculties messmates in SRI AP (nowadays as a part of Fizoptika), and Honeywell in the USA.

Thirdly, results of the theory of SINS based on LG [11] are automatically transferred to the theory of SINS on FOG and other gyros.

Allan variances and asymptotics of Allan deviation for some special cases of the noises are presented in table 7.1. Allan variance and asymptotics of Allan deviation for other type of noise are presented in table 7.3.

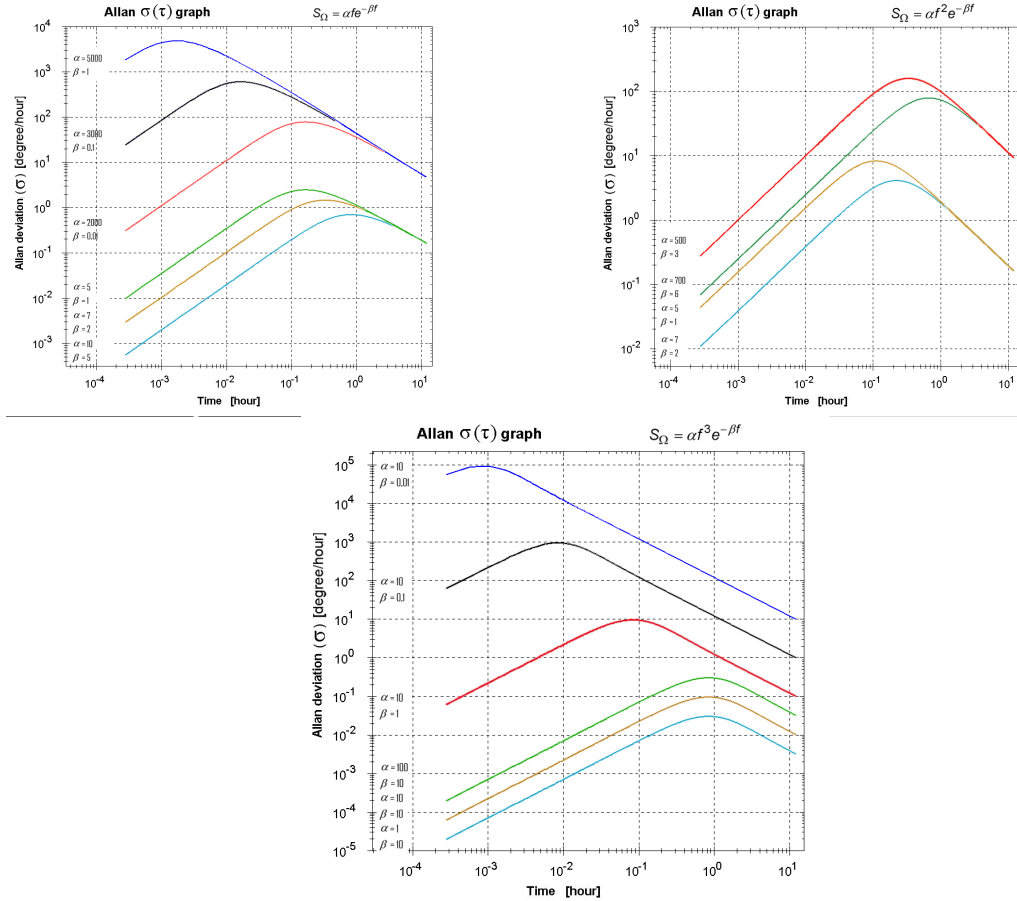
Table 7.2

$S_{\omega}(f)$	$\sigma^2(\tau)$	$\sigma(\tau), \tau \rightarrow 0$	$\sigma(\tau), \tau \rightarrow \infty$
$\alpha f e^{-\beta f}, \beta > 0$	$-\frac{\alpha}{4\pi^2\tau^2} [\ln(\beta^2 + 16\pi^2\tau^2) - 4\ln(\beta^2 + 4\pi^2\tau^2) + 6\ln\beta]$	$\frac{2\sqrt{6\alpha\pi}}{\beta^2} \tau$	$\sqrt{\frac{3\alpha}{2\pi^2\tau^2} \ln\left(\frac{4^{1/3}\pi\tau}{\beta}\right)}$
$\alpha f^2 e^{-\beta f}, \beta > 0$	$\frac{96\alpha^2\pi^2\tau^2}{\beta(\beta^2 + 4\pi^2\tau^2)(\beta^2 + 16\pi^2\tau^2)}$	$4\pi\sqrt{\frac{6\alpha}{\beta^5}}\tau$	$\frac{1}{\pi}\sqrt{\frac{3\alpha}{2\beta}}\tau^{-1}$
$\alpha f^3 e^{-\beta f}, \beta > 0$	$\frac{96\alpha\pi^2\tau^2(5\beta^4 + 60\beta^2\pi^2\tau^2 + 60\pi^4\tau^4)}{\beta^2(\beta^2 + 4\pi^2\tau^2)^2(\beta^2 + 16\pi^2\tau^2)^2}$	$4\pi\sqrt{\frac{30\alpha}{\beta^6}}\tau$	$\frac{1}{\pi\beta}\sqrt{\frac{3\alpha}{2}}\tau^{-1}$
$\alpha f^2 e^{-\beta f^2}$	$\frac{-4\pi^2\tau^2 \frac{\pi^2\tau^2}{\beta} - 4e^{-\frac{\pi^2\tau^2}{\beta}}}{4\beta^{1/2}\pi^{3/2}\tau^2} \alpha(3 + e^{-\frac{\pi^2\tau^2}{\beta}})$	$\sqrt{\frac{3\alpha\pi^{5/2}}{2\beta^{5/2}}}\tau^{-1}$	$\sqrt{\frac{3\alpha}{4\beta^{1/2}\pi^{3/2}}}\tau^{-1}$
$\alpha f^3 e^{-\beta f^2}$	$\frac{\alpha}{\beta^{3/2}\pi\tau} \left(2D\left(\frac{\pi\tau}{\beta^{1/2}}\right) - D\left(\frac{2\pi\tau}{\beta^{1/2}}\right) \right), D(x) \text{ — Dawson function}$	$\sim \tau$	$\sim \tau^{-1}$

Table 7.3

$S_{\omega}(f)$	$\sigma^2(\tau)$	$\sigma(\tau), \tau \rightarrow 0$	$\sigma(\tau), \tau \rightarrow \infty$
$\frac{\alpha f^2}{\beta^2 + f^2}, \beta > 0$	$\frac{\alpha}{4\beta\pi\tau^2} (3 - 4e^{-2\beta\pi\tau} + e^{-4\beta\pi\tau})$	$\sqrt{\alpha}\tau^{-1/2}$	$\left(\frac{3\alpha}{4\beta\pi}\right)^{1/2} \tau^{-1}$

Graphs of Allan deviation for several new types of noises are submitted in Fig. 7.1.



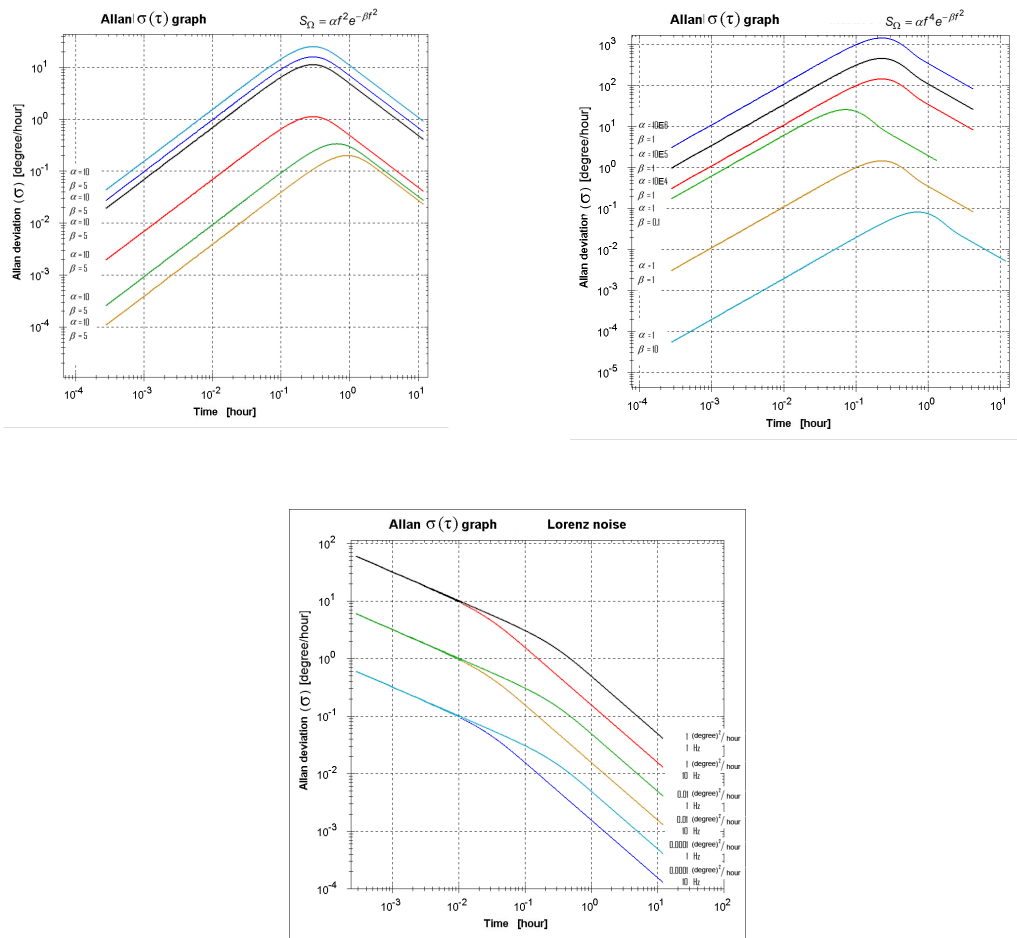


Fig. 7.1. Graphs of Allan deviation for several new types of noises

Conclusions

In the first part of the report it is strictly and visually shown:

- the kinematic error equations of the platform INS and strapdown INS are essentially differ;
- the wide class of noises of gyroscopes which make a contribution to “drift” of GSP only in the second order (therefore – “small”), leads to an error of orientation of SINS in the first order (therefore – “big”) – one and that concrete noise of gyroscopes leads to different SINS orientation errors, depending on a type of rotation of the object (except white noise in angular velocity);
- at one and that rotation of object, different noises are making different contribution to SINS orientation error;
- minimum necessary information about the noises of the three of gyroscopes is a correlation matrix of noises, at acceptance of a hypothesis about Gaussian statistics of noises;
- significantly more “thin” identification of structure of noise of gyroscopes is necessary for the gyroscopes intended for application in SINS in comparison with application of gyroscopes in GSP,

In the second part of the report there are three ideas:

1) Allan variance method is an effective method for identification of noise. The undoubted advantage of a method is the “infrastructure” which is developed in details for half a century [92-95] – justification of a method, the technics – graphs of Allan deviation, the software, IEEE standards with use of Allan variance method.

2) Allan variance method, as well as any other method, it is necessary to study that is given only by practice. And if to use a method because it is “fashionable”, without understanding an essence, it is possible to do many ridiculous mistakes.

3) The following step in study and development of Allan variance method (and its generalizations [21]), from the point of view of the author for the noises of gyroscopes, it is systematic research of noises, elaboration of error models, including taking into account new noise types for various gyroscopes.

The team of designers led by the actively working father of the Russian gyroscopy and inertial navigation technology, intended for marine and oceanic applications rather than space and rocket ones, the Academician V.G. Peshekhonov will probably offer some other promising ways of developing methods for identification of

the structure and parameter estimation of noise in inertial sensors. This team has laid a substantial scientific and technical groundwork in the field of nonlinear filtering [96–99].

The author is grateful to the closest pupils for the operational help with preparation of separate fragments of this report for the "round table" ICINS-2015. A.I. Bidenko, at the request of the author to help him with creation of graphs, has transferred all requests to the programm-mathematical complex (Fig. 3.3-3.6, 5.1, 5.2, 6.5, 6.6, 7.1). N.V. Tribulev, at the request of the author to help him to choose tabular integrals [100] for which the integral (5.1) converges, first of all in cases (2.43), has prepared tables (7.1-7.3), has checked them with program "Mathematics" and simultaneously has added by means of this program some formulas for Allan variance which didn't follow from tabular integrals [100].

"The teacher, prepare pupils that was at whom then to study!"

References

1. **Charles Stark Draper**. URL: https://en.wikipedia.org/wiki/Charles_Stark_Draper.
2. **Charles Stark Draper Laboratory**. URL: https://en.wikipedia.org/wiki/Charles_Stark_Draper_Laboratory#Inertial_navigation
3. **Draper at 25**. Innovation for the 21st Century. URL: <http://www.draper.com/Documents/draperat25.pdf>.
4. **Dreiper**. Priboenaya tekhnika i inertsial'noe navedenie, Voprosy raketnoi tekhniki, 1961, no.1, pp. 70-91; no. 2, pp. 46-73.
5. **Advanced Inertial Reference Sphere**. URL: http://en.wikipedia.org/wiki/Advanced_Inertial_Reference_Sphere.
6. **Advanced Inertial Reference Sphere**. URL: <http://nuclearweaponarchive.org/Usa/Weapons/Airs.html>.
7. **Krobka, N.I.** Strategiya resheniya otkrytykh zadach i assimetriya vrashcheniya vokrug tochki vpravo i vlevo, Kontsept, 2014, Sovremennye nauchnye issledovaniya, no. 2, ART 55199. URL: <http://e-koncept.ru/2014/55199.htm>.
8. **Javan, A., Bennett, W.R. and Herriott, D.R.**, Population Inversion and Continuous Optical Maser Oscillation in a Gas Discharge Containing a He-Ne Mixture, Phys. Rev. Lett., 1961, vol. 63, pp. 106-110.
9. **Macek, W.M., Davis, D.T.M.**, Rotation rate sensing with travelling-wave ring laser, Appl. Phys. Lett., 1963, vol. 2, no. 3, pp. 67-68.
10. **Branets, V.N., Shmyglevskii, I.P.**, Primenenie kvaternionov v zadachakh orientatsii tverdogo tela, Moscow, Nauka, 1973.
11. **Krobka, N.I.** The triaxial laser gyroscopes and the theory their application in strapdown inertial systems: Cand. Sci. Dissertation, NII prikladnoi fiziki, Moscow, 1985.
12. **Krobka, N.I.** Nekommutativnye kinematicheskie efekty i ikh osobennosti v lazernoi giroskopii i besplatformennoi inertsial'noi navigatsii, II Sankt-Petersburgskaya mezhdunarodnaya konferentsia po giroskopicheskoi tekhnike I navigatsii. Ch. I., Sankt-Petersburg, Nauchnyi sovet RAN po problemam upravleniya dvizheniem i navigatsii. TsNII Elektropribor, 1995, pp. 151-151.
13. **Krobka, N.I.**, Nekommutativnye kinematicheskie efekty vrashcheniya tverdogo tela vokrug tochki i ikh proyavleniya v osobennostyax postroyeniya besplatformennykh sistem orientatsii na lazernykh i volokonno-opticheskikh giroskopakh, Vestnik Nizhegorodskogo universiteta im. N.I. Lobachevskogo, 2011, no. 4 (2), pp. 181-183.
14. **Krobka, N.I.**, Accurate error equations of the strapdown inertial navigation systems, The Second Soviet-Chinese Symposium of Inertial Tecnology, Chief editor V.G. Peshekhonov, Saint Petersburg, The Scientific Council on Problems of Motion Control and Navigation of the Academy of Sciences, Chinese Society of Inertial Technology, CSRI "Elektropribor", 1992, pp. 43-50.
15. **Krobka, N.I.**, Application features of three-axis laser gyros in strapdown inertial navigation systems, The IV Russian-Chinese Symposium on Inertial Technology, Saint Petersburg, St. Petersburg Section of the Scientific Council on Movement Control and Navigation Problems of the RAS, Chinese Society on Inertial Technology, 1993, pp. 54-63
16. **Krobka, N.I.**, The features of the strapdown inertial orientation systems based on three-axis fiber-optic gyros with one common light source, Jubilee 15th Saint Petersburg International Conference on Integrated Navigation Systems, Saint Petersburg, The SRC of the RF Central Scientific and Research Institute "Elektropribor", 2008, pp. 89-91.
17. **Krobka, N.I.**, Non-commutative kinematic effects and laws of fiber-optic gyro noise accumulation in strapdown inertial orientation systems, 16th Saint Petersburg International Conference on Integrated Navigation Systems, Saint Petersburg, SRC of the Russian Federation Central Scientific and Research Institute "Elektropribor", 2009, pp. 69-72.
18. **Krobka, N.I.**, A New Noncommutative Kinematic Effect and Its Manifestations in Strapdown Inertial Orientation Systems Based on Fiber Optic Gyros, Gyroscopy and Navigation, 2010, vol. 1, no. 1, pp. 26-36.
19. **Krobka, N.I.** The concept of accurate equations of errors and estimations of quantum limits of accuracy of strapdown inertial navigation systems based on laser gyros, fiber-optical gyros, and atom interferometers on de Broglie waves, 17th Saint Petersburg International Conference on Integrated Navigation Systems, Saint Petersburg: State Research Center of the Russian Federation Concern CSRI Elektropribor, JSC, 2010, pp. 95-112.
20. **Krobka, N.I.**, Differential methods for identification the structure of noises of fiber-optical and other gyros, 17th Saint Petersburg International Conference on Integrated Navigation Systems, Saint Petersburg: State Research Center of the Russian Federation Concern CSRI Elektropribor, JSC, 2010, pp. 63-66.
21. **Krobka, N.I.**, Differential Methods of Identifying Gyro Noise Structure, Gyroscopy and Navigation, 2011, vol. 2, no. 3, pp. 126-137.
22. **Krobka, N.I.**, Estimating Quantum Limits on SINS Accuracy Based on Accurate Error Equations, Gyroscopy and Navigation, 2014, vol. 5, no. 1, pp. 9-19.
23. **Klauder, J.R., Sudarshan, E.C.G.**, Fundamentals of Quantum Optics, New York-Amsterdam, Bell Telephone Laboratories, Syracuse University, 1968.
24. **Akhmanov, S.A., D'yakov, Yu.E., Chirkin, A.S.**, Vvedenie v statisticheskuyu radiofiziku i optiku, Moscow, Nauka, 1981.
25. **Sveshnikov, A.A.** Prikladnye metody teorii metody sluchainykh funktsii, Moscow, Nauka, 1968.
26. **Krobka, N.I., Sviridov, M.V.**, On the influence of random perturbations of the angular velocity on the solution of the kinematic problem, Izvestiya AN SSSR, MTT, 1984, no. 1, pp. 145-150.
27. **Krobka, N.I., Sviridov, M.V.**, Influence of a random frequency bias in a ring laser on the accuracy of rotation measurements, Kvantovaya elektronika, 1985, vol. 12, no. 2, pp. 363-367.

28. **Krobka, N.I.**, On the orders of the Chief Designer of NPO "Rotor" Academician V.I. Kuznetsov, the concept of strict errors equations and the new algorithm of strapdown inertial navigation systems (dedicated to the 100th anniversary of Academician VI Kuznetsov), IX Mezhdunarodnaya nauchno-tehnicheskaya konferentsiya "Girotehnologii, navigatsiya, upravlenie dvizheniem i konstruirovaniye aviatsionno-kosmicheskoi tekhniki", Kiev, NTUU "KPI", 2013, pp. 195-208.
29. **Gilvarry, J.J., Browne, S.H., Williams, I.K.**, Theory of Blind Navigation by Dynamical Measurements, J. of Applied Physics, 1950, vol. 21, no. 8, pp. 753-761.
30. **Andreev, V.D.**, Teoriya inertsial'noi navigatsii. Avtonomnye sistemy, Moscow, Nauka, 1966.
31. **Andreev, V.D.**, Teoriya inertsial'noi navigatsii. Korrektiruemye sistemy, Moscow, Nauka, 1967.
32. **Klimov, D.M., Rabinovich, Yu.I.**, About kinematic errors of inertial navigation systems, Izvestiya AN SSSR. Mekhanika, 1965, no. 6, pp. 49-52.
33. **Branets, V.N.**, On the accuracy of solutions of kinematic equations. 1. Error equations, Kosmicheskie issledovaniya, 1982, vol. 20, no. 2, pp. 145-150.
34. **Branets, V.N.**, On the accuracy of solutions of kinematic equations. 2. Using a quasi-coordinates, Kosmicheskie issledovaniya, 1982, vol. 20, no. 3, pp. 323-331.
35. **Jekeli, C.**, Navigation Error Analysis of Atom Interferometer Inertial Sensor, Navigation. Journal of the Institute of Navigation, 2005, vol. 52, no. 1, pp. 1-14.
36. **Golovan, A.A., Parusnikov, N.A.**, Matematicheskie osnovy navigatsionnykh sistem. Ch. I., Moscow, MGU, 2010, 2-e izdanie.
37. **Ishlinskii, A.Yu.**, Mekhanika sprtsial'nykh giroskopicheskikh sistem, Kiev, AN USSR, 1952.
38. **Goodman, L.E., Robinson, A.R.**, Effect of finite rotations on gyroscopic sensing devices, J. of Appl. Mech., 1958, vol. 25, no. 2, pp. 210-213.
39. **Devyanin, E.A., Ishlinskii, A.Yu., Klimov, D.M.**, Mekhanika giroskopicheskikh i navigatsionnykh sistem, Mekhanika v SSSR za 50 let. T. 1. Obschaya i prikladnaya mekhanika, Moscow, Nauka, 1968, s. 245-264.
40. **Andreev, V.D., Blyumin, I.D., Devyanin, E.A., Klimov, D.M.** Obzor razvitiya teorii giroskopicheskikh i inertsial'nykh navigatsionnykh sistem, Razvitie mekhaniki giroskopicheskikh i inertsial'nykh sistem, Moscow, Nauka, 1973, s. 33-72.
41. **Andreev, V.D., Devyanin, E.A.**, Avtonomnye inertsial'nye navigatsionnye sistemym, Razvitie mekhaniki giroskopicheskikh i inertsial'nykh sistem, Moscow, Nauka, 1973, s. 307-321.
42. **Doc Draper**. URL: <http://www.draperprize.org/docdraper.php>
43. **Krobka, N.I., Sviridov, M.V.**, Effect of random perturbations of the angular velocity on the solution of the kinematic problem, Mechanics of solids, 1984, vol. 19, no. 1, pp. 139-144.
44. **Krobka, N.I., Sviridov, M.V.**, Influence of a random frequency pedestal in a ring laser on the accuracy of rotation measurements, Sov. J. Quantum Electron, 1985, vol. 15, no. 2, pp. 232-234.
45. **SAO/NASA Astrophysics Data System (ADS)**. URL: http://adsabs.harvard.edu/cgi-bin/nph-abs_connect?return_req=no_params&author=Krobka,%20N.%20I.&db_key=PHY
46. **Peshkhonov, V.G.**, Leaders of national gyroscopy, Giroskopiya i navigatsiya, 2013, no. 3, s. 139-154.
47. **Krobka, N.I.**, Rabotu po lazernoi giroskopii v NII prikladnoi mekhaniki. Vospominaniya Krobki N.I. – zamestitelya Glavnogo konstruktora NII PM po napravleniyu lazernoi giroskopii, Prioritet – tochnost'. FGUP "NII PM im. Akademika V.I. Kuznetsova". 50 let, Pod obshechiy red. I.N. Sapozhnikova. Moscow, RESTART, 2006, pp. 161-165.
48. **Krobka, N.I., Balandin, A.I., Bidenko, A.I., Tribulev, N.V., Chernichenko, V.S.**, On a Misconception in the Theory of Inertial Navigation Passed Unnoticed for Many Decades, 20th Saint Petersburg International Conference on Integrated Navigation Systems. Proceedings, Saint Petersburg, SRC of the RF Concern CSRI Elektropribor, JSC, 2013, pp. 80-86.
49. **Krobka, N.I., Balandin, A.I., Bidenko, A.I., Keda, S.V., Tribulev, N.V., Chernichenko, V.S.**, Development of a Program-Mathematical Software Package for Identification of a Gyroscope Noise Structure and Simulation of Strapdown Inertial Orientation Systems, 20th Saint Petersburg International Conference on Integrated Navigation Systems. Proceedings, Saint Petersburg, SRC of the Russian Federation Concern CSRI Elektropribor, JSC, 2013, pp. 87-92.
50. **Effa Mark Leopoldovich**. URL: <http://pomnipro.ru/memorypage56484/biography>
51. **Prioritet – tochnost'**. FGUP "NII PM im. Akademika V.I. Kuznetsova". 50 let, Pod obshechiy red. I.N. Sapozhnikova. Moscow, RESTART, 2006.
52. **Matveev, V.A.**, Giroskop – eto prosto, Moscow, MGTU im. N.E. Baumana, 2012.
53. **Effa M.L.** Razrabotchik – tvorcheskii shans inzhenera, Referat zadumanoi M.L. Effoi knigi, kotoruyu on mechtal napisat', no ne uspel: "Ya – Razrabotchik".
54. **Krobka, N.I., Sapozhnikov, I.N.** Works on laser Gyroscopy in Applied Mechanics Scientific Research Institute named after academician V.I. Kuznetsov, The First International Conference on Inertial Technology, Saint Petersburg, Central Scientific and Research Institute "Elektropribor", 1994, pp. 3-12.
55. **Krobka, N.I.**, The results of the development of laser gyroscopes for strapdown inertial navigation systems, Giroskopiya i navigatsiya, 1995, no. 3, pp. 82-83.
56. **Allan, D.W.**, Statistics of Atomic Frequency Standards, Proc. of the IEEE, 1966, vol. 54, no. 2, pp. 221-230.
57. **Moscow Institute of Physics and Technogy**. State University. URL: <http://mipt.ru/en/>.
58. **Fiztekhportal. MFTI**. Internet-portal "Legendarnyi Fiztekhp". URL: <http://info.mipt.ru/>.
59. **50 let v stroyu Fiztekha**, Sostaviteli: Nozdrin, V.I., Prusakov, I.B., Sedov, B.S., Moscow, MFTI, 2004.
60. **Karlov, N.V. Oni sozdavali Fiztekhp**. (Po arkhivnym materialam i vospominaniyam), Moscow, MFTI, 2007.
61. **Kafedra fizicheskoi elektroniki**. Vypuskniki kafedry. URL: <http://mipt.ru/education/chairs/fizelectro/alumni/>.
62. **Mazan'ko, I.P.**, On the question of limiting the width of the spectral lines of the signal propagating in a medium with "negative temperature", Optika i spektroskopiya, 1964, vol. 17, no. 2, s. 203-208.
63. **Krobka, N.I.** Vliyaniye prostranstvennoi neodnorodnosti sil'nogo polya na spektral'nye kharakteristiki spontannogo izlucheniya: diplomnaya rabota, Moscow, MFTI. FFKE, 1979.
64. **Kur'yatov, V.N., Nasedkin, E.F., Semenov, B.N., Zhuravleva, E.N.**, Napravlenie lazernoi giroskopii vysokoi tochnosti, Lazery dlya mira i sozdaniya. NII "Polyus" imeni M.F. Stel'makha. 50 let, 2012.
65. **Rytov, S.M.**, Vvedeniye v statisticheskuyu radiofiziku, Moscow, Nauka, 1966.
66. **IEEE Std 952-1997**. IEEE Standard Specification Format Guide and Test Procedure for Single-Axis Interferometric Fiber Optic Gyros.

67. **IEEE Std 952-1997 (R2008)**. IEEE Standard Specification Format Guide and Test Procedure for Single-Axis Interferometric Fiber Optic Gyros.
68. **Krobka, N.I.**, On the concept of "error model" in the laser gyroscopy, XVIII mezhvedomstvennaya nauchno-tekhnicheskaya konferentsiya pamyati N.N. Ostryakova, Saint Petersburg, CSRI "Elektropribor", 1993, pp. 49-49.
69. **About Fizoptika**. URL: <http://www.fizoptika.ru/about/index.html>.
70. **Krobka, N.I.**, Gyroscopy on the Sagnac effect: Yesterday, Today and Tomorrow, XII konferentsiya molodykh uchenykh "Navigatsiya i upravlenie dvizheniem" (XII KMU 2010), Saint Petersburg, CSRI "Elektropribor", 2010. [Invited lecture].
71. **Krobka, N.I.** Eksperimental'nye issledovaniya shumov VOG filiala TsENKI "NII PM imeni Akademika V.I. Kuznetsova, Moscow, filial TsENKI "NII PM imeni Akademika V.I. Kuznetsova", KIND. E001.2402, 2008.
72. **Benzin – vash, idei – nashi**. URL: <http://dic.academic.ru/dic.nsf/proverbs/11939/>
73. **Topology**. URL: <https://en.wikipedia.org/wiki/Topology>.
74. **Krobka, N.I.**, On the influence of non-ideal onboard time scale on the structure of error equations and the accuracy of strapdown inertial navigation systems, 21st Saint Petersburg International Conference on Integrated Navigation Systems, Saint Petersburg, SRC of the Russian Federation Concern CSRI Elektropribor, JSC, 2014, pp. 361-364.
75. **Krobka, N.I.**, Differential methods of identifying gyro noise structure, Giroskopiya i navigatsiya, 2011, no. 1, pp. 59-77.
76. **Krobka, N.I.**, The conditions for Euler-Poisson kinematic equations integrability in quadratures, 5th Saint Petersburg International Conference on Integrated Navigation Systems, Saint Petersburg, Scientific Council of the RAS on the Problem of Motion Control and Navigation. State Scientific Center of Russia – CSRI "Elektropribor", 1998, pp. 37-44.
77. **Krobka, N.I.** Solution of the Euler kinematic problem, Giroskopiya i navigatsiya, 2005, no. 3, pp. 105-122.
78. **Krobka, N.I.**, The symmetry and asymmetry of three-dimensional rotations. Three reductions of the problem of integrating the kinematic equations in quadratures, Naukovo-tekhnichniy zbirnyk "Informatsiini systemy, mekhanika ta keruvannya", Kuiv, KPI, 2012, no. 7, pp. 05 [14 p.]. URL: http://ismk.kpi.ua/sites/default/files/ISMC_7/p_05.pdf.
79. **Mezentsev, A.P., Frolov, E.N., Klimkin, M.Yu., Mezentsev, O.A.**, Development, production and test results for a medium-accuracy MEMS INS "AIST-320" based on Colioliis vibratory gyro "AIST-100", 14th Saint Petersburg International Conference on Integrated Navigation Systems, Saint Petersburg, SRC of the RF CSRI "Elektropribor", 2007, pp. 9-18.
80. **iSense. About us**. URL: <http://www.isense.ru/en/o-kompanii/>.
81. **Pochemu logika veshch zheleznaya?** URL: <http://otvet.mail.ru/question/45099950>.
82. **Anekdot of Balagura**. URL: <http://balagur.info/anec/2011-01-06/9323a002c0a9d6d9/>.
83. **Anekdot**. URL: http://pikabu.ru/story/anekdot_1623090.
84. **IEEE Std. 1554-2005**. IEEE Recommended Practice for Inertial Sensor Test Equipment, Instrumentation, Data Acquisition and Analysis.
85. **Lefevre, H.C.**, The fiber-optic gyroscope: achievement and perspective, 19th Saint Petersburg International Conference on Integrated Navigation Systems. Proceedings, Saint Petersburg, SRC of the RF Concern CSRI "Elektropribor", 2007, pp. 122-126.
86. **Lefevre, H.C.**, The Fiber-Optic Gyroscope, Artech House, Boston-London, 1993.
87. **Sanders, S.J., Strandjord, L.K., and Mead, D.**, Fiber optic gyro technology trends – a Honeywell perspective, Optical Fiber Sensors Conference Technical Digest, 2002. OFS 2002, 15th, vol. 1, pp. P. 5-8.
88. **Pavlat, G.A.**, Fiber optic gyro based inertial navigation systems at Northrop Grumman, Optical Fiber Sensors Conference Technical Digest, 2002. OFS 2002, 15th, vol. 1, pp. 9-9.
89. **Krobka, N.I.**, Quantum micro-mechanics: gyros based on de Broglie waves and quantum features of superfluid liquids. State of the arts and development tendencies, 16th Saint Petersburg International Conference on Integrated Navigation Systems, Saint Petersburg, SRC of the RF CSRI "Elektropribor", 2009, pp. 150-163.
90. **Vali, V., Shorthill, R.W.**, Fiber Ring Interferometer, Appl. Opt., 1976, vol. 15, pp. 1099-1099.
91. **Krobka, N.I.**, The features of calibration of three-axis laser gyros with single vibrator and with recessively rotating basis (30 and 20 years later), 17th Saint Petersburg International Conference on Integrated Navigation Systems, Saint Petersburg, State Research Center of the Russian Federation Concern CSRI Elektropribor, JSC, 2010, pp. 67-70.
92. **Allan's TIME**. URL: <http://www.allanstime.com/>
93. **Research**. URL: <http://www.allanstime.com/Research/index.html>
94. **David W. Allan Publications**. URL: <http://www.allanstime.com/Publications/DWA/index.html>.
95. **It's About Time**. URL: <http://itsabouttimebook.com/>
96. **Stepanov, O.A.**, Primenenie teorii nelineinoy fil'tratsii v zadachakh obrabotki navigatsionnoy informatsii (Application of Nonlinear Filtering Theory for Processing Navigation Information), St. Petersburg, TsNII Elektropribor, 2003.
97. **Stepanov, O.A.**, Osnovy teorii otsenivaniya s prilozheniyami k zadacham obrabotki navigatsionnoy informatsii (Fundamentals of the Estimation Theory with applications to the problems of navigation information processing), Part 1, Vvedenie v teoriyu otsenivaniya (Introduction to the Estimation Theory), St. Petersburg, TsNII Elektropribor, 2010.
98. **Stepanov, O.A.**, Osnovy teorii otsenivaniya s prilozheniyami k zadacham obrabotki navigatsionnoy informatsii (Fundamentals of the Estimation Theory with applications to the problems of navigation information processing), Part 2, Vvedenie v teoriyu fil'tratsii (Introduction to the Filtering Theory), St. Petersburg, TsNII Elektropribor, 2012.
99. **Stepanov, O., Motorin, A.**, Identification of sensor errors: Allan variance vs nonlinear filtering, 21st Saint Petersburg International Conference on Integrated Navigation Systems, St. Petersburg, TsNII Elektropribor, 2014, pp. 123-128.
100. **Gradshteyn, I.S., Ryzhik, I.M.**, Tablitsy integralov, summ, ryadov i proizvedenii, Moscow, Gos. Izdatel'stvo fiziko-matematicheskoy literatury, 1963, izd. 4-e.

ACCURACY OF SENSOR BIAS ESTIMATION AND ITS RELATIONSHIP WITH ALLAN VARIANCE

O.A. Stepanov¹

Concern CSRI Elektropribor, JSC, ITMO University, St. Petersburg, Russia

I.B. Chelpanov²

State Polytechnical University, St. Petersburg, Russia

A.V. Motorin³

Concern CSRI Elektropribor, JSC, ITMO University, St. Petersburg, Russia

Abstract

Key words: sensor errors; parameter identification, Allan variance

The paper discusses the relationship between Allan variance and error variance of sensor bias estimation obtained by averaging over a certain time interval. Allan variance is shown to coincide with this variance in some cases. Thus, Allan variance plots can be used to predict the accuracy of bias estimation, which is critical for the sensors whose signals are integrated in inertial systems. Improving of bias estimation accuracy using nonlinear filtering methods is discussed.

Introduction

Identification of sensor error model and determination of its parameters form an important problem to be solved by tests and calibration. Traditionally, algorithms for determining the spectral densities and correlation functions are used to design the model of error random components [1-6]. Allan variance method is also extensively used [7-13]. New methods are searched for, based, for example, on nonlinear filtering methods [14-17]. Determination of time-invariant error components (random bias) is also important, especially when the signals of sensors incorporated in IMUs are integrated and thus lead to accumulation of errors. Bias is often determined by usual averaging of sensor errors over a finite time period. Then the question arises, how the averaging time should be rationally selected so that for example error variance of the obtained estimate be minimum. On the other hand, the estimate obtained by averaging obviously will not be optimal (in terms of minimum error variance) if nonwhite noise components of sensor errors are present. Therefore, bias estimation accuracy can also be improved by using more advanced algorithms which are not reduced to simple averaging but account for the additional error components. As is known, Allan variance is insensitive to the presence of bias, since error increments rather than errors are used to calculate the Allan variance. However, Allan variance plots are still used to estimate the so called bias instability [18, 19], which is actually associated with the problem of estimating the random bias. Discussion of these issues is given in the paper.

Estimation accuracy of the sensor bias by averaging. Connection with Allan variance

Let the sensor error $z(t)$ be measured, which can be described in the form

$$y(t) = c + z(t); \quad (1)$$

where $z(t)$ is a nonstationary zero-mean random process, c is the random bias. It is required to estimate c using measurements $y(t)$. This kind of problem often occurs in sensor calibration performed at the test bench or in comparison of their signals with a reference more precise sensor. It is often solved by simple averaging of the measured error over finite time interval τ , i.e.

$$\hat{c}_\tau = \frac{1}{\tau} \int_0^\tau y(t) dt = c + \frac{1}{\tau} \int_0^\tau z(t) dt. \quad (2)$$

¹ D. Sci., Professor. Head of Scientific and Educational Center, CSRI Elektropribor.

² D. Sci., Professor.

³ Postgraduate.

Obviously, the following can be written for the estimate error and its variance:

$$\hat{c}_\tau - c = \frac{1}{\tau} \int_0^\tau z(t) dt, \quad (3)$$

$$M \left\{ (\hat{c}_\tau - c)^2 \right\} = M \left\{ \left(\frac{1}{\tau} \int_0^\tau z(t) dt \right)^2 \right\}.$$

Considering variance (3) to be the variance of increments of process $\frac{1}{\tau} \int_0^\tau z(t) dt$ and denoting $\bar{z}(t, \tau) = \frac{1}{\tau} \int_{t-\tau}^t z(t^*) dt^*$, we get

$$M \left\{ (\hat{c}_\tau - c)^2 \right\} = M \left\{ (\bar{z}(t + \tau, \tau) - \bar{z}(t, \tau))^2 \right\}. \quad (4)$$

Assume that the following limiting relationship holds true:

$$M \left\{ (\hat{c}_\tau - c)^2 \right\} = \frac{1}{2} \lim_{T \rightarrow \infty} \frac{1}{T} \int_{-T}^T (\bar{z}(t + \tau, \tau) - \bar{z}(t, \tau))^2 dt, \quad (5)$$

meaning that calculation of mathematical expectation in (4) can be replaced with time averaging for one sample.

It can be easily seen that (5) coincides with the Allan variance [6, 8, 23]. Therefore, Allan variance coincides with the error variance of bias estimation calculated by averaging if (5) is valid for process $\bar{z}(t, \tau)$. Then optimal averaging time can be determined by Allan variance minimum point, and thus, corresponding minimum error variance of bias estimate found by averaging. Respectively square root of the Allan variance also called the Allan deviation [8,9,11] is the same as the root mean square (RMS) for the bias estimation error. The established relation seems helpful because it lets assess the accuracy of bias estimation by Allan variance plots insensitive to bias.

Consider an example. Let

$$y(t) = x(t) + \rho v(t), \quad (6)$$

where $x(t)$ is the random walk (Wiener process) set in the form $\dot{x} = qw$, $x(0) = 0$; qw , $\rho v(t)$ are independent zero-mean white noises with power spectral densities (PSD) q^2 and ρ^2 , noises $w(t)$, $v(t)$ have unit PSDs. In other words, process $y(t)$ is a sum of random walk and white noise. Searching for estimate in the form (2), we can write:

$$\hat{c}_\tau - c = \frac{1}{\tau} \int_0^\tau x(t) dt + \frac{\rho}{\tau} \int_0^\tau v(t) dt. \quad (7)$$

It can be easily seen that the following relation is true for estimate error variance:

$$M \left\{ (c - \hat{c}_\tau)^2 \right\} = \frac{q^2}{\tau^2} M \left\{ \left(\int_0^\tau \int_0^\tau w(t) dt dt \right)^2 \right\} + \frac{\rho^2}{\tau^2} M \left\{ \left(\int_0^\tau v(t) dt \right)^2 \right\}. \quad (8)$$

Note that squared first and second integrals of white noise are under the signs of mathematical expectation in (8). Therefore, these mathematical expectations determine the variances of the first and second integrals. Using the known expressions for these variances [6], we obtain the expression

$$\sigma_{\Delta c}^2 = M \left\{ (c - \hat{c}_\tau)^2 \right\} = \frac{q^2 \tau}{3} + \frac{\rho^2}{\tau}, \quad (9)$$

coinciding with the Allan variance for the sum of random walk and white noise. Differentiating (9) with respect to τ and setting the derivative equal to zero provides optimal (in terms of minimum variance) average time and corresponding minimum estimate variance:

$$\tau_{opt} = \frac{\sqrt{3}\rho}{q}, \quad \sigma_{\Delta c(\min)}^2 = \frac{2\rho q}{\sqrt{3}}. \quad (10)$$

Therefore averaging time optimal in the given sense is directly proportional to the square root of the ratio between white noise PSD and PSD of generating noise of random walk, and error variance is directly proportional to their product.

This example is illustrated by the simulation. Figure 1 shows real bias estimation RMS error calculated using 500 samples for six various time intervals vs Allan deviation for one sample. Note that the calculated from finite length sample AV is the estimate the true AV (5). This explains the incomplete match graphs in Figure 1, especially for large averaging time.

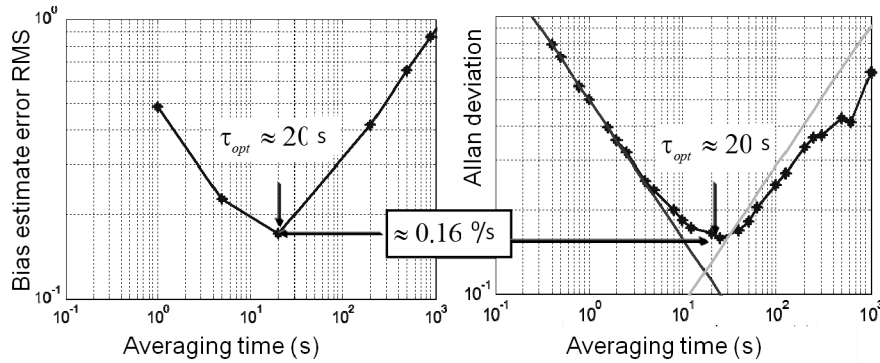


Fig. 1. Real RMS: bias estimation by averaging (left) and Allan deviation (right).

Note that the location of Allan variance minimum point in this statement depends on the ratio between PSDs of white noise and generating noise of random walk, as follows from (10). This is also illustrated in Fig. 2 showing Allan variances for four variants of error components

$$y_{11}(t) = x_1(t) + \rho_1 v(t); y_{12}(t) = x_1(t) + \rho_2 v(t); y_{21}(t) = x_2(t) + \rho_1 v(t); y_{22}(t) = x_2(t) + \rho_2 v(t),$$

where $\dot{x}_1(t) = q_1 w(t)$; $\dot{x}_2(t) = q_2 w(t)$.

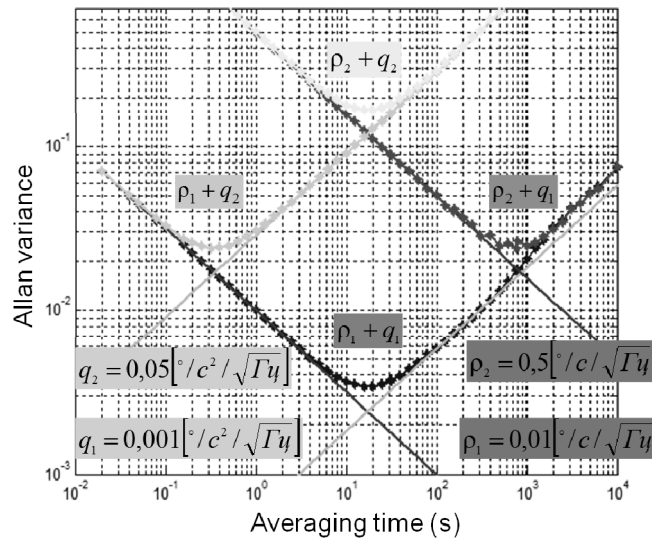


Fig. 2. Allan variance for sum of white noise and random walk of PSDs ρ_1^2, ρ_2^2 , and q_1^2, q_2^2 respectively

Standards [18, 19] introduce the stability as “a measure of the ability of a sensor performance coefficient to remain invariant when continuously exposed to a fixed operating condition”. Note that no quantitative measures determining this ability are given. Let us discuss the possibility of introducing such quantitative measure for random bias of sensor error model (1). Obviously, in this case, the bias non stability is determined by the PSD of random walk generating noise q . In [9, 10, 18, 19] the minimum of AV plot is used to characterize bias instability in assumption that it is the flicker noise PSD. As follows of the aforementioned results, the AV may have an extremum in the absence of flicker noise in the error model. Thus the quantitative measure of stability depends on the model. For the model (1) the maximum averaging time leading to an increase in the bias estimation accuracy, and the corresponding RMS can be considered as the bias stability characteristic as well. However, these values also depend on the white noise PSD (as shown in Fig. 2) and does not consider the possibility of bias estimation by other methods, which are discussed below.

Improving the accuracy of bias estimation using nonlinear filtering

As mentioned in the Introduction, [15, 16] propose an approach based on nonlinear filtering for identification of sensor error models. Its idea lies in finding an optimal Bayesian estimate of composite filter including the state subvector of shaping filter of the studied process and the subvector of unknown parameters specifying this shaping filter. Following these references, formulate the statement of bias estimation problem with inaccurately known parameters of measurement error models. Introduce a composite vector $\tilde{x}_i^T = [X_i, \theta]^T$, where $X_i = [x_i, c]^T$, $\theta = [q, \rho]^T$, then nonlinear filtering problem in discrete form can be written as

$$\begin{aligned} x_i &= x_{i-1} + q\sqrt{\Delta t}w_i, \\ c_i &= c_{i-1} + c, \\ q_i &= q_{i-1} = q, \\ \rho_i &= \rho_{i-1} = \rho, \\ y_i &= c_i + x_i + (\rho / \sqrt{\Delta t})v_i, \end{aligned} \quad (11)$$

where w_i and v_i are zero-mean Gaussian white noise sequences with unit variance, Δt is the sampling interval.

Introducing probability distribution function (PDF) $f(\theta)$ for vector θ and applying partitioning method (Rao-Blackwellization method), the following can be written for optimal estimate $\hat{\theta}_i(Y_i)$ and corresponding computational covariance matrix $P_i^0(Y_i)$ [14, 20]:

$$\hat{\theta}_i(Y_i) = \int \theta f(\theta / Y_i) d\theta, \quad P_i^0(Y_i) = \int (\theta - \hat{\theta}_i)(\theta - \hat{\theta}_i)^T f(\theta / Y_i) d\theta, \quad (12)$$

where $Y_i = [y_1, \dots, y_i]$ is the vector of measurements obtained by the time i . A posteriori PDF $f(\theta / Y_i)$ is defined as

$$f(\theta / Y_i) = \frac{f(\theta)f(Y_i / \theta)}{\int f(\theta)f(Y_i / \theta)d\theta}, \quad (13)$$

where $f(Y_i / \theta) = f(y_i / Y_{i-1}, \theta)f(y_{i-1} / Y_{i-2}, \theta) \dots f(y_1 / \theta)$ is the likelihood function.

The distinctive feature of the problem is that with fixed $\theta = \theta^j$, Eqs. (11) set the linear gaussian filtering problem, and therefore PDFs

$$f(y_i / Y_{i-1}, \theta = \theta^j) = N\left(y_i; H\hat{X}_{i/i-1}(\theta^j), D_i^{cond}(\theta^j)\right), \quad (14)$$

where $H = [1 \ 1]$; are also Gaussian. Incoming optimal prediction estimates $\hat{X}_{i/i-1}(\theta^j)$ and measurement residual variances $D_i^{cond}(\theta^j) = M\left\{\left(y_i - H\hat{X}_{i/i-1}(\theta^j)\right)^2\right\}$ are calculated using the bank of Kalman filters. To calculate the optimal estimate and conditional covariance matrix (12), the point-mass method can be used. Then it is implied that a priori PDF $f(\theta)$ is approximated as [14, 22]

$$f(\theta) = \sum_{j=1}^L \mu_0^j \delta(\theta - \theta^j), \quad \mu_0^j = \frac{f(\theta = \theta^j)}{\sum_{j=1}^L f(\theta = \theta^j)}, \quad (15)$$

where θ^j , $j = \overline{1, L}$ is the set of possible values of parameters defining the point masses. Substituting (15) to (13), the following expressions can be written for a posteriori PDF $f(\theta / Y_i)$:

$$f(\theta / Y_i) = \sum_{j=1}^L \mu_i^j \delta(\theta - \theta^j), \quad \mu_i^j = \frac{\mu_{i-1}^j \cdot f(y_i / Y_{i-1}, \theta = \theta^j)}{\sum_{j=1}^L \mu_{i-1}^j f(y_i / Y_{i-1}, \theta = \theta^j)}. \quad (16)$$

With account for (12), the following relationships can be easily obtained for the estimates and conditional covariance matrix:

$$\hat{\theta}_i(Y_i) \approx \sum_{j=1}^L \mu_i^j \theta_i^j, \quad P_i^0(Y_i) \approx \sum_{j=1}^L \mu_i^j \theta_i^j (\theta_i^j)^T - \hat{\theta}_i \hat{\theta}_i^T. \quad (17)$$

Nonlinear filtering can be used to get the bias estimate and its variance in the form

$$\hat{c}_i(Y_i) \approx \sum_{j=1}^L \hat{c}_i^j \mu_i^j, \quad P_i^c(Y_i) \approx \sum_{j=1}^L P_i^{cj} \mu_i^j, \quad (18)$$

where \hat{c}_i^j ; P_i^{cj} are the bias estimates and variances of obtained in each local Kalman filter.

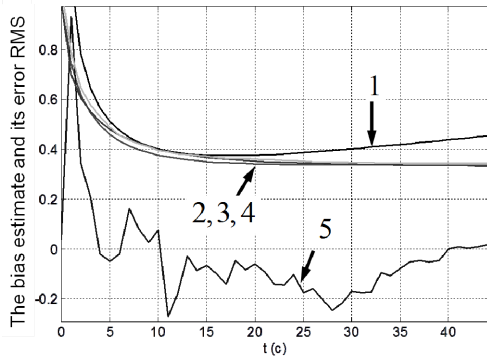


Fig. 3. Allan deviation (I), bias estimation error RMS for optimal KF (2), calculated (3) and real (4) bias estimation error RMS and bias estimation error sample (5) for adaptive filter

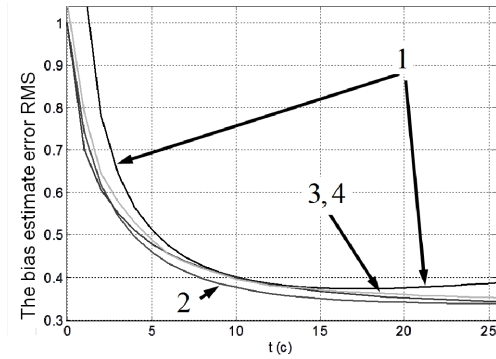


Fig. 4. Allan deviation (I), bias estimation error RMS for optimal KF (2), calculated (3) and real (4) bias estimation error RMS for adaptive filter

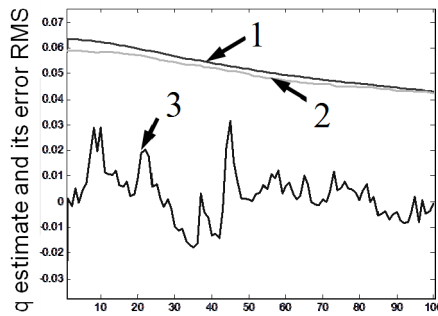


Fig. 5. Calculated (1) and real (2) estimation error RMS for q ; estimation error sample (3)

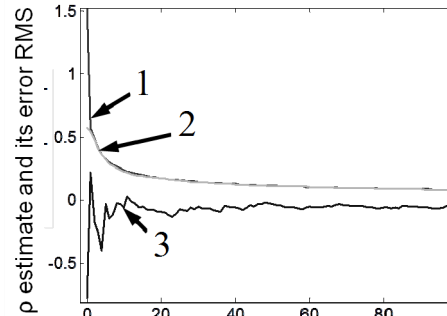


Рис. 6. Calculated (1) and real (2) estimation error RMS for ρ ; estimation error sample (3)

The efficiency of the adaptive filtering method have been proved by simulation. The values q and ρ that are determined noise PSDs were assumed as $q_{ad} \in [0.01 \ 0.21]$ $\rho_{ad} \in [0.1 \ 2.1]$, and initial bias RMS was 1. The simulation results are shown on figures 3-6. In comparison the Allan deviation plot and the RMS error of optimal Kalman Filter (KF) bias estimates is shown on figures 3, 4 for $q_{opt} = M\{q_{ad}\} = 0.11$, $\rho_{opt} = M\{\rho_{ad}\} = 1.1$. Figures 3, 4 shows that use of adaptive filtering allows keeping the optimal estimation accuracy for an infinite interval, and adaptive filtering accuracy is not very different from KF accuracy for this level of uncertainty. The 'real' RMS value is determined by averaging the estimation error squared (17) (18) using all samples. The 'calculated' RMS value is the square root of the mean value of the variances calculated by (17) (18). The coincidence of these values indicates the correctness of their calculation. The transition process for model parameter estimation is slower compared to the estimation of the bias (Fig. 5.6). Note that the similar problem of determining the PSDs of noise components can be solved using the Allan variance as in [16]. The results have shown that optimal estimation provides a 3-5 times better accuracy than for the Allan variance method.

This fact proves that the integrated problem of bias optimal estimation and model identification can be efficiently solved by nonlinear filtering methods using the bank of Kalman filters. It should be also noted that in designing the error model, both the problems of parameter estimation and structure identification prove important [21].

Conclusions

The paper establishes the relationship between Allan variance and variance of bias estimation error received by averaging. These variances are shown to coincide under some conditions. Thus, Allan variance can be used to estimate the minimum error variance of bias estimation by averaging and the corresponding averaging

time, which is exactly important in sensor calibration. This relationship is illustrated by a model being a sum of white noise and random walk.

The paper discusses an approach improving the bias estimation accuracy with unknown sensor error model based on nonlinear filtering methods. It should be also noted that nonlinear filtering provides both estimation of error model parameters and identification of model structure.

This work was supported by the Russian Foundation for Basic Research no. 14-08-00347.

References

1. **Sveshnikov, A.A.**, Prikladnye zadachi teorii sluchainykh funktsii (Applied Problems of Theory of Random Functions), Nauka, 1968.
2. **Bendat, J., Allan, G.P.** Random Data: analysis and measurement procedures, Wiley Interscience, New York (2nd ed 1986, 3rd ed. 2000, 4th ed. 2010)
3. **Prokhorov, S.A.**, Prikladnoi analiz sluchainykh protsessov (Applied Analysis of Applied Processes), Samara, 2007.
4. **Shevlyakov, G.L. and Lyubomischenko, N.S.**, Robust Estimation of Time Series Spectra: Brief Overview of Methods and Algorithms, Materialy XXIX konferentsii pamyati N.N. Ostryakova (Proceedings of the 29th Conference in Memory of N.N. Ostryakov), 2014.
5. **Sergienko, A.B.**, Tsifrovaya obrabotka signalov (Digital Signal Processing), St. Petersburg, 2002.
6. **Stepanov, O. A.**, Osnovy teorii otsenivaniya s prilozheniyami k zadacham obrabotki navigatsionnoi informatsii. Part 1. Vvedenie v teoriyu fil'tratsii (Fundamentals of the Estimation Theory with Applications to the Problems of Navigation Information Processing. Part 2. Introduction to Filtering Theory), St. Petersburg: CSRI Elektropribor, 2012.
7. **Allan, D.W.**, Statistics of Atomic Frequency Standards, Proc. of the IEEE, 54(2), 1966, pp. 221-230.
8. **Howe, D., Allan, D. and Barnes, J.**, Properties of Signal Sources and Measurement Methods, Proceedings of the 35th Annual Symposium on Frequency Control, 1981, pp. 464-469.
9. **Tehrani, M. M.**, Ring Laser Gyro Data Analysis with Cluster Sampling Technique, Proceedings of SPIE, vol. 412, 1983.
10. **Ng, L.C. and Pines, D.J.**, Characterization of Ring Laser Gyro Performance Using the Allan Variance Method, Journal of Guidance, Control, and Dynamics, Vol. 20, No. 1 (1997), pp. 211-214.
11. **Kucherkov, S.G. et al.**, Using Allan Variance in Characterization of MEMS Gyro, Giroskopiya i Navigatsiya, №2 (41), 2003, pp. 98-104.
12. **Siraya, T.N.**, Allan Variance as an Estimate of Measurement Error, Giroskopiya i Navigatsiya, 2010, №2(69), pp. 29-36.
13. **Krobka, N.I.**, Differential Methods Of Identifying Gyro Noise Structure Gyroscopy And Navigation, 3, vol.2, 2011, hh. 126-137
14. **Stepanov, O.A., Toropov, A.B.** Comparison of Point Mass and Particle Filters in Map-aided Navigation // 17 St. Petersburg International Conf. on Integrated Navigation System, ICINS 2010 – Proceedings, pp. 381-384.
15. **Stepanov, O.A., Toropov, A.B.** Application of the Monte Carlo Methods with Partial Analytical Integration Techniques to the Problem of Navigation System Aiding // 20th Saint Petersburg International Conference on Integrated Navigation Systems, ICINS 2013 – Proceedings pp.298-301.
16. **Motorin, A.V. and Stepanov, O.A.**, Identification of Sensor Errors: Allan Variance vs Nonlinear Filtering, 21st St. Petersburg International Conference on Integrated Navigation Systems, 2014, pp. 123-128.
17. **Stepanov, O.A., Motorin, A.V., Vasil'ev, V.A., and Toropov, A.B.**, Using Nonlinear Filtering Methods in Designing Models for Sensor and Map Errors, Materialy XXIX konferentsii pamyati N.N. Ostryakova (Proceedings of the 29th Conference in Memory of N.N. Ostryakov), 2014.
18. **IEEE Std 528-2001**, IEEE Standard for Inertial Sensor Terminology, IEEE Aerospace and Electronic Systems Society, 2001.
19. **IEEE std. 1554-2005**, IEEE Recommended Practice for Inertial Sensor Test Equipment, Instrumentation, Data Acquisition, and Analysis. IEEE Aerospace and Electronic Systems Society, 2005.
20. **Stepanov, O.A. and Toropov, A.B.**, Using Sequential Monte-Carlo Methods and Analytical Integration in Navigation Data Processing, XII Vserossiiskoe soveshchanie po problemam upravleniya (12th Russian Meeting on Control Problems), Russia, Moscow, 16-19 June 2014.
21. **Motorin, A.V., Toropov, A.B., and Stepanov, O.A.**, Applying Multiple Model Filtering to the Estimation of Sensor Error Model, Materialy XVII konferentsii molodykh uchenykh "Navigatsiya i Upravlenie Dvizheniem" (Proceedings of the 17th Conference of Young Scientists "Navigation and Motion Control", 2015.
22. **Bucy, R. S.** Digital synthesis of non-linear filters./ R. S. Bucy and K. D. Senne //Automatica 7(3), 1971, pp.287-298, 1971.
23. **Allan, D. W.** Historicity, Strengths, and Weaknesses of Allan Variances and Their General Applications // Methods for Navigation Sensor erformance Determination, SPb, CSRI Elektropribor, 2015, pp. 509-526.

**22nd SAINT PETERSBURG INTERNATIONAL CONFERENCE
ON INTEGRATED NAVIGATION SYSTEMS, 2015**

**Panel discussion
METHODS FOR NAVIGATION SENSOR PERFORMANCE DETERMINATION**

Editors *L.B.Bakonina, A.K.Krytova*
Cover design *A.A.Reznikova*

Подписано в печать 20.05.15. Формат 70×108/16. Бумага офсетная. Гарнитура Таймс и Ариал.
Усл.-печ. л. 4,81. Тираж 400 экз.

Государственный научный центр Российской Федерации АО «Концерн «ЦНИИ «Электрон»
197046, С.-Петербург, ул. Малая Посадская, 30

Отпечатано с готового оригинал-макета, представленного оргкомитетом конференции,
в типографии Издательства Политехнического университета.
195251, Санкт-Петербург, Политехническая ул., 29

